Doctor of Philosophy, PhD

Alessia Calcagnì

OU personal identifier: C2646402

Analysis of TFEB function in Ksp-Cadherin16 CRE mouse lines to model a particular type of Renal Cell Carcinoma

The Open University

Discipline: Life and Biomolecular Sciences

Affiliated Research Centre: Telethon Institute of Genetics and Medicine

Thesis submitted in accordance with the requirements of the Open University for the degree of “Doctor of Philosophy”.

July 2016

A mia sorella

TABLE OF CONTENTS

LIST OF FIGURES

LIST OF TABLES

ABBREVIATIONS

AD	Transcription activating domain
AL	Autolysosome
AMLs	Angiomyolipomas
APC	Adenomatous polyposis coli
APS	Alveolar soft part sarcoma
AQP	Aquaporin
Areg	Amphiregulin
BAP1	BRCA1 associated protein 1
BCR	Breakpoint cluster region
BHD	Birt-Hogg-Dubè syndrome
bHLH	Basic helix-loop-helix domain
bHLH-LZ	Basic helix–loop–helix leucine zipper
bTrCP	b-transducin-repeat-containing protein
CAG	Cycken beta actin
CBP	Creb binding protein
CCND1	Cyclin D1
cc-RCC	Clear cell Renal cell carcinoma
CDH16	Cadherin 16
CDKN1A	Cyclin-dependent kinase inhibitor 1A
CDKN2A	Cyclin-dependent kinase inhibitor 2A
ChIP	Chromatin immunoprecipitation
CIMP	CpG island methylator phenotype

CK1	Casein Kinase I
CK7	Cytokeratin 7
CLEAR	Coordinated Lysosomal Expression and Regulation
CLTC	Clathrin heavy chain
CM	Cap mesenchyme
CMA	Chaperon-mediated autophagy
CRD	Cysteine rich domain
CRD	Contex-dependent regulatory domain
CtBP	C-terminal binding protein
DKK	Dickkopf
DVL	Dishevelled
E-box	Enhancer box
EGFR	Epitelial growth factor receptor
EL	Endo-lysosomes
ER	Endoplasmic reticulum
ERK	Extracellular signal-regulated kinase
eSC	embryonic Spinal cord
FAP	Familial adenomatous polyposis
FDA	Food and drug administration
FDR	False Discovery Rate
Fgf	Fibroblast growth factor
FGFR	Fibroblast growth factor receptor
FH	Fumarate hydrolase
FLCN	Folliculin
FNIP	Folliculin interacting protein

FZD	Frizzled
GLUT1	Solute carrier family 2 member 1
GPNMB	Glycoprotein (transmembrane) nmb
Gro	Grucho
GSK	glycogen synthase kinase
GTP	Guanosine triphosphate
HbEGF	Heparin binding EGF like growth factor
HE	Hematoxylin and eosin
HGF	Hepatocyte growth factor
HPRC	Hereditary papillary renal cell carcinoma
HSPG	Heparan sulphate proteoglycan
INT1	WNT family member 1
IWP	Inhibitor of Wnt production
JMD	Juxtamembrane domain
KDM6a	Lysine demethylase 6A
KW/BW	Kidney to Body Weight ratio
LAMP2A	Lysosomal associated membrane protein 2A
LE	Late ebdosome
LEF1	Lymphoid enhancer binding factor 1
Lhx1	LIM homeobox 1
LRO	Lysosome related organelles
LRP5/6	Low density lipoprotein receptor related protein 5/6
LSD	Lysosomal storage disorder
LYNUS	Lysosome nutrient sensing
lysoNaATP	Lysosomal ATP-sensitive Na+ channels

LZ	Leucine zipper domain
MALAT1	Metastasis associated lung adenocarcinoma transcript 1
MAX	MYC associated factor X
mBM	Multi-layered basement membrane
MCLN1	Mucolipin 1
mCy	Multilayered cysts
MET	Hepatocyte growth factor receptor
MET	Mesenchymal-to-epithelial transition
MiT/TFE	Microphthalmia/transcription factor E
MITF	Microphthalmia-associated transcription factor
MM	Metanephric mesenchyme
mTOR	Mechanistic target of rapamycin
MVB	Multivescicular body
MYC	Myelocytomatosis viral oncogene homolog
MyoD	Myogenic differentiation
NFAT	Nuclear factor of activated T-cells
NLS	Nuclear Localization Signal
NONO	Non-POU domain containing, octamer-binding
OCT4	Octamer-binding transcription factor 4
O/N	Over-night
PAK	p21-activated kinase
PARP	Poly-(ADP-ribose) polymerase
PAS	Periodic acid–Schiff
Pax8	Paired box 8
PBRM1	Polybromo 1

PCP	Planar cell polarity
PCR	Polymerase chain reaction
PEComas	Perivascular epithelioid cell neoplasms
PET/CT	Positron emission tomography coupled with computed tomography
PKA	Protein kinase A
PKCb	Protein kinase C beta
PM	Plasma-membrane
PORC	Porcupine
PP1	Serine/threonine protein phosphatase
PP2C	Putative protein phosphatase
PRCC	Papillary renal cell carcinoma (translocation-associated)
PSF	Splicing factor proline/glutamine-rich
Rag	Ras-related GTP binding protein
RCC	Renal cell carcinoma
Rheb	Ras homolog enriched in brain
RMA	Robust Multiarray Average
RNF146	Ring finger protein 146
RTK	Receptor tyrosine kinase
sCy	Single cysts
SDHB	Succinate dehydrogenase complex iron sulfur subunit B
SDHD	Succinate dehydrogenase complex iron sulfur subunit D
SETD2	SET domain containing 2
SFQP	Splicing factor proline/glutamine-rich
sFRP	frizzled secreted proteins
SIX2	sine oculis-related homeobox 2

TCF	Transcription factor
TCF/LEF	T-cell factor/lymphoid enhancer factor
TCGA	The Cancer Genome Atlas
TFE3	Transcription factor E3
TFEB	Transcription factor EB
TFEC	Transcription factor EC
TGN	Trans-Golgi network
THP	Tamm horsfall protein
TSC	Tuberosclerosis
TSS	Transcription start site
UB	Ureteric bud
v-ATPase	Vacuolar H[+]-ATPase
VEGF	vascular endothelial growth factor
VHL	von Hippel-Lindau tumor suppressor
Wg	wingless
WIP	WAS/WASL interacting protein
WLS	Wntless
WTX	APC membrane recruitment protein 1

PROLOGUE

A pool of literature has emerged recently, describing the Microphthalmia/transcription factor E (MiT/TFE)*TFEB* as a potent inducer of the lysosomal and autophagic machineries through the activation of the *CLEAR* network (Sardiello *et al*, 2009; Settembre *et al*, 2011; Ballabio, 2016). TFEB regulation and activity has been widely investigated, and several papers have been published describing how this factor can be regulated by cellular metabolic status(Settembre *et al*, 2013), and how it can lead to the induction of lysosomal and autophagy pathways, mediating responses important for cell homeostasis, growth, and differentiation (Levy *et al*, 2006; Sardiello *et al*, 2009; Settembre *et al*, 2011). Moreover, *MITF*, *TFE3* and *TFEC*, the other closely-related members of the MiT/TFE subfamily (MiT/TFE) (Steingrímsson *et al*, 2004), have been shown to regulate a similar subset of target genes, many of which function in autophagy and lysosome (and lysosome-related organelle) biology (Martina *et al*, 2014).

The MiT/TFE transcription factors have also been linked to cancer development. Indeed, the Microphthalmia-associated transcription factor (*MITF)* has been described as a key transcription factor in melanoma progression (Garraway *et al*, 2005), while *TFEB* and *TFE3* have been implicated in the development of a group of novel-identified Renal Cell Carcinomas that are known as *TFE*-translocation Renal Cell Carcinomas (*TFE*-tRCCs) (Kauffman *et al*, 2014). Fusion genes arise from chromosomal translocations involving the *TFE3* and *TFEB* genes with different partners. In *TFEB*-tRCC patients, TFEB protein levels are amplified and TFEB is mainly found in the nucleus(Kuiper *et al*, 2003), while the TFE3 fusion gene product was found to be more stable and transcriptionally

active than it's wild-type counterpart (Weterman *et al*, 2000). It has been almost two decades since the initial identification of these chromosomal rearrangements, however, the mechanisms responsible for kidney tumour development after *TFE3/TFEB* gene overexpression remains largely uncharacterized (Kauffman *et al*, 2014). Due to this, effective targeted therapies have yet to be identified, hence the immediate need to model these diseases in experimental animal systems (Kauffman *et al*, 2014).

ABSTRACT

TFE-fusion renal cell carcinomas (*TFE*-fusion *RCCs*) are caused by chromosomal translocations that lead to the overexpression of the *TFE3* and *TFEB* genes (Kauffman *et al*, 2014). The mechanisms causing kidney tumour development starting from *TFE3/TFEB* gene overexpression, remain largely uncharacterized and effective targeted therapies are yet to be identified, hence the need to model these diseases in an experimental animal system (Kauffman *et al*, 2014). Here we show that kidney-specific *TFEB* overexpression, in both constitutive and inducible conditional transgenic mouse lines, resulted in a phenotype characterized by renal clear cells, multi-layered basement membranes, severe cystic pathology, and ultimately papillary carcinomas with hepatic metastases. These features closely recapitulate the phenotype observed in both *TFEB*- and *TFE3*-mediated human kidney tumors. Analysis of kidney samples from these mice revealed both transcriptional induction of genes belonging to the WNT pathway and enhanced WNT βcatenin signalling. The use of specific WNT signalling inhibitors normalized the proliferation rate of primary kidney cells derived from transgenic mice and significantly rescued the disease phenotype in the mouse model. These data shed new light on the mechanisms underlying *TFE*-fusion *RCCs* and suggest a possible therapeutic strategy based on the inhibition of the WNT pathway.

INTRODUCTION

CHAPTER 1. MiT/TFE family of bHLH-LZ transcription factors

MITF, *TFEB*, *TFE3* and *TFEC* are closely related basic helix–loop–helix leucine zipper (bHLH-LZ) transcription factors that belong to the MiT/TFE subfamily (MiT/TFE) (Hemesath *et al*, 1994). Many genes important for cell proliferation and development belong to the mammals bHLH-LZ factors, such as Myc/Max and MyoD (Hemesath *et al*, 1994). Most of these family members are able to bind the hexamer core CACGTG or (E-box), while the MiT/TFE factors showed an higher specificity of binding for M-box, or non-canonical E-box (TCATGTG, CATGTGA or TCATGTGA) sites (Hemesath *et al*, 1994; Aksan & Goding, 1998). All the members of the MiT/TFE family share an high homology that include three regions: the basic motif that recognizes a specific DNA sequence, the helix-loop-helix (HLH), and the leucine-zipper (LZ) domain, which are essential for protein-protein interactions (Steingrímsson *et al*, 2004). HLH-LZ domains are able to homo/hetero-dimerize among themselves, and through these interactions are able to bind specific sequences of DNA (Hemesath *et al*, 1994). Structural studies have revealed that these factors share a three-residue shift, defined as “kink”, in their Zip domain that allows specific hetero-dimerization among themselves, while preventing binding with other bHLH-Zip factors (Pogenberg *et al*, 2012). Specific deletions of the leucine zipper domain are indeed able to abolish the DNA-binding ability of these proteins (Hemesath *et al*, 1994).

However, the functional relevance of this hetero/homo-dimerization is still not known. TFEB, MITF, and TFE3 can promote transcription through an activation domain that is highly conserved among the family members (Beckmann *et al*, 1990). This domain, however, is not present in the *TFEC* gene, which is the most divergent family member and seems to act as an inhibitory factor, unlike the other three members that activate transcription (Zhao *et al*, 1993).

1.1 MiT/TFE factors: protein function

A recent but large body of evidence underscores the important roles played by these transcription factors in many cellular and developmental processes. MITF (Mi) protein is mainly expressed in melanocytes, which are the pigment-producing cells, but it has also been found to have crucial functions in osteoclasts, mast-cells, and in the retinal pigmented epithelium (Steingrímsson *et al*, 2004). In melanocytes, it is able to provide a melanocyte-specific signal that activates the pigmentation program and is needed for melanocyte survival. It is indeed considered a master regulator for melanocyte development (Hemesath *et al*, 1994). MITF is able to induce the expression of specific melanocyte-related genes, such as *Tyrosinase* and *TRP-1,* through the recognition of an M-box element in which the 5'-T (flanking the canonical CATGTG sequence) is highly recognized by the MITF gene (Aksan & Goding, 1998). Mice lacking MITF are albino, due to the absence of pigmented cells, and have a characteristic microphthalmia phenotype (undeveloped eyes) due to the RPE (Retinal Pigmented Epithelium) transdifferentiation of the ectopic neural retina (Bumsted & Barnstable, 2000). Moreover, in humans, mutations of the MITF gene have

been associated with the Waardenburg syndrome Type 2, an inherited syndrome associated with hearing loss and pigmentary disturbances (Tassabehji *et al*, 1994). TFEC protein expression is restricted to cells of myeloid origin; indeed proximal promoter analyses revealed macrophagic-specific features that caused *TFEC* to be classified as a macrophage-specific gene (Rehli *et al*, 1999). In contrast, *TFEB* and *TFE3* genes are broadly expressed (Kuiper *et al*, 2004). The *TFE3* gene was initially identified as a protein that binds the mE3 motif within the immunoglobulin heavy chain enhancer (Beckmann *et al*, 1990), and is implicated, together with *TFEB*, in humoral immunity (Huan *et al*, 2006) and placental vascularization (Steingrimsson *et al*, 1998), and together with MITF in osteoclastogenesis (Hershey & Fisher, 2004). Also, the *TFEB* gene is considered to be a master-regulator of the auto-lysosomal pathway (Ballabio, 2016; Sardiello *et al*, 2009).

1.2 The Lysosomes

Lysosomes are cytoplasmic organelles specialized in the degradation and recycling of cellular waste. The lysosomal compartment can receive material from the extracellular space mainly through endocytosis and phagocytosis, while intracellular material is largely delivered by the autophagy pathway (Luzio *et al*, 2007). A number of cellular functions depend on a normal lysosomal function: cellular constituent turnover, cholesterol homeostasis, antigen presentation, plasma membrane remodelling, and bone remodelling (Saftig & Klumperman, 2009). Lysosomal function can be subdivided into three main activities: degradation, secretion, and signalling.

1.2.1 Lysosome function: degradation

Lysosomal degradation occurs through the endocytosis of extracellular material and delivery of intracellular material via the autophagy machinery. Endocytosis is a term that encompasses many degradative pathways, which include phagocytosis, macropinocytosis, clathrin- and caveolin-mediated endocytosis, and clathrin- and caveolin-independent pathways. Fission of plasma-membrane (PM) invaginations (a dynamin-driven process), results in endocytic vesicles, which then undergo several maturation steps to become late endosomes (LEs). In LEs, endocytic cargos are sorted into intraluminal vesicles (Xu & Ren, 2015). Mature LEs, also known as Multivesicular Bodies (MVB), fuse with lysosomes to become endo-lysosomes (ELs). This event is also required for the transport of lysosomal hydrolases from the trans-Golgi network (TGN) to lysosomes (Xu & Ren, 2015). During endosome-to-lysosome maturation, there is a progressive reduction of the luminal pH due to the activation of ATPases that pump protons into the lysosome, and of lysosomal membrane channels, such as the cation transporter MCOLN1 that mediates Ca^{2+} release from the lysosomal lumen (Mindell, 2012). Alternatively, intracellular material can reach lysosomes through the autophagy pathway, a bulk-degradative process used by cells to breakdown/recycle cytoplasmic material, including damaged organelles (i.e. mitochondria via mitophagy). Autophagy can be further classified into different subtypes: microautophagy, chaperon-mediated autophagy (CMA), and macroautophagy (which will be called autophagy from hereon). In microautophagy, cytosolic proteins are directly engulfed by the lysosomal or endosomal membranes (Sahu *et al*, 2011). In the CMA, proteins are transported into the lysosomes through chaperones and receptors, and they need to be

unfolded and translocated through the LAMP2A protein (Kaushik & Cuervo, 2012). Autophagy requires the biogenesis of double membrane vesicles known as autophagosomes, which sequester cytoplasmic material. Autophagosomes can subsequently fuse directly to lysosomes, or indirectly through LEs, becoming autolysosomes (ALs), which then fuse with lysosomes to generate autophago-lysosomes (Settembre *et al*, 2013b).

1.2.2 Lysosome function: secretion

The mechanism associated with lysosome secretion is known as "lysosomal exocytosis", where lysosomes migrate toward the periphery of the cell, fuse with the plasma-membrane in a calcium-dependent manner, and subsequently release their content into the extracellular matrix (Verhage & Toonen, 2007). Lysosomal exocytosis proceeds in two steps; first, upon stimulation, kinesin-associated lysosomes move from the perinuclear region to the cell periphery along microtubules. Second, a pool of pre-docked lysosomes can fuse with the plasma membrane in response to calcium-elevation (Jaiswal *et al*, 2002).

Initially, this mechanism was considered to be associated only with specialized cells containing a subset of lysosome-related organelles (LROs) (Stinchcombe & Griffiths, 1999), such as bone resorption in osteoclasts, T lymphocytes degranulation, and pigmentation in melanocytic cells (Settembre *et al*, 2013b). However, it has since been shown in all cell types (Rodríguez *et al*, 1997). Lysosomal exocytosis is not only required to admit the release of lysosomal material into the extra-cellular space, but it is also really important in the process of plasma membrane repair, providing a source of membranes needed during injuries (Settembre *et al*, 2013b).

1.2.3 Lysosome function: signalling

Lysosomes are no longer thought just as organelles involved in degradation and cellular clearance, importantly, their activity has now been demonstrated to affect a myriad of cellular functions, including lipid homeostasis, plasma membrane repair, energy metabolism, bone remodelling, and pathogen defence. Indeed, lysosomal activity needs to adapt to external cues and to be finely regulated by the metabolic status of the cell (Settembre *et al*, 2012). The mTORC1 (mechanistic Target of Rapamicin 1) kinase complex, is a master controller of cell and organism growth, and recently it was shown to perform this function on the lysosomal membrane (Sancak *et al*, 2010). The amount of amino acids inside lysosomes influences the activation status of mTORC1, thus allowing it's docking on the lysosomal membrane in nutrient replete conditions. Briefly, the v-ATPase complex promotes the activation of Rag GTPases, thus recruiting mTORC1 to the lysosomal membrane and inducing it's activation through the small GTPase Rheb (Sancak *et al*, 2010, 2008). During nutrient removal, mTORC1 is released from the surface of lysosomes, and this, in turn, allows the activation of a $lysoNa_{ATP}$ channel that becomes constitutively open and controls lysosomal membrane potential, pH, and amino acid homeostasis (Cang *et al*, 2013). Thus, complex protein machinery, involving mTORC1 and other proteins, relies on regulation that occurs on the surface of lysosomes and is known as LYNUS (**Ly**sosome **nu**trient **s**ensing). It senses the metabolic status of the cells by sensing lysosomal amino acid content, and, subsequently, transmit this information to the cytoplasm and the nucleus (Settembre *et al*, 2013b).

1.3 Transcription factor EB (TFEB): a master regulator of the autophagic-lysosomal network

Initially, lysosomal activity was considered as a constitutive process, but the continuous discovery of new cellular functions that are dependent on these organelles, led to the idea that it could be finely regulated. Indeed, Ballabio and colleagues recently discovered that lysosomal genes have a coordinated expression. Microarray analyses showed that genes encoding for lysosomal proteins are co-expressed in different cell types and conditions (Sardiello *et al*, 2009). Moreover, a palindromic sequence of 10 base-pairs (GTCACGTGAC) localized mainly within 200 base-pairs from the transcription start site (TSS) was identified in the promoter region of these genes (Sardiello *et al*, 2009) and was therefore aptly named *Coordinated Lysosomal Expression and Regulation* (*CLEAR*) element, which contained the consensus E box (CANNTG) that is typically recognized by bHLH-LZ transcription factors (Sardiello *et al*, 2009).

TFEB directly binds to the *CLEAR* element located in the promoter of lysosomal genes, including v-ATPase, lysosomal hydrolases, and lysosomal transmembrane proteins, thus inducing their expression (Sardiello *et al*, 2009; Palmieri *et al*, 2011). Consequently, TFEB overexpression was associated with higher levels of lysosomal enzymes, thus enhancing lysosomes catabolic capacity (Sardiello *et al*, 2009). This was the first evidence showing that lysosomal function was globally regulated, and that TFEB function is indispensable for proper cellular metabolic homeostasis. Subsequent work revealed that TFEB can also exert its transcriptional control on genes associated with autophagy and lysosomal exocytosis (Palmieri *et al*, 2011). Specifically, it

was shown that TFEB can induce autophagy by prompting autophagosome formation and autophagosome-lysosome fusion (Settembre *et al*, 2011). Accordingly, TFEB overexpression increased degradation of bulk autophagy substrates, such as long-lived proteins (Settembre *et al*, 2011). TFEB can also regulate lysosomal exocytosis (Medina *et al*, 2011), a process involving the trafficking of lysosomes toward the PM, and their subsequent fusion with it, thus releasing their content in the extracellular space. Therefore, TFEB coordinates a complex transcriptional program that regulates the main degradative cellular pathways and thus promoting cellular clearance. Several pathological conditions characterized by lysosomal dysfunction can be ameliorated by *TFEB* overexpression in mouse models of human diseases. These include LSDs but also α1-anti-trypsin deficiency and other more common diseases such as Parkinson's, Alzheimer's, and Huntington's (Ballabio, 2016; Settembre *et al*, 2013b).

1.4 TFEB regulation

The concept that lysosomes can act as sensing platforms for signals regulation resulted in the idea that these organelles are not only required for degradation and cellular clearance but are also required as sensors for a variety of cell function and homeostasis. The recent discoveries identifying *TFEB* as the master regulator of the "lysosomal gene network" supports this concept. TFEB regulation is dependent on post-transcriptional modifications, spatial localization, and protein-protein interactions. Under basal conditions, TFEB is mainly localized in the cytoplasm of the cell. Specific stimuli, such as starvation, can induce a rapid

TFEB translocation in the nucleus (Sardiello *et al*, 2009; Settembre *et al*, 2011), where it can exert its transcriptional function. Important for TFEB nuclear translocation is it's phosphorylation status; indeed phosphorylated TFEB is mainly cytoplasmic, while the dephosphorylated form accumulates in the nucleus. Two specific serine residues are essential for TFEB subcellular localization, Ser142 (Settembre *et al*, 2011) and Ser211 (Martina *et al*, 2012; Roczniak-Ferguson *et al*, 2012), and at least three kinases can phosphorylate TFEB: ERK2, mTORC1 (Settembre *et al*, 2012), and PKCb (Ferron *et al*, 2013). Phosphorylation of Ser142 by ERK2 and of both Ser142 and Ser211 by mTORC1 are crucial for TFEB localization, and indeed mutants of these residues result in nuclear TFEB localization (Settembre *et al*, 2011; Roczniak-Ferguson *et al*, 2012; Ferron *et al*, 2013; Martina *et al*, 2012). During feeding conditions, TFEB is phosphorylated and is found in the cytoplasm and on lysosomes due to interactions with 14-3-3 protein (Roczniak-Ferguson *et al*, 2012) and mTOR and LYNUS machinery, respectively (Settembre *et al*, 2012; Martina & Puertollano, 2013). Interestingly, active Rag GTPases also bind TFEB, mediating its recruitment to the lysosomal membrane, promoting its phosphorylation by mTORC1 (Martina & Puertollano, 2013). During starvation, lysosomes sense the metabolic status through their v-ATPase pumps, thus releasing the mTORC complex from their surface as previously described (Sancak *et al*, 2010). Consequently, TFEB is no longer phosphorylated and translocates to the nucleus. Moreover, nutrient depletion also coincides with lysosomal calcium release from the calcium channel mucolipin 1 (MCOLN1), which in turn activates the calcineurin phosphatase that dephosphorylates TFEB, promoting nuclear translocation (Medina *et al*, 2015). This signalling network is of significant relevance for the coordination and activation of a transcriptional program that

allows cells to sense and adapt to nutrient status. Furthermore, it has been demonstrated that TFEB regulates the transcription of many genes important for its own regulation, such as v-ATPase subunits, MCOLN1 and numerous lysosomal enzymes. This reinforces the idea that lysosomal adaptation to external stimuli is regulated by multiple feedback loops. In accordance with this, TFEB nuclear translocation can also induce its own transcription, in a positive autoregulatory loop that is dependent on the presence of CLEAR elements located in its promoter. Thus, starvation can induce TFEB activity using dual mechanisms (Fig. 1) (Roczniak-Ferguson *et al*, 2012; Settembre *et al*, 2013a, 2012).

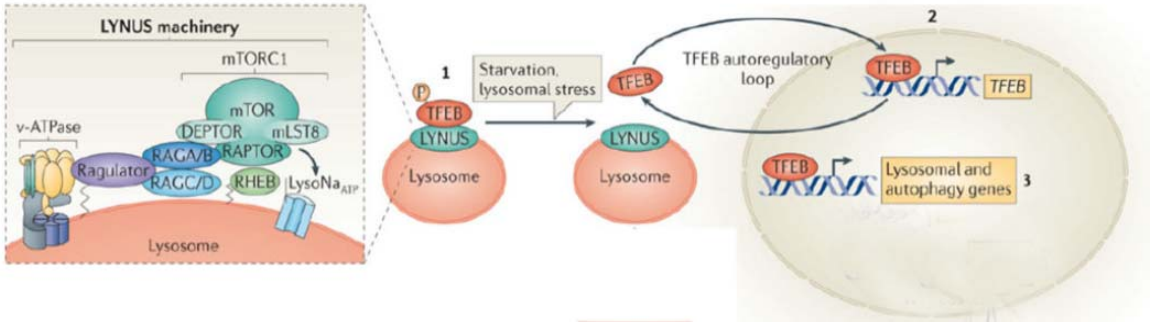

modified from Settembre et al., Nat Rev Mol Cell Biol 2013

Figure 1. TFEB regulation model.

TFEB is induced by starvation and mediates the starvation response. In the presence of nutrients, TFEB interacts with the LYNUS machinery and is phosphorylated by mTORC1, on the lysosomal surface. This phosphorylation inactivates TFEB keeping it in the cytoplasm. During starvation, mTORC1 is no longer on the lysosome, and consequently TFEB is not phosphorylated and it translocates into the nucleus, where it induces its own transcription and the transcription of its target genes, like the genes involved in the lysosomal-autophagy pathway.

Importantly, similar regulation mechanisms were also observed for the other MiT transcription factors(Martina *et al*, 2014; Martina & Puertollano, 2013). Finally,

recent data showed a possible role of WNT pathway in the regulation of the TFE-factors. MITF was shown to be regulated by the GSK kinase, whose activation is important for the regulation of the WNT pathway (Ploper *et al*, 2015). MITF protein has three C-terminus phosphorylation sites that are phylogenetically conserved and also found in TFEB (S397, S401 and S405) and are efficiently phosphorylated by GSK (Ploper *et al*, 2015). Considering that GSK protein kinase activation triggers the proteasomal degradation of βcatenin, a key player in WNT pathway, Ploper *et al.* postulated that these kinase could be important to regulate the stability of the MITF protein, and possibly of the other MiT-TFE factors (Ploper *et al*, 2015).

In conclusion, identification of TFEB, and the study of its transcriptional network, underlined new mechanisms through which cells can respond to metabolic changes, such as nutrient availability. In the lysosomal context, TFEB resulted to participate in a lysosome-to-nucleus signalling, converting lysosomal status in a transcriptional response. However, how different stimuli can activate different MiT members, and which cell responses they modulate, still need to be investigated. Regarding this, in the past few years, mutations involving *TFEB*, *TFE3* and *MITF* genes had been identified in different cancerous condition. Amplifications and activating mutations of the MITF gene had been observed in melanoma, and in some forms of hereditary Renal Cell Carcinoma (Ugurel *et al*, 2007; Bertolotto *et al*, 2011), whereas chromosomal translocations leading to the overactivation of *TFEB* and *TFE3* genes had been identified in sporadic Renal Cell Carcinomas herein referred as *TFE*-fusion RCC (Kauffman *et al*, 2014). These findings opened a new field of study, thus conveying the interest for these factors toward the cancer field.

CHAPTER 2. Renal Cell Carcinomas

Kidney cancer is a complex disease, because of its heterogeneity in terms of genetic background, histology, therapies and prognosis. A lot of efforts have been spent to unravel the nature of the different forms of cancer that occur in the kidney. Kidney cancer results from mutations in a number of different genes, which have unique histology profiles, require different therapies resulting in poor and promising prognoses, as some kidney lesions are aggressive and others quite indolent (Linehan *et al*, 2010). Renal Cell Carcinomas (RCCs) originate from the renal epithelium and include several heterogeneous subgroups defined according to their histological phenotype. The most frequent sporadic forms of RCCs are Clear Cells (65-70%) , type 1 papillary (10%), type 2 papillary (5%), *TFE*-fusion RCC (1-5%), cromophobe (5%) and oncocytoma (5%) (Amin *et al*, 2002; Linehan, 2012). Each of these kidney cancer subtypes has its own histology profile, outcome and responds to different therapies.

2.1 Renal Cell Carcinoma: genes and syndromes

Studies of the inherited forms of kidney disease, such as von Hippel-Lindau (VHL) syndrome and the Birt-Hogg-Dubé (BHD) syndrome, have led to the identification of genes important for RCC. To date, mutations in 12 different genes (*VHL*, *MET*, *FH*, *FLCN*, *SDHB*, *SDHC*, *SDHD*, *TSC1*, *TSC2*, *PTEN*, *MiTF* and *BAP1*) have been associated with an increased susceptibility in the

development of RCC (Linehan & Ricketts, 2013). Consistent with this, mutations in the *VHL* gene, that are responsible of the VHL syndrome, are found in the majority of cases with sporadic Clear Cell RCCs. Moreover, the *Met* gene is mutated in all patients with hereditary papillary renal carcinoma, and is also found mutated in a small population of patients with sporadic, type 1 papillary kidney cancer. Mutations of the fumarate hydrolase gene (*FH*) are responsible for the inherited form of type 2 papillary kidney cancer associated with the leiomyomatosis renal cell carcinoma (HLRCC), but in this case sporadic type 2 RCC is a mixture of kidney cancers, and the gene(s) responsible are currently under investigation. Folliculin (*FLCN*) is mutated in 96% of patients with inherited chromophobe RCC and oncocytoma associated with BHD syndrome. *TFEB*, *TFE3,* and *MITF*, are however only mutated in non-hereditary papillary kidney cancers, whereas germline gain-of-function mutations of MITF have been discovered in patients with melanoma, but rarely with kidney cancer (Linehan, 2012) (see Fig. 2).

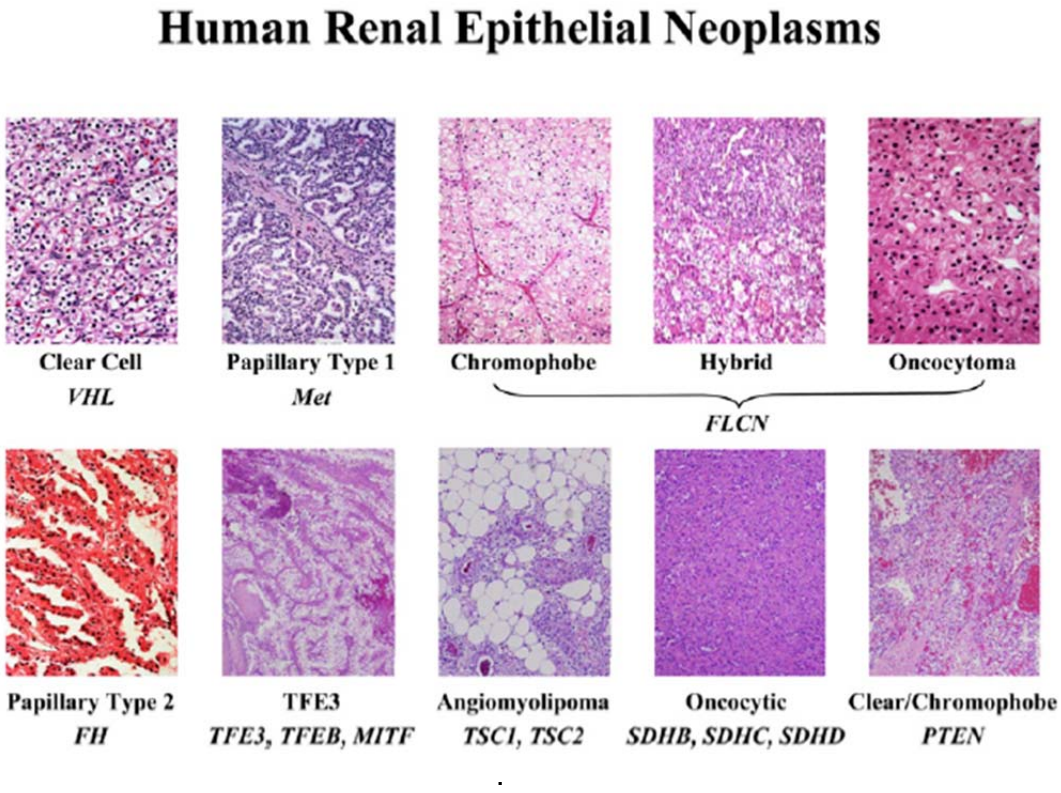

From Linehan et al., Genome Research 2012

Figure 2. Description of the main RCC subtypes.

Classification of the main forms of kidney cancers accordingly with their histology and genetic mutations.

2.2 Clear Cell Renal Cell Carcinoma (ccRCC): The VHL gene

Clear Cell Renal Cell Carcinoma (ccRCC) is the most common type of RCC. Initially, it was associated with deletions of the short arm of chromosome three (Linehan & Zbar, 1987). Subsequently, investigators identified mutations in the *VHL* gene causing the hereditary form of ccRCC, VHL syndrome. Patients with VHL syndrome also have a higher risk of developing cancers in a number of other organs, including the kidney, where they can develop, in early stages, a

multifocal clear cell kidney cancer. It is reported that almost 35-45% of patients with the VHL syndrome ultimately die of kidney cancer (Linehan, 2012). Indeed, renal kidney tumours continuously develop, and they are surgically resected when a 3cm threshold is reached (Herring *et al*, 2001).

To understand if mutations in the *VHL* gene were also responsible of the non-hereditary sporadic forms of kidney cancers, an in-depth mutational analysis of the *VHL* gene was performed in patients with kidney cancer. Gene alterations were found in nearly 90% of patients with ccRCC (Nickerson *et al*, 2008), whereas they were not observed in patients with other forms of RCC, like papillary or cromophobe RCC, thus underscoring the relevance of this gene in ccRCCs. The VHL protein binds the HIF-1alpha and HIF-2alpha transcription factors, thus enabling their targeting for ubiquitin-dependent proteasomal degradation. In normoxia, the VHL complex binds and ubiquitylates the hypoxia-inducible factors, conversely, under hypoxia, formation of the VHL complex is inhibited allowing for HIF factors to accumulate in the nucleus and subsequently to transcribe their target genes, like the vascular endothelial growth factor (*VEGFA*), the glucose transporter *GLUT1*, and the epidermal growth factor (EGFR*)* (Kaelin, 2008). HIF-1aplha is ubiquitously expressed and primarily targets genes involved in glycolysis, whereas HIF-2alpha is the primary regulator of erythropoietin and of the stem cell factor OCT4 (Shen & Kaelin, 2013). Targeting the vascular endothelial growth factor receptor is still the most effective treatment for advanced ccRCC.

More recently, new genes responsible of sporadic forms of ccRCC are being discovered. These genes are involved in the maintenance of chromatin status, like the histone modifier *SETD2* and the SWI/SNF chromatin remodeller complex gene *PBRM1*(Dalgliesh *et al*, 2010; Varela *et al*, 2011). Detailed mechanistic

analyses will be required for the better understanding of the role of these genes in kidney cancer.

2.3 Hereditary forms of kidney cancer

Mutations in the proto-oncogene *MET* are responsible for hereditary papillary renal cell carcinoma (HPRC), and have also been found in patients with nonhereditary papillary kidney cancer (Schmidt *et al*, 1997). *MET* gene encodes for the cell surface receptor for hepatocyte growth factor (HGF) and cancerous mutations usually occur in the tyrosine kinase domain of *MET*, thus enabling the use of molecules with dual kinase activity able to target both MET and VEGF receptors in patients with HPRC and sporadic papillary RCC (Choueiri *et al*, 2013). However, therapeutic treatments for these patients also require the surgical removal of tumours larger than 3cm.

Patients affected by the Birt-Hogg-Dubè (BHD) syndrome are at risk of developing bilateral, multifocal kidney cancer as well as pulmonary cysts and fibrofolliculomas (Zbar *et al*, 2002). While patients affected by VHL or HPRT develop respectively ccRCC or papillary RCC, BHD patients can develop different histological types of kidney cancer, but more frequently hybrid oncocytic tumours and chromophobe renal carcinoma are observed. These patients are managed in the same way of patients with VHL and HPRC, tumours are surgically resected at 3cm (Pavlovich *et al*, 2005). Recently, linkage analysis on BHD families led to the identification of mutations in the Folliculin (*FLCN*) gene. *FLCN* works as a tumour suppressor gene, and mutations have been found in a high percentage of BHD families (Nickerson *et al*, 2002). FLCN interacts with two

proteins, FNIP1 and FNIP2, and with AMPK, which negatively regulates mTOR. FLCN can control a number of processes, and interestingly it can modulate amino acid-dependent mTOR activation through Rag GTPases, and TFEB and TFE3 activity (Schmidt & Linehan, 2015; Hong *et al*, 2010; Petit *et al*, 2013).

Hereditary leiomyomatosis renal cell carcinoma (HLRCC) patients can develop cutaneous and uterine leiomyomas, which are fibroid tumours, and type 2 papillary kidney cancer (Launonen *et al*, 2001). Renal cancers are aggressive, and even tumours of small mass have high metastatic potential, thus surveillance is not recommended and extensive surgical procedures typically are performed immediately (Linehan, 2012). The gene responsible for the disease is the fumarate hydrolase (*FH*) gene, a Krebs cycle enzyme. *FH*-deficient kidney cancers have high aerobic glycolysis and are dependent on glucose transport, a hallmark of the Warburg effect, which postulates that some cancers require glycolysis for ATP production, while they have impaired oxidative phosphorylation (Yang *et al*). For this reason new therapies are now in development for HLRCC patients, targeting the tumour vasculature and the glucose transport (Linehan & Rathmell, 2012).

Succinate dehydrogenase renal cell carcinoma is an inherited syndrome associated with the development of pheochromocytomas and paragangliomas, rare tumours arising from the neural crests, and oncocytic kidney cancer (Vanharanta *et al*, 2004). Renal cancers can be very aggressive, and they should be immediately removed as soon as they are identified. Mutations have been identified in the *SDHB* and *SDHD* genes, which are two of the four genes encoding for the mitochondrial succinate dehydrogenase. These cancer also behave in accordance with the Warburg effect theory (Vanharanta *et al*, 2004; Linehan, 2012).

Inactivating mutations of both alleles of *TSC1* or *TSC2*, which are the two members of the tuberosclerosis (TSC) compex, lead to the development of an hereditary syndrome associated with the growth of tumours in a number of tissues, included kidney. Usually, kidneys are affected by angiomyolipomas (AMLs), a kind of benign renal neoplasm composed of smooth muscle, vasculature, and fat cells. Rarely, TSC patients can also develop RCC (Linehan, 2012). TSC1/2 complex, is required for mTOR shut-down, consequently, inactivating mutations activates constitutively the mTOR pathway, increasing cellular growth.

TFEB and *TFE3* genes have been linked to chromosomal translocations associated with the development of Renal Cell Carcinomas (RCCs). These Translocation Renal Cell carcinomas (TRCCs) are rare kidney cancers that were added to the 2004 to the World Health Organization (WHO) classification (Argani & Ladanyi, 2005) and defined as *TFE*-fusion RCCs (Kauffman *et al*, 2014). This group of tumours will be described in detail below.

2.4 Molecular pathways altered in kidney cancer

All the identified cancer genes, *VHL*, *MET*, *FLCN*, *FH*, *SD*, *TSC1*, *TSC2*, *TFEB* and *TFE3*, participate in the control of different aspects of cellular metabolism, including nutrient, oxygen, and energy sensing. The identification of such genes has led to the better understanding of the biochemical basis of kidney cancer and of the principal signalling pathways altered in these cancers (Fig. 3).

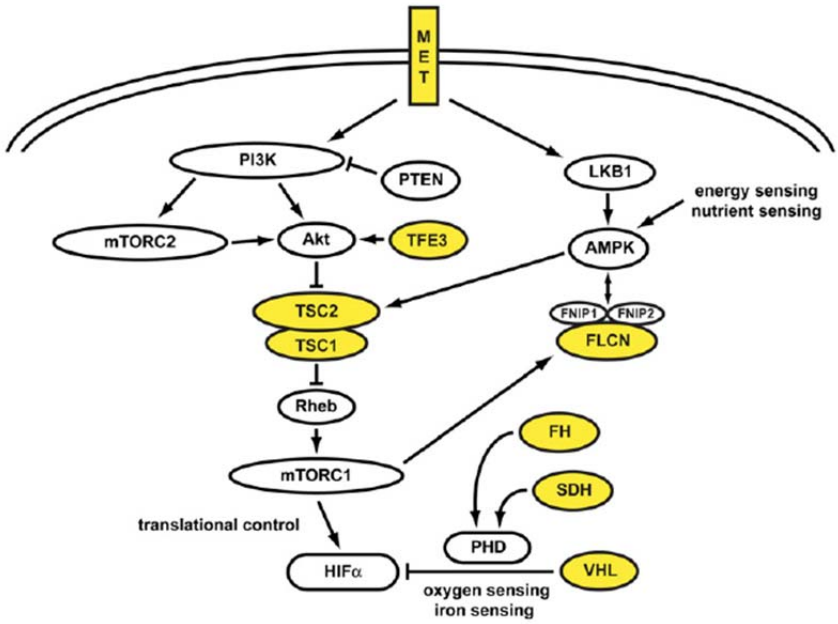

From Linehan et al., *Genome Research* 2012

Figure 3. Kidney cancer gene pathways.

Genes associated to kidney cancer development, VHL, MET, FLCN, FH, SDH, TSC1, TSC2, and TFE3, affects the capability of the cell to sense oxygen, iron, nutrients and energy. VHL targets HIF-1alpha for ubiquitin-mediated degradation. The FLCN/FNIP1/FNIP2 complex can bind AMPK, and FLCN is phosphorylated by mTOR. TSC1/2 are phosphorylated by the LKB/AMPK cascade and mediate cell's response to energy. FH and SDH are Krebs cycle enzymes, when they are deficiently the cell requires glycolysis for energy production. Moreover, their deficiency also dysregulate HIF degradation, and this leads to increase GLUT1 levels which enables transport of glucose and ATP production.

2.6 Sporadic RCCs-papillary kidney cancer

Papillary RCC has been widely characterized, and now is a well-established entity in terms of morphological, immunohistochemical and cytogenetic features. Papillary kidney cancer has been sub-classified in two different types, type 1 and type 2, in accordance with their histology. Type 1 papillary RCC is characterized

by the presence of tightly formed papillae covered by small cuboidal cells, with a single line of uniform nuclei and nucleoli. In type 2, papillae are large and less organized, and are covered by large eosinophilic cells with irregular nuclei. Type 1 papillary kidney cancer is much more frequent then type 2, and patients have a much better prognosis, while type 2 RCCs tend to metastasize early (Leroy *et al*, 2002; Linehan, 2012).

Little is known about the molecular basis of papillary RCC, indeed mutations in the *MET* gene were commonly found only in a subset of patients with sporadic type 1 papillary kidney cancer. However, recent TCGA data collected on a large population of patients, affected by type 1 and 2 papillary RCC, revealed that alterations of *MET* status (defined as mutation, splice variant, or gene fusion) or increased chromosome 7 copy numbers (where the *MET* gene is located) were identified in 81% of type 1 papillary renal-cell carcinomas (Linehan *et al*, 2015). Type 2 RCC showed high heterogeneity. 25% of patients screened showed mutations or alterations in the *CDKN2A* gene, leading to gene silencing. Other type 2 tumours were associated with mutations in the chromatin-modifying genes *SETD2*, *BAP1*, and *PBRM1*, which are frequently mutated in ccRCCs in combination with loss of chromosome 3p. A CpG island methylator phenotype (CIMP) was observed in a sub-group of type 2 RCCs with poor survival and mutations in the FH gene (Linehan *et al*, 2015). Finally, chromosomal translocations involving *TFEB* and *TFE3* genes were also identified in patients with type 2 papillary RCC, suggesting that these tumours are underappreciated in type 2 patients as they are the only recurrent translocation in kidney cancers (Linehan *et al*, 2015; Malouf *et al*, 2014).

CHAPTER 3. *TFE*-fusion RCCs

All the MiT-TFE family members have been associated with cancer development. *MITF* has been associated with Melanoma and with hereditary forms of hereditary RCC. *TFEB* and *TFE3* genes are found fused to different gene partners in sporadic RCCs (see Table 1) (Kauffman *et al*, 2014).

MiT member	Chromosome	Mutations in renal cell carcinoma	Mutations in other neoplasms
MiTF	3p14.1	Germline activating amino-acid substitution	Melanoma: germline activating amino-acid substitution, gene amplification
TFE3	Xp11.2	Gene fusions with *PRCC*, *ASPSCR1*, *SFPQ*, *NONO*, *CLTC*	Alveolar soft part sarcoma: gene fusions with *ASPSCR1* Perivascular epithelioid cell tumours (PEComas): gene fusions with *SFPQ*/other genes?
TFEB	6p21.2	Gene fusion with *MALAT1*	None known
TFEC	7q31.2	None known	None known

From Linehan et al., Nat. Rev. Uorol. 2014

Table 1. Clinical mutations of the Mit family transcription factors.

TFEB and *TFE3*-translocation RCCs are a histologically variable group of sporadic tumours representing almost 2% of all the RCCs (Komai *et al*, 2009) and approximately 12% of type 2 papillary renal cell carcinoma (Cancer Genome Atlas Research Network *et al*, 2016). Initially, *TFE*-fusion RCCs were predominantly observed in paediatric patients, comprising, according to Argani *et al*. (Argani & Ladanyi, 2005), almost one third of all the paediatric cases of RCCs. Currently *TFE*-fusion RCCs are also considered relatively common in adult patients younger than 45 years old (Komai *et al*, 2009). Recent large-scale next-generation genetic analyses evidenced the frequent occurrence of *TFEB* and

TFE3 translocations in RCCs (Linehan *et al*, 2015; Malouf *et al*, 2014). Moreover, recent evidences also showed an association of previous chemotherapy exposure with development of translocation RCC. Approximately 10-15% of tRCCs have been observed after a previous exposure to cytotoxic drugs (Argani *et al*, 2006). *TFE3*-tRCCs are usually aggressive and often metastasize, while *TFEB*-tRCCs usually have a better prognosis. However, the molecular basis of these cancers are currently poorly understood, and this has hampered the identification of a promising pharmacological treatments (Argani & Ladanyi, 2005).

3.1 *TFEB*-translocation RCC: molecular basis

In most cases, *TFEB*-tRCCs are the consequence of a well-characterized chromosomal translocation involving the *TFEB* gene, on chromosome 6p21.2, and the non-coding Alpha gene (or *MALAT1*) located on chromosome 11q13, generating an Alpha-*TFEB* fusion (t(6;11)(p21.2;q13) (Davis *et al*, 2003; Kuiper, 2003). *TFEB* contains two noncoding and eight coding exons. The ATG starting codon is located in exon 3, and the stop codon is situated in exon 10, as depicted in Figure 4. The translocation breakpoint in *TFEB* generally is located in exon 3, just upstream of the ATG start codon, thus resulting in the retention of the entire TFEB coding sequence. At the end of the translocation event, the Alpha promoter drives the expression of the fusion gene. Importantly, the Alpha gene does not contribute to the open reading frame, thus causing only a promoter substitution event (Davis *et al*, 2003; Kuiper, 2003). The consequence of the Alpha-*TFEB* fusion gene is a significant overexpression of the full-length TFEB protein, which accumulates inside the nucleus. Indeed, overexpression and nuclear accumulation

of TFEB are considered to be a diagnostic marker of the disease (Kuiper, 2003). All cases involving *TFEB* breakpoints were observed within a 289bp cluster region (BCR) upstream exon 3, thus retaining the entire *TFEB* coding sequence (Davis *et al*, 2003; Argani *et al*, 2005; Inamura *et al*, 2012). However, only recently a new breakpoint was identified in three patients within exon 4, but the protein size appears to be the same as the wild-type protein (Inamura *et al*, 2012) (Fig. 4).

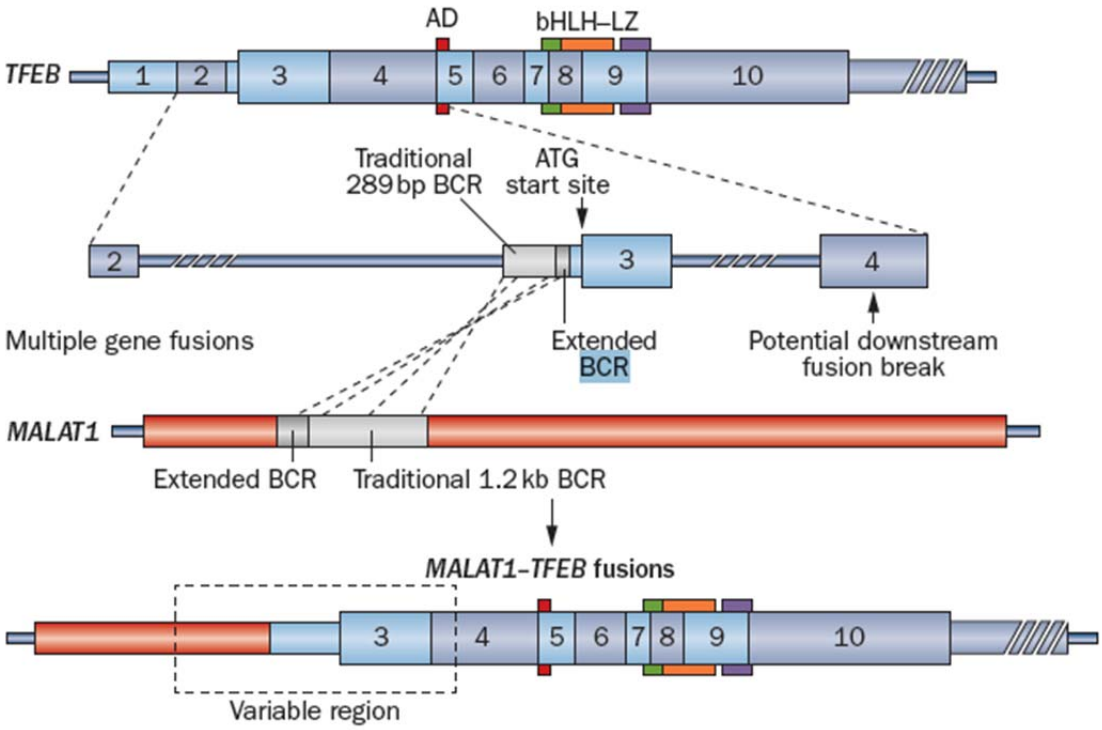

From Linehan et al., Nat. Rev. Urol. 2014

Figure 4. MALAT1-TFEB gene fusions.

The figure is a schematic representing exons and functional domains of the *TFEB* gene. The common breakpoint cluster region (BCR) is represented in light grey, while the darker region is the recently published BCR extension. All the *MALAT1-TFEB* gene fusions contain an upstream *MALAT1* region (red) and most of the *TFEB* gene (blue-grey). Thin regions of the gene represent noncoding regions, whereas the thick region represents the translating reading frame. AD, strong transcription activating domain; BCR, breakpoint cluster region; bHLH, basic helix-loop-helix domain; LZ, leucine zipper domain.

In rare cases of *TFEB*-fusion RCCs, *TFEB* can translocate with the *KHDBRS2* (*inv(6) (p21;q11)*) (Malouf *et al*, 2014) and the *CLTC* (*t(6;17)(p21;q23)*) genes (Durinck *et al*, 2015). *KHDBRS2* is a gene involved in RNA splicing, and the *TFEB* breakpoint was located within the 5' end of the gene, thus retaining most of the *TFEB* coding sequence (Malouf *et al*, 2014). The *TFEB-CLTC* fusion gene was identified in a non-ccRCC sample previously reported as unclassified. In this case, the fusion protein contained the bHLH domain of *TFEB*, suggesting that the retained *TFEB* gene is still functional (Durinck *et al*, 2015). Thus, even if new *TFEB*-fusion RCCs have been recently identified, it looks like TFEB is still the driving force of the neoplastic transformation.

3.2 *TFE3*-translocation RCC: molecular basis

TFE3 chromosomal translocations appear to be more complicated. *TFE3* was found to be involved in translocations with five known gene partners (i.e. *PRCC*, *ASPSCR1*, *SFQP*, *NONO*, *CLTC*) leading to the generation of fusion proteins. The first translocation was the *PRCC-TFE3* t(X;1)(p11.2;q21.2), identified in 1986 in a paediatric patient (de Jong *et al*, 1986) and characterized in 1995 due to the derivation of three cell lines, UOK120, UOK124 and UOK146 (Sidhar *et al*, 1996). Subsequently, this translocation was also identified in young adults (Tonk *et al*, 1995). The following derivation of two additional cell lines, UOK145 and UOK109, led to the identification of novel gene fusion products, the *SFQP-TFE3* (previously known as *PSF*) and the *NONO-TFE3* gene fusions (Clark *et al*, 1997). Finally, Argani *et al.* identified other two gene fusions, *ASPSCR1-TFE3* (Argani *et al*, 2001) and *CLTC-TFE3* (Argani *et al*, 2003). The identification of multiple *TFE3*-

gene partners strongly suggests that RCC is caused by *TFE3*, rather than by its fusion partners (Kauffman *et al*, 2014). The exact breakpoint varies in *TFE3*, and usually occurs in different introns of both *TFE3* and its gene partner. Fusion of chimeric mRNA happens at the exon-exon junctions, retaining the reading frame of the fusion transcript, while containing the N-terminal portion of the gene partner and a variable range of exons located in the C-terminal part of *TFE3* gene. *TFE3* exon 1 is commonly absent, while the universally retained region of the chimeric protein includes exon 6 to 10, encoding for a 208 amino acid C-terminal peptide containing the bHLH/LZ dimerization and DNA binding domain. In total, five translocation gene partners have been identified for *TFE3*-tRCCs. Of these, only *PRCC-TFE3*, *SFQP-TFE3* and *ASPSCR1-TFE3* have been identified as common translocations, while *NONO-TFE3* and *CLTC-TFE3* were observed only in single patients. Moreover, *ASPSCR1-TFE3* was also found in patients with alveolar soft part sarcoma (APS) and *SFPQ-TFE3* was found in a subset of patients with a rare tumour known as perivascular epithelioid cell neoplasms (PEComas). All the identified gene fusions are listed in Table 2.

Chromosomal rearrangement	Type	Cell line	Fusion gene		Fusion protein		Reference
			5' gene exons	TFE3 exons	Amino acids	Predicted mass (kDa)	
PRCC–TFE3							
t(X;1)(p11.2;q21)	1	UOK120, UOK146	1	4–10	553	58.4	Sidhar *et al.*[23]
t(X;1)(p11.2;q21)	2	UOK124	1–4	4–10	790	85.6	Sidhar *et al.*[23]
t(X;1)(p11.2;q21)	3	NA	1	5–10	471	49.8	Argani *et al.*[43]
t(X;1)(p11.2;q21)	4	NA	1–2	6–10	452	47.8	Argani *et al.*[43]
SFPQ–TFE3							
t(X;1)(p11.2;p34)	1	UOK145	1–9	6–10	942	102.0	Clark *et al.*[26]
t(X;1)(p11.2;p34)	2	NA	1–9	5–10	977	105.7	Chang *et al.*,[44] Zhong *et al.*[45]
t(X;1)(p11.2;p34)	3	NA	1–6	2–10	1,102	118.0	Cancer Genome Atlas Research Network[11]
ASPSCR1–TFE3							
t(X;17)(p11.2;q25)	1	FU-UR1	1–7	6–10	591	63.7	Ladanyi *et al.*[29]
t(X;17)(p11.2;q25)	2	NA	1–7	5–10	626	67.4	Ladanyi *et al.*[29]
NONO–TFE3							
inv(X)(p11.2;q12)	1	UOK109	1–9	6–10	657	75.1	Clark *et al.*[26]
inv(X)(p11.2;q12)	2	NA	1–11	6–10	707	80.1	Sato *et al.*[33]
CLTC–TFE3							
t(X;17)(p11.2;q23)	NA	NA	1–17	6–10	1,212	136.1	Argani *et al.*[28]

Abbreviation: NA, not applicable.

From Linehan et al., Nat. Rev. Urol,. 2014

Table 2. TFE3 gene fusions in RCCs.

Recent TCGA analyses showed that among all the screened *TFE*-tRCC tumours, only one had mutations in the *VHL* gene, and none of them had mutations in other genes commonly observed in cc-RCCs (Network *et al*, 2013). Together, these data suggest that the first step, and driving force, of the disease pathological cascade is the overexpression of active TFEB and TFE3 proteins, which is likely associated with an increase of their function as transcription factors.

3.3 Mechanisms of *TFE*-fusion oncogenesis

Fusion genes can cause tumorigenesis mainly through three mechanisms. The "lost activity model" happens when a translocation event causes the loss of function of a tumour suppressor gene. The "novel activity model", presumes that the fusion event generates new protein functions leading to a transformation event. Finally, the "dysregulated activity model" is the commonly accepted model for *TFEB* and *TFE3*-tRCCs. In this case, the *TFE*-fusion event increments a pre-existing oncogenic activity of the wild-type protein through changes in the promoter of the *TFEB* or *TFE3* genes. Indeed, all *TFE3* gene partner promoters are constitutively active causing TFE3 protein to be expressed at higher levels and the fusion protein results in a more stable and transcriptionally active gene product than the wild-type protein (Weterman *et al*, 2000; Clark *et al*, 1997; Argani *et al*, 2003). In *TFEB*-tRCC, there is a promoter substitution leading to the up-regulation of the wild-type TFEB, thus the "dysregulated activity model" is aptly applied. This model implies that *TFEB* and *TFE3* genes have intrinsic oncogenic activities, and this has been demonstrated for some members of the MiT-TFE family. For example, specific *NONO-TFE3* knockdown can inhibit the soft-agar colonization phenotype associated with UOK-109 cells, and this, in turn, can be re-established by the induction of the MITF protein (Davis *et al*, 2006). Moreover, this theory has also been confirmed by clinical observations, considering that MiTF is amplified in 20% of metastatic melanoma and activating mutations of this gene have been identified in hereditary RCC as well as melanoma (Cronin *et al*, 2009; Bertolotto *et al*, 2011).

3.4 Candidate *TFE*-driven signalling pathways

Ones established that *TFEB* and *TFE3* genes overexpression/overactivation are the drivers of carcinogenesis in *TFE*-tRCCs, research interest conveyed toward the identification of molecular pathways that could be altered by these genes and responsible of cancer insurgency. To date, there has been limited data available on the biological pathways involved in these TFE-fusion tumours, and this has hampered the identification of target therapies (Kauffman *et al*, 2014). Argani *et al.* (Argani *et al*, 2010) reported activation of the mTOR pathway in *TFE*-tRCC patients compared to ccRCCs, as shown by increased phosphorylation levels of the downstream mTOR target S6. Unfortunately, selective mTORC1 inhibition performed on patients with *TFE*-tRCCs did not improve the disease phenotype (Malouf *et al*, 2010). Up-regulation of the MET-tyrosine kinase receptor, which in turn activates HGF-signalling, was detected by Tsuda *et al.* in *TFE*-tRCC patients by *in vitro* assays (Tsuda *et al*, 2007), however subsequent analyses on *TFE3*-renal samples failed to identify activated MET protein (Kauffman *et al*, 2014) and treatment of *TFE3*-tRCC patient cells with a MET-inhibitor required an extremely high drug concentration to observe an inhibition of cell growth, consistent with the response observed in cells with no MET activation (Guo *et al*, 2010). Moreover, a clinical trial using tivantinib, a MET inhibitor, demonstrated poor response on *TFE*-RCC patients (Wagner *et al*, 2012). Some patients with metastatic *TFE3*-tRCC have been treated with inhibitors of ErbB receptors and of the mTOR pathway. Unfortunately, most of these patients relapsed after an initial period of remission (Parikh *et al*, 2009; Wu *et al*, 2008). Other hypotheses have been proposed regarding the involvement of possible molecular pathways in carcinogenesis.

TFE3 can interact with SMAD proteins, resulting in TGF-beta signalling (Hua *et al*, 2000), which can have a key relevance in carcinogenesis mediating initiate immune evasion, growth factor production and metastatic dissemination. Moreover, *TFE3* can also bind to the ETS transcription factor, that belongs to a gene family associated with fusion events in prostate cancer and sarcomas (Tian *et al*, 1999). TFEB and TFE3 can also regulate transcription of E-cadherin, important in cell-cell interaction, and CD40L, for primary T lymphocytes activation (Huan *et al*, 2006). Another mechanism putatively involved in carcinogenesis is activation of the lysosomal-autophagy pathway. Considering the well described role of *TFEB* as master regulator of these pathways (Sardiello *et al*, 2009; Settembre *et al*, 2011; Ballabio, 2016) and the recent evidence indicating that activation of autophagy driven by MiT/TFE genes plays an important role in pancreatic cancer (Perera *et al*, 2015), a general idea is that carcinogenesis can be mediated by the autophagy machinery. Autophagy is an essential mechanism for nutrient recycling during cellular starvation, but until now there are no direct evidences of its involvement of in *TFE*-fusion RCC pathogenesis. Further, recent data showed that MITF protein overexpression can positively regulate WNT pathway in melanoma cell lines, and that this, in turn, is able to determine a nuclear accumulation of MITF in a positive feed-back loop (Ploper *et al*, 2015), thus introducing the idea that WNT pathway can mediate a role in the *TFE*-driven carcinogenesis by increasing the nuclear amount of MITF protein and by enhancing the WNT signalling.

In conclusion, nearly two decades have passed from the identification of *TFE*-tRCCs and we currently still do not have effective therapies for these cancers. Significant efforts have been made for the histological and molecular description of these cancers, and recent TCGA data have given new insights in the disease

characterization. Despite this though, the altered molecular events responsible for the disease pathogenesis and progression have to be identified, thus preventing the finding of specific therapies.

CHAPTHER 4. WNT signalling

WNT proteins are a group of 19 highly conserved secreted glycoproteins (Papkoff *et al*, 1987) that direct cell proliferation, migration, survival, polarity and cell fate. WNT pathway is particularly active during embryonic development and tissue homeostasis, and is involved in stem-cell control and renewal (Anastas & Moon, 2013). Considering this, perturbations of this pathway have been associated with different human diseases, including cancer (Anastas & Moon, 2013). Currently, there are three different pathways activated by WNT ligands: the canonical WNT-βcatenin cascade, WNT non-canonical planar cell polarity pathway, and the WNT/Ca^{2+} pathway. Among these three, the canonical WNT/ βcatenin pathway is the best characterized.

4.1 Complexity of WNT glycoprotein secretion

WNT glycoproteins are a family of highly hydrophobic and conserved molecules, and they are characterized by the presence of a N-terminal signal peptide required for their secretion. Lipid modified WNT glycoproteins are widely observed in Metazoans, ranging from the sea anemone Nematostella, to humans, thus

implying that they are involved in a variety of functions (Clevers, 2006). Murine *Wnt1*, also known as *Int1*, was the first discovered WNT gene. It was identified in 1982 as proto-oncogene activated by integration of a mouse mammary tumour virus (Nusse & Varmus, 1982). Later, the identification of the wingless (W*g*) polarity gene as orthologous to *Wnt1* in D. Melanogaster, led to the generation of the name WNT, as a fusion of Wg and INT (Rijsewijk *et al*, 1987). WNT proteins can be distributed in a graded manner among tissues, thus inducing WNT signalling at different levels. Control of WNT proteins secretion is important and needs to be finely regulated (Hausmann *et al*, 2007). Three factors have been recently identified as regulators of WNT secretion: lipoprotein particles (Panáková *et al*, 2005), the retromer complex (Coudreuse *et al*, 2006), and the multi-pass transmembrane protein Wntless (WLS) (Bänziger *et al*, 2006).

.

4.1.1 WNT glycosylation

At the primary sequence level, WNT proteins share a pattern of 23 cysteine residues, that are required for protein palmitoilation (Willert *et al*, 2003), the N-terminal signal sequence, and several glycosylation sites. WNT glycosylation is still not completely understood. It may be required for targeting WNT proteins to the exocytic route and it may also affect the extracellular distribution of WNT proteins. Glycosylated-deficient WNT3a and WNT5a proteins are defective in secretion whereas, glycosylated-deficient WNT1 protein can be secreted and can promote WNT signalling in cultured cells (Tang *et al*, 2012). These results indicate that the involvement of glycosylation in WNT secretion is not a common mechanism among different WNT proteins. Moreover, lipidation-defective Wg protein can be glycosylated, suggesting that glycosylation and lipidation are two

independent processes (Tang *et al*, 2012). Further investigations are still required to completely understand the functions of glycosylation in WNT proteins.

4.1.2 WNT lipidation

WNT lipidation is also essential for WNT proteins localization and function. Two lipid modifications have been identified on mature WNTs, initially identified on WNT3A. Murine WNT3A was the first isolated and characterized WNT protein (Willert *et al*, 2003). This protein is N-glycosylated to allow its secretion, and these lipid modifications are required for its hydrophobicity and poor solubility (Hausmann *et al*, 2007). The first identified lipidation site was cysteine 77, which is conserved in all WNT proteins and mutation of this residue has no effect on protein secretion, but diminished WNT3a ability to activate βcatenin signalling (Willert *et al*, 2003). Another lipidation site was subsequently identified, serine 209, for protein palmitoylation. Lesions in serine 209 result in the accumulation of WNT3A in the endoplasmic reticulum, which fails to be secreted (Takada *et al*, 2006). Thus, cysteine 77 palmitoylation is required for normal function of secreted WNT proteins, while palmitoylation of serine 209 is required for correct protein trafficking. The importance of WNT lipidation is also evident from the discovery of Porcupine (PORC), an acyltransferase that has been proposed to be the enzyme required for the addition of acyl groups to both Cys77 and Ser209 (Willert *et al*, 2003). Porcupine is a multi-pass transmembrane protein active only in WNT-producing cells and belongs to the O-acyltransferase superfamily (Hofmann, 2000; Kadowaki *et al*, 1996). PORC is localized to the ER and WNT secretion is significantly abrogated in PORC null cells. Blocking Ser209 palmitoylation resembles the phenotype of Porcupine loss-of-function, suggesting that Porcupine is responsible for this modification (Takada *et al*, 2006). Finally, the recent solving

of WNT8 crystal structure has revealed that WNT proteins can bind to their Frizzled receptor due to the presence of two domains projecting into the receptor pocket, and one of these domains contains a palmitoleic acid lipid necessary for this interaction. Thus, lipid signalling resulted to play an important role in WNT pathway, as it is required for a correct trafficking, secretion and activity of WNT proteins.

4.1.3 Wntless proteins and the retromer complex

Wntless (Wls) protein is a seven-pass transmembrane protein important for WNT secretion. Wls localizes at the Golgi network, endosomes, and plasma membrane, and binds WNT proteins (Fig. 5). Wls is thought to act as a sorting receptor, shuttling WNT proteins from the Golgi and delivering them to the plasma membrane. Moreover, studies in *C. elegans* demonstrated the importance of the retromer trafficking complex in WNT signalling. This complex involves the retrograde transport of endocytosed transmembrane proteins back to the Trans-Golgi network. In yeast, the retromer complex is important for the recycling of the hydrolase transporter Vps10, while in mammals it is required for mannose-6-phospate receptor trafficking. Recent evidences revealed that the retromer complex also retrieves endosomal Wls protein, avoiding its lysosomal degradation and mediating its trafficking back to the trans-Golgi network (Belenkaya *et al*, 2008) (Fig. 5).

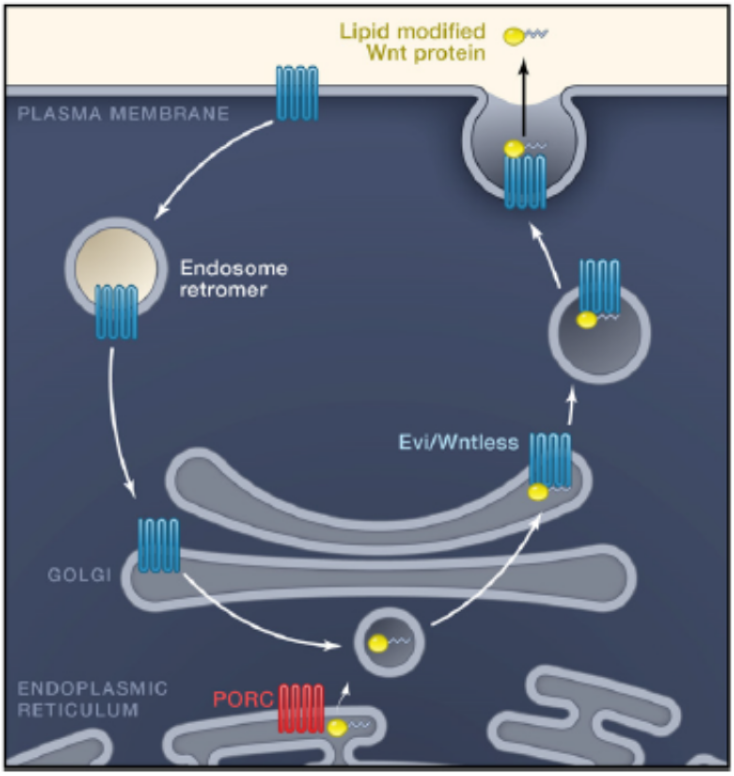

From Clevers et al., Cell 2012

Figure 5. The WNT secretion machinery.

WNT proteins are lipidated in the ER by the PORC enzyme. Subsequently, trafficking and secretion is dependent from the Wls transmembrane proteins. The retromer complex is required for recycling the Wls endosomal vesicles.

Indeed, the loss of retromer function leads to degradation of Wls in lysosomes and reduction in WNT secretion. Vacuolar acidification is required for the release of WNT proteins from the Wls molecule and drugs inhibiting the V-ATPase proton pump can prevent the release of WNT protein, thus leading to an accumulation of WNTs-Wls complexes both in cells and plasma-membrane (Willert & Nusse, 2012).

4.1.4 WNT proteins are not classical morphogens

WNT proteins are normally considered morphogens, meaning that these molecules are able to exert their function across long distances. A well-known example of WNT morphogen action occurs at the wing imaginal disk of *Drosophila*. Wg protein is produced by a thin layer of cells, which subsequently dispersed from this tissue, mediating varying molecular responses over long distances. Wg proteins can mediate this kind of action in two ways: by their association with lipoprotein particles (Panáková *et al*, 2005) or by their interaction with specific binding partners, like the Swim protein (Mulligan *et al*, 2012). However, with the exception of wing development in Drosophila, Wg rarely mediates long-range signals, rather they usually mediate contact-dependent signalling. In other animals, WNT signalling appears to occur predominantly in cells that are close to each other, thus these molecules are not considered classical morphogens, but they can signal at short distances (Clevers & Nusse, 2012).

4.2 The βcatenin cytoplasmic destruction complex

In the absence of WNT morphogen stimulation, WNT pathway is not active and βcatenin protein is degraded by the proteasome. βcatenin is a key player in the canonical WNT pathway and its levels and localization need to be finely regulated. βcatenin levels are strictly controlled by the cytoplasmic destruction complex, which is a complex made up of multiple proteins, like Axin and APC. Axin is a tumour suppressor gene that acts as the scaffold for the destruction complex, it can interact with βcatenin, the tumour suppressor proteins APC, and WTX, with

the two constitutively active serine-threonine kinases CK1 and GSK3. Axin is phosphorylated by the kinases CK1 and GSK3, while it is dephosphorylated by the PP1 and PP2C phosphatases. There are two Axin genes in the human genome and they encode for Axin1 and Axin2. Axin is a member of the βcatenin degradation complex, yet Axin 2 expression levels are upregulated by the WNT/βcatenin pathway. Moreover, there are three Nuclear Localization Signals (NLS) in Axin that may serve as a shuttle for βcatenin between the cytoplasm and nucleus (Cong & Varmus, 2004). APC is the largest structural protein of the destruction complex. It interacts with both βcatenin and Axin due to the presence of three Axin-binding motifs interposed between 15-20 amino acids repeats that bind βcatenin. The APC-βcatenin binding domains are thought to be required for the exposure of βcatenin phosphorylation residues to the destruction complex. APC can be phosphorylated by the CK1 kinase and this phosphorylation outcompetes Axin to form a complex with βcatenin. Additionally, it has been proposed that coordination of Axin, APC, and βcatenin phosphorylation is necessary for βcatenin processing in the degradation complex (Verheyen & Gottardi, 2010). APC function is still not completely understood, although it is clear that it is essential for the destruction complex activity. APC has also been demonstrated to function as a nuclear shuttling protein, indeed APC has two NLSs required to shuttle APC into the nucleus (Zhang *et al*, 2000). Further, nuclear APC was shown to negatively regulate the transcriptional activity of βcatenin (Voronkov & Krauss, 2013). Finally, WTX is another member of the destruction complex and it is mutated in some forms of paediatric kidney cancer (Rivera *et al*, 2007), however, the exact function of WTX is not well defined.When the WNT pathway is inactive, WNT receptors are not engaged and CK1/GSK3 kinases phosphorylate

Axin-bound βcatenin at N-terminal Ser/Thr residues (Verheyen & Gottardi, 2010). Initially, CK1 phosphorylates βcatenin at Ser45, enabling a subsequent phosphorylation by GSK on Ser33, Ser37, and Ser41. These phosphorylation events increase APC affinity for βcatenin, thus allowing the transfer of βcatenin from Axin to APC and the loading of a new βcatenin molecule on Axin . Finally, APC exposes the phosphorylated motif to the Fbox/WD repeat protein βTrCP (Voronkov & Krauss, 2013) that is part of an E3 ubiquitin ligase complex. βcatenin is then ubiquitinated and ultimately degraded by the proteasome (Aberle *et al*, 1997).

4.3 WNT receptors

Activation of WNT signalling requires the binding of the secreted WNT proteins to WNT receptors. WNT proteins can bind a heterodimeric receptor complex located on the cell surface, composed of Frizzled (FZD) and LRP5/6. FZD proteins are seven transmembrane receptors with a large N-terminal cysteine-rich domain (CRD) important for WNT binding (Janda *et al*, 2012). FZDs interact with a single pass transmembrane protein of the LRP family, known as LRP5/6 in vertebrates (Pinson *et al*, 2000). Currently, the most popular model proposes that WNT binds to FZD, which triggers the hetero-oligomerization of the FZD-LRP5/6 complex, also known as the WNT signalosome, thus activating WNT/βcatenin signalling (Tolwinski *et al*, 2003)**.** WNT signalosome oligomerization is induced on its cytoplasmic domain by Dishevelled (DVL). DVL can interact with the cytoplasmic tail of FZD (Clevers & Nusse, 2012) and can oligomerize through its DIX domains,

which are motifs that share homology with the Axin domain (Voronkov & Krauss, 2013; Fiedler *et al*, 2011). The DVL-mediated FZD-LRP5/6 oligomerization is then needed for Axin recruitment to the WNT signalosome, inducing Axin polymerization on the cytoplasmic side of the signalosome (Voronkov & Krauss, 2013). Axin and the kinases CK1 and GSK3 are recruited to LRP5/6 (Del Valle-Pérez *et al*, 2011). First, CK1–mediated phosphorylation acts as a primer that allows for GSK3-mediated phosphorylation of LRP5/6. CK1 and GSK3 can recognize and phosphorylate PP(S/T)PX(S/T) repeats in the cytoplasmic tail of LRP5/6, initiating the crucial event of βcatenin stabilization, as these kinases can switch from phosphorylating βcatenin to phosphorylate LRP5/6. The degradation complex subsequently becomes rapidly saturated by phospho-βcatenin, and the newly synthesized protein accumulates in the cytoplasm and translocates into the nucleus, thus activating the transcription of its target genes (Li *et al*, 2012) (Fig. 6).

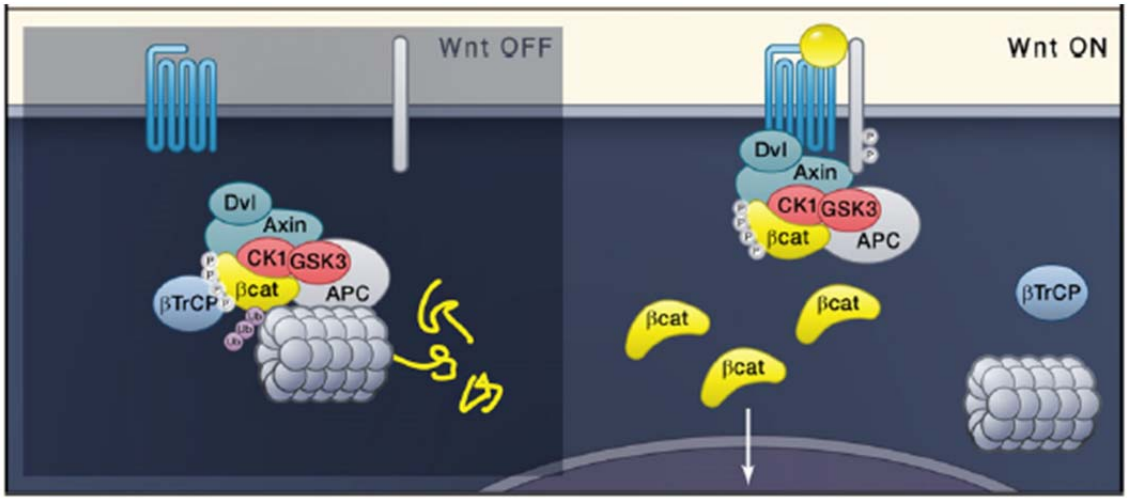

Modified from Clevers et al., Cell 2012

Figure 6. The WNT signalosome and the degradation machinery.

In the absence of Wnt, the destruction complex localizes in the cytoplasm where it binds, phosphorylates, and ubiquitinates βcatenin through b-TrCP. Wnt induces the association of the intact complex with phosphorylated LRP. After binding to LRP, the destruction complex stills

captures and phosphorylates βcatenin, but ubiquitination by b-TrCP is blocked. Newly synthesized βcatenin accumulates.

The WNT signalosome can also activate WNT pathway indirectly, by inducing Axin degradation and GSK3 inhibition (Cselenyi *et al*, 2008) or by sequestering GSK3 in multivesicular endosomes that reduce the kinase presence at the cell surface (Taelman *et al*, 2010).

4.4 Adherens complex and βcatenin signalling

βcatenin can also mediate a transcriptional-independent function, which happens at the cell surface. In this context, βcatenin can bind different cadherins, like E-cadherin, mediating the generation of adherens junctions (Clevers & Nusse, 2012). The adherens junction pool is highly stable, and it has multiple functions in the cell, like structural adhesion functions, protective roles, and it participates in signalling pathways, with a prominent role in WNT/ βcatenin signalling (Brooke *et al*, 2012). Cadherins are a family of single-pass transmembrane proteins and the central components of the adherens junctions. Changes in cadherins concentration are referred to as “switch”, as for example the increase in N-cadherins against E-cadherins observed in epithelial to mesenchymal transition (EMT). Cadherins switch is important for cell motility, migration, invasiveness and metastasis in cancer (Voronkov & Krauss, 2013). As an example of the importance of cadherins switch, E-cadherin adhesion complexes are considered to be one of the key regulators of cytoplasmic βcatenin pool, and a reduction of E-cadherin

content is sufficient to induce an increase of βcatenin levels and transcriptional activity (Brembeck *et al*, 2006). E-cadherin is a single-pass transmembrane protein that has an N-terminal extracellular domain which is important for cell-cell adhesion and consists of five repeats that are stabilized by calcium (Voronkov & Krauss, 2013). The intracellular part of the protein contains a juxtamembrane domain (JMD) that promotes adhesion complexes to bind βcatenin, plakoglobin, as well as p120 and αcatenin (Ishiyama *et al*, 2010). There are different mechanisms by which βcatenin can be modulated at the adherens junctions. For example, βcatenin phosphorylation by PKA appears to promote its stability and, subsequently, binding to the Creb binding protein CBP, thus inducing βcatenin-mediated signalling (Hino *et al*, 2005). Moreover, the cellular kinase Src (c-Src) can phosphorylate βcatenin, impairing its binding with E-cadherin, and leading to an increase in its cytoplasmic levels (Voronkov & Krauss, 2013). Finally, WNT binding to FZD/LRP receptors also induces a CK1-dependent E-cadherin phosphorylation that reduces the affinity of βcatenin to E-cadherin, leading to the release of βcatenin. Hence, WNT signalling stimulation can also induce a release of the membrane-bound form of βcatenin, further increasing its protein levels (Voronkov & Krauss, 2013).

4.4.1 Additional transmembrane receptors influencing βcatenin

c-Met, the receptor of the hepatocyte growth factor/scatter factor (HGF), has been associated with WNT/βcatenin signalling, and it has been shown that it can activate βcatenin at the site of the adherens junctions (Nelson & Nusse, 2004). HGR binding to c-Met stimulates an autophosphorylation of the receptor that in turn mediates βcatenin phosphorylation on Tyr654 and Tyr670, leading to βcatenin

dissociation from E-cadherin (Nelson & Nusse, 2004). HGF can also induce βcatenin release through a matrix metalloproteinase-7 (MMP-7)-dependent E-cadherin degradation (Pan *et al*, 2010), or through the induction of the transcription factor Snail, that represses E-cadherin expression (Leroy & Mostov, 2007). HGF/c-Met-mediated stabilization of β-catenin has been associated with several types of tumours (Ranganathan *et al*).

4.5 βcatenin nuclear function

Once released from the destruction complex, cytoplasmic βcatenin translocates into the nucleus where it can exert its main functions. Here βcatenin interacts with a number of transcription factors and predominantly with the zinc-finger transcriptional factors of the Tcf/Lef (T-cell factor/lymphoid enhancer factor) family. These factors were originally identified in the immune system, however the discovery of the interaction between TCF/LEF and βcatenin revealed a wider role in WNT signalling. All the members of the Tcf/Lef family (Tcf1, Tcf3, Tcf4, and Lef1) have an N-terminal βcatenin binding domain, followed by a context-dependent regulatory domain (CRD) able to bind the co-repressor Grucho (Gro), a HMG-box DNA-binding domain, and a C-terminal domain with binding sites for the co-repressor C-terminal binding protein (CtBP) (Arce *et al*, 2006). Lef1 generally works as a transcriptional activator when complexed with βcatenin. Tcf3 is instead predominantly considered as a repressor. Tcf1 and Tcf4 are context-dependent and can work both as repressors or activators of transcription (Arce *et al*, 2006). The consensus TCF cognate motif in vertebrate is AGATCAAAGG (van

de Wetering *et al*, 1997) and it has been used for the generation of a WNT/TCF reporter, the pTOPflash plasmid containing concatamers of this motif (Korinek *et al*, 1997). In the absence of βcatenin, Tcf/Lef members bind DNA and form a repressor complex with Grucho, CtBP and HDAC, leading to transcriptional repression (Clevers & Nusse, 2012). When βcatenin translocates into the nucleus, it displaces the repressor complex bound to Tcf/Lef factors, facilitating the Tcf/Lef binding with co-activators such as CBP/p300, and BCL9/LGS and Pygo, which can activate transcription of target genes (Fig. 7) (Clevers & Nusse, 2012).

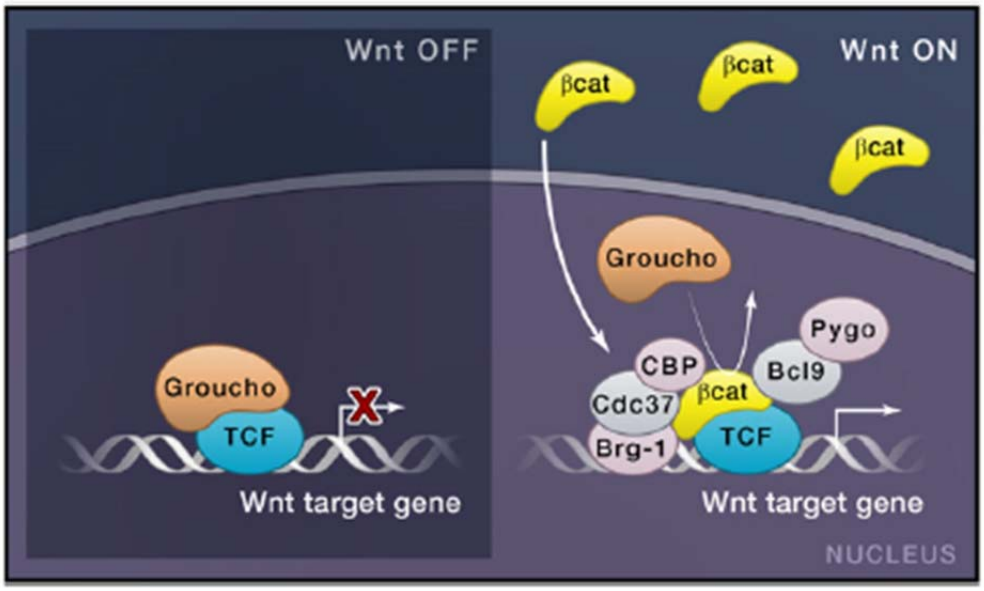

Modified from Clevers et al., Cell 2012

Figure 7. WNT signalling in the nucleus.

In the absence of WNT signals, TCF represses its target genes through the binding with corepressors such as Groucho. Upon WNT signalling, βcatenin replaces Groucho from TCF and recruits transcriptional coactivators and histone modifiers such as Brg1, CBP, Cdc47, Bcl9, and Pygopus to drive target gene expression.

There is no consensus on the mechanism by which βcatenin travels between cytoplasm and nucleus, and in many cases WNT stimulation leads to an overall increase in βcatenin protein levels, without a clear nuclear localization. βcatenin nuclear import depends from the Nuclear Localization Signal/importin machinery and it can be actively exported back to the cytoplasm either by an export signal or as cargo of Axin or APC (Clevers, 2006). A number of WNT target genes have been identified in different biological systems. Until now, the direct "WNT target genes", contain a TCF binding site. To this category of genes belong cMyc, Cyclin D1 and Axin2 (Clevers 2006).

4.6 WNT antagonists

WNT signalling pathway can be inhibited at different levels. One possibility is to inhibit WNT signalling through the use of secreted molecules able to antagonize WNT ligands, which include frizzled secreted proteins (sFRPs), WNT inhibitory proteins (WIPs), Dickkopf (DKK) and Cerberus. sFRP, WIP and Cerberus inhibit WNT by blocking the interaction between WNT ligands and Fzd receptors (Bovolenta *et al*, 2008). DKK1 molecules act by disrupting the Fz-LRP complex (Clevers & Nusse, 2012). Moreover, the WNT pathway can be targeted by Axin degradation; Axin N-terminal phosphorylation results in increased affinity for βcatenin and thus, βcatenin degradation. Inhibition of the Axin phosphatases PP2A and PP1, via okadaic acid, can induce βcatenin degradation (Voronkov & Krauss, 2013). Other druggable molecules include the Tankyrase proteins, Tankyrase 1 (PARP5a) and Tankyrase 2 (PARP5b), which are Poly (ADP-ribose)

polymerases (PARPs) that are implicated in WNT signalling. PARPs mediate the addition of a multimeric side chain by the use of a NAD+ molecule as a substrate, and these proteins appear to interact with the ubiquitin ligase RNF146, which is essential for Axin degradation by the destruction complex. Thus, Tankyrase inhibitors can inhibit WNT signalling by blocking Axin degradation (Voronkov & Krauss, 2013). Porcupine is another protein that could be a target for the modulation of WNT signalling, as it is required for proper WNT secretion. IWP are a class of potent small molecules targeting Porcupine, and thereby inhibiting WNT secretion. (Voronkov & Krauss, 2013). Finally, a group of small molecules were found to disrupt the β-catenin/Tcf-4complex: CGP049090, PKF118-310, PKF115-584 and ZTM000990. Studies revealed that the binding sites for these molecules in βcatenin corresponds to a cavity located inside amino-acids Arg469, Lys435, Lys508, Glu571 and Arg515 which interacts with Tcf-4 (Voronkov & Krauss, 2013). The use of these small molecules, which sterically hindered substrate binding, inhibited colon cancer cell lines proliferation *in vitro* (Wei *et al*, 2010), disrupted the β-catenin/Tcf-4complex *in vivo*, and was able to eradicate breast cancer in a Her2/Neu mouse model of breast cancer (Hallett *et al*, 2012).

CHAPTHER 5. WNT signalling in the kidney

WNT signalling plays important roles during embryonic kidney development. WNT-mediated signalling regulates kidney development from early stages of renal organogenesis, and aberrant WNT signalling can lead to kidney diseases ranging from fatal kidney agenesis to milder phenotypes.

5.1 Renal organogenesis

Renal organogenesis starts from early metanephros, which begins with the outbranching of the Wolffian duct, the ureteric bud (UB), and the metanephric mesenchyme (MM). The MM is subdivided into cap mesenchyme (CM) that is adjacent to the UB, and cortical interstitial stroma that surrounds the CM (Halt & Vainio, 2014). After the metanephros establishment, the UB undergoes iterative branching, while the CM begins to differentiate into nephrons in the regions surrounding the UB. Progenitor cells located in this position, generate pre-tubular aggregates that subsequently undergo a Mesenchymal-to-epithelial (MET) transition to generate a renal vesicle, which will ultimately differentiate into the collecting duct system generated by the UB (Halt & Vainio, 2014). Renal vesicles mature into functional nephrons through the evolution of comma-bodies into S-shaped bodies, elongating along the corticomedullary axis, and forming the region that contains the Bowman's capsule, the proximal convoluted tubule, the loop of Henle, the distal convoluted tubule, and the collecting tube. On the vascular side

of the kidney, the nephron connects with the glomerulus, which is composed of endothelial and mesangial cells (Halt & Vainio, 2014) (Fig. 8).

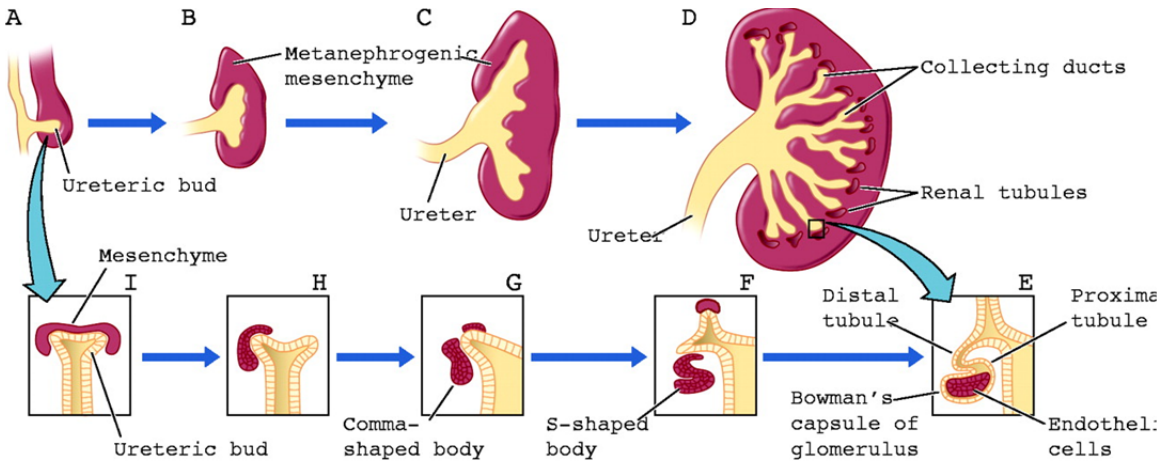

From Sampogna et al., Physiology 2004

Figure 8. Renal branching morphogenesis and nephron formation.

Ureteric bud (UB) outgrowth is induced by signals arising from the metanephric mesenchyme (A, B). This is followed by iterative branching of the UB and stalk elongation (C, D). At the branch tips, the UB induces a mesenchymal-to-epithelial transformation (E, F) via the formation of comma- and S-shaped bodies (G, H), ultimately forming various nephron components (I).

In this context, generation and study of several knockout models has helped the understanding of the transcriptional program responsible for nephrogenesis. The sine oculis-related homeobox 2 (Six2) gene is essential for the developing kidney, as it is expressed in the nephron stem cell population needed to maintain the self-renewal potential, while its expression is rapidly down-regulated in the pre-tubular cell aggregates to allow differentiation initiation (Halt & Vainio, 2014). Upon induction, cells of the cap mesenchyme down-regulate Six2 and activate genes like Fgf8, Wnt4, Lhx1 and Pax8 to allow pretubular aggregate formation (Halt & Vainio, 2014). In these developmental stages, WNT signalling plays important roles. It is involved both during the initial induction of the CM and during nephron

maturation, and alterations of WNT signalling in this stage can severely affect renal organogenesis, resulting in different pathological conditions like polycystic kidney disease and Wilms tumour.

5.2 WNT signalling in nephrogenesis

In vitro experiments have revealed that contacts between CM and UB is the key stimulus for successful kidney development. Indeed, separation of CM from MM leads to a regression of both tissues in culture (Kispert *et al*, 1998). In this context, MM development can be rescued from degeneration and differentiate into nephrons through the addition of the embryonic spinal cord (eSC). eSC can mediate MM development mainly through the production of WNTs. WNT4 was identified as the major molecule expressed in the CM and the principal nephrogenic inducer (Halt & Vainio, 2014), while WNT9b was also shown to be essential to induce CM differentiation (Carroll *et al*, 2005). WNT9b was identified as the primary UB-derived factor able to stimulate exit of CM from a stemness state. WNT9b is mainly expressed in the Wolffian duct and in the UB, and its expression is retained in collecting ducts until adulthood. In mice, Wnt9b expression induced the production of Wnt4, Fgf8, Pax8, and Lhx1, while these genes were not expressed in the CM of Wnt9b-deficient kidneys, thus resulting in the absence of nephron generation (Halt & Vainio, 2014). Similar to Wnt9b, Wnt4 depletion inhibits nephron differentiation, resulting in a vestigial kidney (Stark *et al*, 1994). The *WNT4* gene acts in the CM downstream of *WNT9b*, inducing LHX1 activation in pre-tubular aggregates, and subsequently promoting renal vesicle epithelialization and thus MET progression (Halt & Vainio, 2014). Several studies

have been performed to address the effects of WNT signalling in nephron maturation. In one study, TCF-reporter mouse lines revealed an activation of WNT/TCF pathway in embryonic kidney (Barolo, 2006). Moreover, WNT activation was observed only in the UB and not in the MM, and addition of βcatenin stabilizing small molecules or GSK3β inhibitors in the separated MM promoted the expression of the WNT/βcatenin/TCF feedback genes: Lef1, Tcf1, and Wnt4 (Kuure *et al*, 2007). Further, kidney specific βcatenin knock-out mice demonstrated a failure to induce CM development due to reduction in the expression of Fgf8, Pax8, Wnt4, and Lhx1, whereas ectopic expression of an active βcatenin form led to an ectopic CM induction and to a premature depletion of the renal stem cell pool (Halt & Vainio, 2014). In summary, βcatenin is sufficient to activate the nephron stem cell pool to promote nephron differentiation, via the the β-catenin/TCF/Lef pathway mediated up-regulation of Fgf8 and Wnt4. Additionally, *WNT4*-dependent MET induction does not proceed through canonical βcatenin signalling, indeed, forcing an aberrant βcatenin response in mice resulting in negatively regulation of the epithelialization process (Park *et al*, 2007). In this context, the WNT/Calcium/NFAT (nuclear factor of activated T cells) signalling was shown to function as a downstream effector of WNT4 in pre-tubular aggregates (Tanigawa *et al*, 2011). During MET initiation, early nephrons expressed the calcineurin-dependent NFAT factor, while the calcineurin inhibitor increased nephrogenesis. In addition, WNT4 also induced calcium influx together with the calcium/calmodulin-dependent protein kinase II phosphorylation in primary MM cells. This data indicated that WNT4 functions in the CM, at least in part through the Calcium/NFAT pathway. After MET establishment, nephrons need to growth in an oriented manner along their Y-axis. This complex architecture requires an oriented

cell division and coordinated motility, and WNT signalling has been shown to control these processes through the coordination of a planar cell polarity (PCP) pathway. De-regulation of WNT leads to pathophysiological changes and kidney cystic disease (Lancaster & Gleeson, 2010), thus it is reasonable to conclude that the WNT/PCP pathway plays an essential role after MET establishment. Given that the WNT/βcatenin pathway needs to be suppressed in order to initiate the WNT/PCP pathway and nephron elongation after MET establishment, mechanisms balancing this transition have been explored. MET failure and prolonged WNT/βcatenin activation was shown to provoke Wilms tumour and renal cysts formation (Qian *et al*, 2005). Inversin is a WNT signal regulator that was shown to reduce βcatenin levels by increasing proteasomal degradation of cytoplasmic dishevelled, moreover it was shown to promote βcatenin-independent WNT signal transduction (Simons *et al*, 2005). It has been speculated that inversin could signal through the primary cilium and that urine flow in early tubules can regulate the cellular response to WNT via the primary cilium (Simons *et al*, 2005). However, it appears that the WNT pathway signals through βcatenin, in a canonical way, until MET establishment. Subsequent nephron maturation requires a switch from the “canonical” to the “non-canonical” WNT pathway, which is essential for PCP-oriented cell division that needs βcatenin suppression.

In conclusion, WNT signalling is critical for kidney organogenesis and it plays an active role from early inductive stages to later steps of tubular epithelial maturation.

5.3 WNT signalling alterations in the kidney: cystic disease

Disorders associated with the development of cystic changes in the kidney are known as cystic kidney disease. Among these, polycystic kidney disease (PKD) is a genetic disorder caused by the progressive development of cysts in nephrons and collecting ducts, commonly leading to end-stage renal failure. PKD can be classified as two types: autosomal dominant PKD (ADPKD) and autosomal recessive PKD (ARPKD) (Harris & Torres, 2009). The genes responsible for ADPKD diseases are polycystic kidney disease gene 1 (*PKD1*) and polycystic kidney disease gene 2 (*PKD2*) encoding respectively for polycystin-1 and polycystin-2 (Harris & Torres, 2009). ARPKD is instead caused by mutations in the polycystic kidney and hepatic disease 1 (*PKHD1*) gene, which encodes the fibrocystin protein (FPC). In ADPKD, cysts arise slowly from any segment of the nephron and increase in number and dimension over time. However, other tissues are also affected by cysts formation, including liver and pancreas (Boletta & Germino, 2003). Conversely, ARPKD has an early and severe onset, and is associated with cyst development in kidneys and liver (Harris & Torres, 2009). The exact mechanism of how these proteins lead to PKD pathogenesis remains unclear, but recently many papers have been published evidencing new roles for such proteins. As an example, PC2 is a calcium-sensitive cation channel, and it can sense fluid flow in the renal epithelial cells (Nauli *et al*, 2003), whereas PC1 and FPC may function as PC2 modulators (Nauli *et al*, 2003). There are significant evidence linking canonical WNT signalling to cystic renal disease development. First, PC1 was shown to regulate the canonical WNT response. Indeed, the C-terminal PC1 region resulted in augment WNT/βcatenin signalling, and this was also observed in different types of cancer cells, like osteoblasts (Lancaster &

Gleeson, 2010; Zhang *et al*). These results were in contrast with more recent data revealing that the C-terminal part of PC1 is able to facilitate the nuclear accumulation of βcatenin, however transcription of the βcatenin downstream target genes was decreased. PC1 seems to inhibit WNT signalling by reducing the affinity between βcatenin and TCF (Lal *et al*, 2008). The inhibitory effects on canonical WNT signalling is also consistent with the observation that overexpression of c-Myc, a β-catenin/TCF-regulated oncogene, induces a renal cystic phenotype in transgenic mice, and it has been shown to be overexpressed in ADPKD and other renal diseases (Lal *et al*, 2008). Finally, this inhibitory effect was also observed with *PC2* deletion in kidney cells, but in this case it was not clear if it was due to a direct effect of *PC2* or through an indirect effect that *PC2* can have on *PC1* (Kim *et al*, 2009). Interestingly, it was observed that cysts arise in animal models of PKD with complete or partial loss of polycystin proteins (Lantinga-van Leeuwen *et al*, 2007), but also with their overexpression (Thivierge *et al*, 2006), leading to the concept that the kidney is particularly sensitive to gene dosage. Also alterations in the regulation of the WNT signalling pathway have been demonstrated to be involved in the pathogenesis of cystic renal disease. For example, conditional WNT mutant mice such as mice with βcatenin overexpression or APC inactivation (Qian *et al*, 2005) revealed that canonical WNT pathway over-activation leads to cystic renal phenotypes, further supporting a role for WNT/βcatenin signalling in cystogenesis. However, contradictory results indicate that canonical WNT loss-of-function mutants also display renal cysts (Lancaster & Gleeson, 2010). Again, this suggests that canonical WNT/βcatenin must be delicately balanced in the kidney.

5.3.1 A kidney injury model

The cystic diseases can have an early or a late onset. In the latter, patients do not exhibit symptoms until adulthood when the kidney is fully developed. Considering that cyst generation is strictly linked to the renal developmental stage, is possible that tubules pass through a "developing-like" state, thus re-activating some of the developmental programs. Injury has been proposed as a cause of resetting developmental programs. Indeed, in a predisposed subject, as a PKD patient, injury can be sufficient to trigger the rapid development of the cystic disease (Lancaster & Gleeson, 2010). The activation of WNT signalling during injury has already been confirmed (Lin *et al*, 2010), but the relevance of WNT pathway in such condition is still an open question (Fig. 9) .

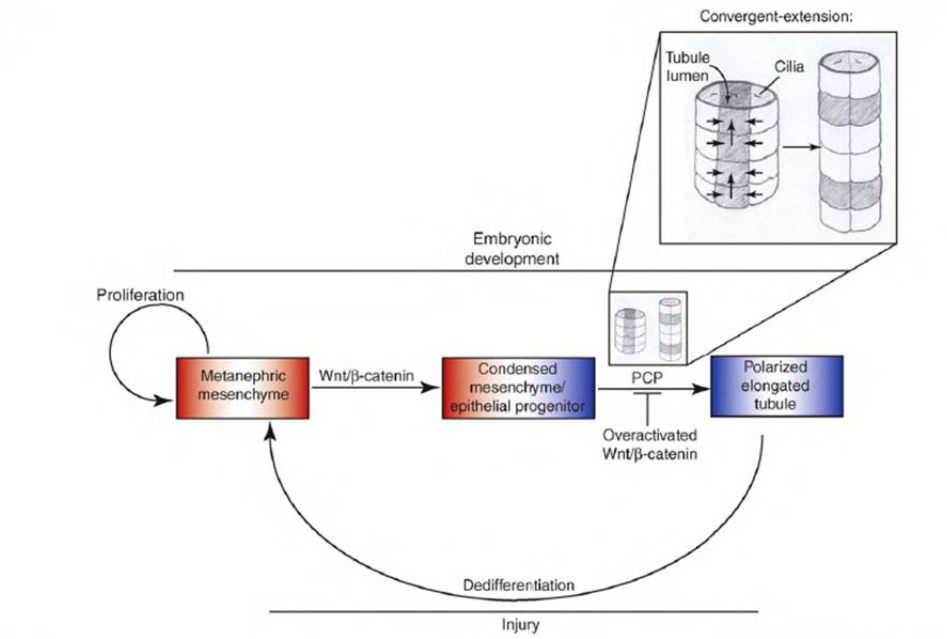

From Lancaster et al., Trends in Molecular Medicine 2010

Figure 9. Cyst formation during development and injury.

The developing kidney tubule epithelium forms from the differentiation of mesenchymal precursor cells. This process is triggered by canonical WNT signalling, which induces pretubular aggregates, a cluster of cells that are epithelial progenitors. Subsequently, canonical WNT signalling must be turned off and non-canonical WNT signalling takes over to form the epithelium

and the polarized tubule structure. When injury occurs, this process or a similar one is reactivated and both canonical and non-canonical WNT signalling are again required for new tubule formation. Cyst formation results from abnormalities in any of these cellular processes during development or injury repair.

5.4 WNT signalling alterations renal cancer

Aberrant regulation of WNT pathway has emerged as a frequent theme in cancer. Indeed, it was shown that the proviral insertion of the *Wnt1* gene into the mouse genome was leading to the development of mammary hyperplasia in mice (Nusse & Varmus, 1982). Hyperactive WNT-βcatenin signalling was also observed in colorectal cancer (Korinek *et al*, 1997). *APC* inactivating mutations are associated with familial adenomatous polyposis (FAP), which can progress to colorectal carcinomas (Korinek *et al*, 1997), and mutations in APC and βcatenin are also observed in colorectal cancers of non-FAP patients (Anastas & Moon, 2013). As previously discussed, proper βcatenin regulation is essential in the kidney. βcatenin activating mutations are common events in Wilms tumour (Koesters *et al*, 1999), and mice with *Apc* gene inactivation in the kidney are prone to the development of Renal Cell Carcinoma (Sansom *et al*, 2005). Finally, mutations or alterations in the regulation of βcatenin have been identified in RCC patients (Kim *et al*, 2000). These data suggest that the activation of the βcatenin signalling pathway, which has been associated with several cancerous conditions (Anastas & Moon, 2013), may also play a role in RCC development.

AIM OF THE THESIS

The aim of my PhD project was to identify molecular mechanisms/pathways that can be altered during overexpression/overactivation of the *TFE* transcription factors, which can drive carcinogenesis, and ideally to identify novel druggable targets. To answer this question, we had to generate an experimental animal system able to recapitulate the disease observed in *TFE*-fusion RCC patients.

The specific aims of my PhD were:

- ***To generate renal specific Tcfeb (murine Tfeb gene) overexpressing mouse lines.***

  We generated both a constitutive and a tamoxifen-inducible kidney-specific Tcfeb-overexpressing mouse line by crossing conditionally *Tcfeb* overexpressing mice with both a constitutive and an inducible *KSPcdh16-CRE* (kidney-specific Cadherin16 CRE) mouse line. These mice developed both cystic and cancerous renal pathologies.

- ***To evaluate if the transgenic mouse lines recapitulated the pathology observed in TFEB-fusion RCC patients.***

  Extensive histological analyses were performed to fully characterize both the cystic and cancerous renal phenotypes observed in the animal models to understand if these models resembled the human disease.

- ***To identify altered molecular pathways.***

  Microarray analysis was performed on newborn transgenic mice to identify altered molecular pathways, which were subsequently validated by quantitative real-time PCR. Biochemical and *in-vitro* assays were

performed to demonstrate the relevance of the WNT pathway, which was found altered in the transcriptional analyses. Finally, *Tcfeb*-overexpressing mice were treated with a drug that inhibits the WNT pathway to understand the relevance of this pathway in renal cystic and cancerous disease development. Importantly, a significant regression of both diseases was demonstrated in the presence of WNT signalling inhibition.

MATERIALS AND METHODS

Mouse models:

CondTg-Tcfeb transgenic mice (generated by Dr. Settembre (Settembre *et al*, 2011)) were crossed with *KSPcdh16-CRE* (Jackson laboratories) and *indKSPcdh16-CRE* (generated by Dr. Peters (Lantinga-van Leeuwen *et al*, 2006)) mice to obtain *KSPcdh16/Tcfeb* and *indKSPcdh16/Tcfeb* mice. The *ATG7* conditional KO mice (Komatsu *et al*, 2005) (*ATG7* fl/fl mice) were a generous gift from T.Eissa. Mice were crossed with *KSPcdh16-CRE* and *CondTg-Tcfeb* mice to obtain kidney-specific ATG7 deletion and Tcfeb overexpression (*ATG7-/-;KSPcdh16/Tcfeb)*. All mice were mated starting from 8 weeks and were maintained in a C57BL/6 background genotype. To genotype all the mouse lines, tails were cut and lysed in 500µl lysis Buffer (50mM TrisHCl pH 8, 100mM EDTA, 100 mM NaCl, SDS 1%), supplemented with 20µl proteinase K (20mg/ml) at 55°C O/N. After removal of cellular debris (5 min centrifugation at maximum speed), DNA was precipitated by adding 1 ml of 100% ethanol (EtOH) to each tube and gently mixed by inverting the tubes. Subsequently, DNA was washed once with 70% EtOH air-dried and resuspended in 500µl H_2O. Mice were genotyped by PCR on the tail DNAs using specific primers:

KSPcdh16-CRE-forward: 5'-GCA GAT CTG GCT CTC CAA AG-3'

KSPcdh16-CRE-revers: 5'-AGG CAA ATT TTG GTG TAC GG-3'

cotrolKSPcdh16-CRE-forward: 5'-CAA ATG TTG CTT GTC TGG TG-3'

controlKSPcdh16-CRE-revers: 5'-GTC AGT CGA GTG CAC AGT TT-3'

indKSPcdh16-CRE-forward: 5'-CATTCTCTCCCACTGAATGGA-*3'*

indKSPcdh16-CRE-revers-1: 5'-ACAGAGTGGGGTTTGTGTCTG-*3'*

*indKSPcdh16-CRE-revers-2: 5'-*AACTGTCCCCTTGTCATACCC*-3'*

CondTg-Tcfeb-forward: 5'-TGAGAGAAGACGCAGGTTCA-3'

CondTg-Tcfeb-revers: 5'-AATCACCGTCATGGTCTTTG-3'

ATG7fl/fl-forward: 5'-TGGCTGCTACTTCTGCAATGATGT-3'

ATG7fl/fl-revers: 5'- CAGGACAGAGACCATCAGCTCCAC-3'

PCR conditions using the LA Taq mixture (Takara Bio Inc, Japan) were:

- for *KSPcdh16-CRE genotype:*
    1. 94°C 3 min;
    2. 94°C 30 sec/65°C 1 min/72°C 1 min for 33 cycles;
    3. 72°C 3 min (final extension).

- *for indKSPcdh16-CRE* genotype:
    1. 95°C 3 min;
    2. 95°C 30 sec/59°C 30 sec/72°C 1 min for 35 cycles;
    3. 72°C 3 min (final extension).

- for *CondTg-Tcfeb genotype:*
    1. 95°C 3 min;
    2. 95°C 30 sec/61°C 30 sec/72°C 30 sec for 30 cycles;
    3. 72°C 3 min (final extension).

- for ATG7-flox/flox genotype:
    1. 95°C 3 min;
    2. 98°C 30 sec/62°C 30 sec/72°C 1 min for 30 cycles;
    3. 72°C 7 min (final extension).

PCR products of the different PCRs are showed in figure 10.

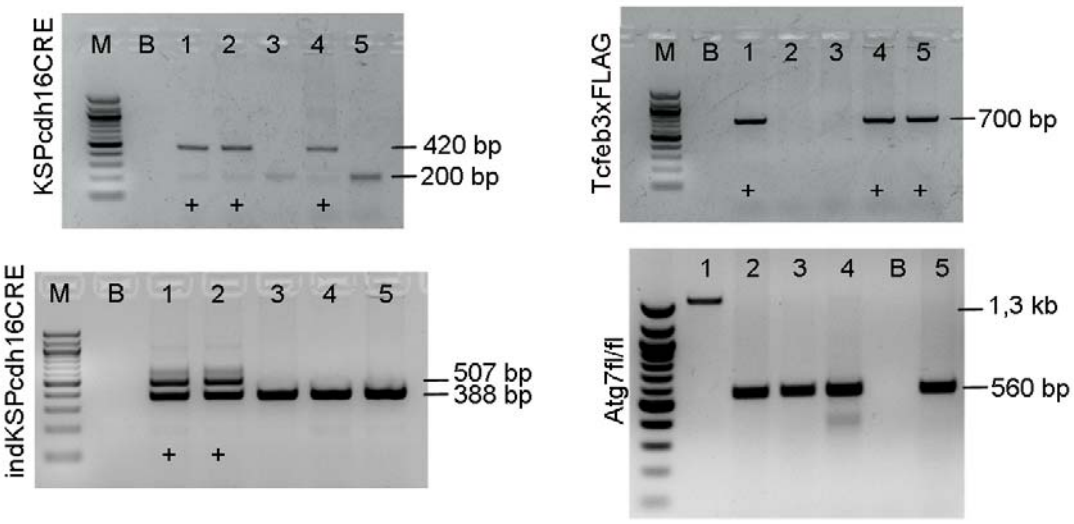

Figure 10. Genotypes of representative litters.

Representative genotypes of *KSPcdh16CRE*, *indKSPcdh16CRE*, *Tcfeb3xFLAG* and *ATG7fl/fl* mice. In the *KSPcdh16CRE* PCR, lanes 1, 2 and 4 show *KSPcdh16*$^{+/-}$ animals (420 bp *CRE* band, 200 bp *wild-type* band) . In the *indKSPcdh16CRE* PCR, lanes 1 and 2 indicate *indKSPcdh16CRE*$^{+/-}$ mice (507 bp *CRE* band, 388 bp *wild-typet* band) . In the *Tcfeb-3xFLAG* PCR, lanes 1, 4 and 5 represent *Tcfeb-3xFLAG*$^{+/-}$ positive mice (700 bp band). In the ATG7fl/fl PCR lane 1 indicate a wild-type animal (1,3kb wild type band), lane 2,3 and 5 are ATF7fl/fl animals (560 bp ATG7^{flox} band), lane 4 is an ATG7flox/+ mouse (1.3 kb wild-type band, 560 bp ATG7^{flox} band) (M, marker; B, Blank).

For the tamoxifen injections, *IndKSPcdh16*$^{+/-}$*;wt and indKSPcdh16*$^{+/-}$*;tgTcfeb*$^{+/-}$ mice were weighted first, and then injected Intra-Peritoneally (IP) with tamoxifen at a dosage of 100 micrograms/gram of mouse weight for three consecutive days to obtain an efficient recombination.

Experiments were conducted in accordance with the guidelines of the Animal Care and Use Committee of Cardarelli Hospital in Naples and authorized by the Italian Ministry of Health.

Tissue collection

For all the tissue collection procedures, age-matched mice were weighted and then anesthetised with an IP injection of avertin at 2ml/100 gr. To collect kidney and liver samples, animals were perfused with PBS, pH 7,4, to completely clear blood from tissues. Pictures from kidneys and livers were taken. Both kidneys were weighted and then divided in two halves, one half from each kidney was frozen in dry ice and stored at -80ºC for molecular analyses, and the other ones were fixed in 4% paraformaldehyde (for immuno-staining). Regarding liver samples, a small piece was fixed in 4% paraformaldehyde and the remaining part was cut in small pieces and frozen in dry ice.

Biochemical analysis:

Blood samples were collected from the retro-orbital vein in heparinized tubes, and then centrifuged at 10,000 g for 10 min at 4ºC to obtain the plasma. Plasma was harvested and stored frozen until use. Plasma urea was measured using standardized clinical diagnostic protocols of the Academical Medical Center Amsterdam. Albumin (Bethyl Laboratories, Montgomery, TX) was measured in urines collected for 24h in metabolic cages and analysed in the Academical Medical Center with standardized procedures. The biochemical measurements were performed by Lotte Kors in the Academical Medical Center in Amsterdam.

High Frequency Ultrasound and PET/CT scan analyses.

All the imaging procedures were performed at the CEINGE institute in Naples, Italy, by Luigi Auletta. Mice were under general anesthesia. Anesthesia was

produced in an induction chamber, saturated with 5% isoflurane (Iso-Vet 1000 mg/g Inhalation Vapor, Piramal Healthcare UK Ltd., Northumberland, UK) in oxygen (2 L/min) and subsequently maintained during all procedures with a conenose delivering isoflurane at 1.5% in oxygen at 2 L/min.

For High Frequency Ultrasound, each mouse was placed in dorsal recumbency on a dedicated, heated, small animal table (VEVO Imaging Station 2, FUJIFILM VisualSonics, Inc., Toronto, Ontario, Canada) and hairs were removed with a small clipper and then with the application of a depilatory cream, and a pre-warmed ultrasound-coupling gel was applied to the skin to improve ultrasound transmission and reduce contact artefacts. A 40 MHz transducer (MS 550 D, FUJIFILM VisualSonics, Inc., Toronto, Ontario, Canada) was mounted on the dedicated stand of the imaging station, and B-mode and Color-Doppler mode images were obtained on the ultrasound equipment (VEVO 2100, FUJIFILM VisualSonics, Inc., Toronto, Ontario, Canada).

Positron emission tomography (PET) coupled with computed tomography (CT) was performed with a dedicated small animals PET/CT scanner (eXplore Vista, GE Healthcare), with a trans-axial field of view of 6.7 cm and an axial field of view of 4.8 cm. Animals, fasted overnight, were injected under general anesthesia in the lateral caudal vein with 300 μCi of [^{18}F]-fluorodeoxyglucose (FDG). Mice were left to recover from anesthesia under a heating lamp and PET/CT acquisitions were started after 90 minutes of biodistribution. Static emission scans of 30 minutes with energy window of 250–700 keV were acquired. The PET datasets were reconstructed by 2D FORE/3D OSEM algorithm and corrected for random coincidences, scatter, physical decay to the time of injection (voxel size: 0.3875 × 0.3875 × 0.775 mm^3). The mean specific uptake value (SUV) was

obtained for each region of interest using the visualization and analysis software of the scanner (version 4.11 Build 701, MMWKS Image Software: Laboratorio de Imagen, HGUGM, Madrid, Spain).

Survival analysis:

Survival curves were calculated for a period of 8 months on a total of 15 *KSPcdh16/Tcfeb* mice, 10 *indKSPcdh16/Tcfeb* mice (Tam P12), 12 *indKSPcdh16/Tcfeb* mice (Tam P14) and 12 *indKSPcdh16/Tcfeb* mice (Tam P30) grown in the same animal facility, all in same background (C57BL/6). Values were plotted by the product-limit method of Kaplan and Meier; statistical analyses were carried out applying the Log Rank (Mantel-Cox) test.

Cell culture, transfections and plasmids:

Primary kidney cells were obtained from P30 *KSPcdh16*$^{+/-}$*;wt* and *KSPcdh16*$^{+/-}$*;tgTcfeb*$^{+/-}$ mice. Animals were first anesthetised as already described, and then sacrificed by cervical dislocation. Primary kidney cells were derived following the protocol described in Leemans *et al.* (Leemans *et al*, 2005). Kidneys were collected, uncapsulated and washed shortly in ethanol 70% and then PBS to prevent contaminations. Tissue from the outer cortex and inner medulla was cut into approximately 1mm^3 pieces, washed in pre-warmed PBS and centrifuged at 1200 rpm for three minutes. Kidney pieces were subsequently digested by 1mg/ml collagenase type 1A (Sigma-Aldrich) at 37°C for one hour and then filtered in 40µm filters. Finally the cell suspension was washed with PBS, and spinned at 1500 rpm for five minutes twice. Primary tubular epithelial cells (TECs) were grown to confluence in DMEM-F12 culture medium supplemented with 10% FCS, 100IU/ml penicillin, 100mg/ml streptomycin, 2mM L-glutamine (Gibco; Invitrogen

Corp.), 1% ITSe (Thermo-Fisher) and 1% S1 hormone mixture (Sigma-Aldrich) and were cultured in 5% CO_2 at 37 degrees. TECs were identified by characteristic cobblestone-shaped morphology.

HEK293 and HK2 cells were purchased from ATCC. HEK293 cells were cultured in DMEM (Euroclone) supplemented with 10% FBS, 100IU/ml penicillin, 100mg/ml streptomycin and 2mM L-glutamine (Gibco; Invitrogen Corp.). HK2 cells were grown in DMEM-F12 (Invitrogen) supplemented with 5% FBS, 100IU/ml penicillin, 100mg/ml streptomycin, 2mM L-glutamine (Gibco; Invitrogen Corp.) and 1% ITSe. Cells were grown at 5% CO_2 at 37 degrees.

Human full-length TFEB-FLAG was previously described (Settembre *et al*, 2011). The TopFlash and FopFlash plasmids (Upstate), the pCS2+MT-Myc-tagged β-CATENIN (full-length β-CATENIN), and the Evr2-Tcf1E plasmid (Tcf1E) were kindly provided by Dr. M. Plateroti.

Cells were transfected with Lipofectamine LTX and Plus reagent (Invitrogen) following the manufacturer's protocol. Luciferase activity was measured 48h post-transfection using the Dual-Luciferase Reporter Assay System (Promega). To normalize transfection efficiency in reporter assays, the HEK293 and HK2 cells were co-transfected with a plasmid carrying the internal control reporter *Renilla reniformis* luciferase driven by a TK promoter (pRL-TK; Promega). Data are representative of three independent experiments and statistical significance was determined using Student's *t*-test. $P<0.05$ was considered as significant.

In-vitro drug treatments and MTT proliferation assay:

Cultured primary kidney cells derived from the cortex and medulla of *KSPcdh16/wt* and *KSPcdh16/Tcfeb* mice were seeded in 96-well plates at the density of $5x10^3$cells/well, maintained overnight at 37°C, and incubated in the presence of

the test compounds at the different concentrations. PKF118-310 and CGP049090 were added at different dosages (0μm, 0.2μm, 0.4μm, 0.8μm, 1.6μm, 3.2μm) for 24 hours. 0μm represents the basal proliferation of cells after 48 hours of plating. MTT assay was used to assess cell proliferation. This assay is based on the protocol initially described by Mossmann (1983) and subsequently optimized for the cell lines used in these experiments. Briefly, 5mg of MTT powder was solubilized in 1mL of PBS and filtered. 10μL of this solution was added to 100μl of cell culture medium without phenol red. At the end of the incubation time, cells were washed twice with PBS and incubated with MTT-media solution to form formazan crystals. After four hours, media was removed and 100μl/well of a solubilisation solution was added to the cells (2.1mL HCl 10N, 500mL isopropanol) for four hours at 37°C to obtain a complete solubilisation of the crystals. As a readout, absorbance of the 96-well plate was measured recording the Optical Density (OD) at 570nm with a microplate spectrophotometer system. Results are representative of three independent experiments performed on three different *KSPcdh16/wt* and *KSPcdh16/Tcfeb* mice. *T*-test is referred to cells without drug (0μm) taken from *KSPcdh16/Tcfeb* mice versus cells without drug (0μm) taken from *KSPcdh16/wt* mice. Data are representative of three independent experiments and statistical significance was determined using Student's *t*-test. $P<0.05$ was considered as significant.

In vivo drug treatments:

P21 *KSPcdh16/wt* and *KSPcdh16/Tcfeb* mice were intraperitoneally injected daily, from Monday to Friday, with the PKF118-310 drug at the dose of 0.85mg/kg or with an equal amount of vehicle (DMSO). Mice were weighted every day from Monday to Friday. After 30 days from the beginning of the treatment, animals were

sacrificed and kidneys were collected, weighted and processed for further analyses. Six animals for each group and genotype were collected.

Quantitative real-time PCR:

Total RNA was isolated from frozen samples by adding 1ml of Trizol solution (Life Technologies) per piece, and lysed using a TissueLyser (Qiagen). After that, 200μl of chloroform were added, tubes were shacked for 15 seconds and centrifuged to obtain three phases, a lower red phase, an interphase, and a colorless upper aqueous phase containing the RNA. The aqueous phase was collected and 500μl of isopropanol were added to ensure RNA precipitation. After ten minutes, samples were centrifuged, the supernatants were removed and RNA pellets were washed with ethanol 75%, centrifuged, and then air-dried and resuspended in 30-50μl of RNase-free water. After complete RNA resuspension, 1μg of the RNA solution was reverse transcribed to single-stranded cDNA by using QuantiTect Rev Transcription Kit (Qiagen) in a final reaction volume of 20μl. cDNA mixes were diluted 1:3 in water, and 2μl of the diluted cDNA solution was analysed by Real-Time PCR. Real-time PCR was performed using SYBR Green (Roche Diagnostics) and performing the reaction in the LightCycler® System 2.0 (Roche Applied Science). The parameters of Real-time PCR amplification were defined according to Roche recommendations. To quantify gene expression, Gapdh mRNA expression was used as an internal reference. All the values are shown as fold activation respect to w-type levels. Data are representative of three independent experiments and statistical significance was determined using Student's *t*-test. $P<0.05$ was considered as significant.

The following primers were used in this study: Gapdh; forward (fw) tgcaccaccaactgcttagc, reverse (rev) tcttctgggtggcagtgatg; Tcfeb; fw gcagaagaaagacaatcacaa, rev gccttggggatcagcatt; Ccnd1; fw ccttgactgccgagaagttgtg, rev gttccacttgagcttgttcacca; Axin2; fw gatgcatcgcagtgtgaagg, rev ggttccacaggcgtcatctc; c-Myc; fw ccagcagcgactctgaagaa, rev acctcttggcaggggtttg; Fzd3; fw gcatctgggagacaacatgg, rev caggtctggacgactcatctg; Rnf146; fw agcggaggagaaaagactgc, rev acatagccctttctcggtccg; Kdm6a; fw tgacagcggaggagagggag, rev ccttcatcctggcgccatct; Cdkn1a; fw gtctgagcggcctgaagatt, rev caatctgcgcttggagtgat; HbEgf; fw tccacaaaccagctgctacc, rev ccttgtggcttggaggagaa; Pak1; fw ttcctgaaccgctgtcttga, rev tcaggctagagaggggcttg; Areg; fw tattggcatcggcatcgtta, rev tgcacagtcccgttttcttg; Crk; fw cgcgtctcccactacatcat, rev tctcctattcggagcctgga; Tgfa; fw agtgcccagattcccacact, rev cgtacccagagtggcagaca; Gpnmb, fw tggctacttcagagccacca, rev ggcatggggacatctgctat.

Microarray hybridization:

Microarray analysis was performed in collaboration with the Coriell Genotyping and Microarray Center, in Camden, New Jersey. Total RNA (3µg) was reverse transcribed to single-stranded cDNA with a special oligo (dT) 24 primer containing a T7 RNA promoter site, added 3' to the poly-T tract, prior to second strand synthesis (One Cycle cDNA Synthesis Kit by Affymetrix, Fremont, CA, USA). Biotinylated cRNAs were then generated, using the GeneChip IVT Labeling Kit (Affymetrix). 20µg of biotinylated cRNA was fragmented and 10µg hybridized to the Affymetrix GeneChip Mouse 430A_2 microarrays for 16 hours at 45°C using an Affymetrix GeneChip Fluidics Station 450 according to the manufacturer's standard protocols.

For the analysis at P0, the total RNA was extracted from the kidney of three *KSPcdh16/Tcfeb* mice and of two control *KSPcdh16/wt* mice. For the analysis at P14 total RNA was extracted from the kidney of three *KSPcdh16/Tcfeb* P14 mice and three control *KSPcdh16/wt P14* mice.

Microarray data processing:

Microarray data processing were performed by Rossella De Cegli in Tigem, Naples, Italy. The data discussed in this publication have been deposited in NCBIs Gene Expression Omnibus (GEO) (Edgar *et al*, 2002) and are accessible through GEO Series accession number GSE62977 (KSP_P0 dataset) and GSE63376 (KSP_P14 dataset). Low-level analysis to convert probe level data to gene level expression was performed using Robust Multiarray Average (RMA) implemented using the RMA function of the Bioconductor project (Gentleman *et al*, 2004).

Statistical analysis of differential gene expression:

For each gene, a Bayesian t-test (Cyber-t) (Baldi & Long, 2001) was used on RNA normalized data to determine if there was a significant difference in expression between *KSPcdh16/Tcfeb* mice versus *KSPcdh16/wt* mice both at P0 (GSE62977-KSP_P0 dataset) and at P14 (GSE63376-KSP_P14 dataset). P-value adjustment for multiple comparisons was done with the False Discovery Rate (FDR) of Benjamini-Hochberg (Klipper-Aurbach *et al*, 1995). The threshold for statistical significance chosen was FDR≤0.05. In the KSP_P0 dataset we selected 361 probe-sets corresponding to 294 significantly induced genes (GSE62977). In the KSP_P14 dataset we selected 729 probe-set corresponding to 628 genes (GSE63376).

(Immuno-) histological analysis:

All the tissues were embedded in paraffin. Immediately after dissection, tissues were stored O/N in 4% paraformaldehyde and then they underwent to an ascending scale of alcohols for complete dehydration. They were kept one hour in ethanol 70%, one hour in ethanol 80%, one hour in ethanol 95%, one hour in ethanol 100% and O/N in a second wash of ethanol 100%. The day after they underwent to two washes of 1 hour each of Xylene, three washes of paraffin and then they were included. For all the staining and immunohistochemistry procedures, 4μm tissue sections were first de-paraffinized with a descending scale of alcohols, and then they were analysed using standard hematoxylin and eosin (HE) staining, periodic acid Schiff (PAS) staining, Sirius Red (SR) staining, or immunohistochemistry. Some of these stainings were performed in collaboration with Prof. Dorien Peters at the Leiden University Medical Center in Netherlands, as specified in the figure legends. For the HE staining, tissue sections were stained with haematoxylin for two minutes, then rinsed in running tap water, rapidly dipped 8-10 times in acid ethanol (1% HCl in 70% ethanol) to allow de-staining, rinsed in running tap water, and then in deionized water, finally stained in eosin for five minutes, dehydrated and mounted with Eukitt. For the PAS-D procedure, tissue sections were brought to distilled water, and then digested 30 minutes with 0,25% diastase (alpha-amylase). After that sections were washed with RX water and stained following the standardized protocol (BIOPTIKA), dehydrated and mounted with Eukitt. For staining with Sirius Red de-paraffinized sections were incubated in 0.2% phosphomolybdic acid hydrate for five minutes and 0.1% Sirius red for 90 minutes. Subsequently sections were incubated for one minute in saturated picric acid and then placed in 70% ethanol, dehydrated and mounted with Eukitt. For immunohistochemistry procedures, sections were subjected to

heat mediated antigen retrieval procedure (10mM citrate buffer pH 6.0) followed by 1hr preincubation with normal goat serum (1:200; DakoCytomation, Glostrup, Denmark). After blocking of endogenous peroxidase activity for 15 minutes in 0.1% H_2O_2 in water, sections were incubated with primary antibodies diluted in 1% BSA in PBS. Then sections were washed three times in PBS, and incubated for 30 minutes with the secondary antibody. Immune reactions were revealed using NovaRed or diaminobenzidine chromogen and counterstained with haematoxylin diluted 1:10 in RX water. Sections were washed five minutes in running tap water, dehydrated, and mounted with Eukitt.

Primary antibodies: rabbit polyclonal anti-megalin (1:750, Pathology LUMC, Leiden, the Netherlands), goat polyclonal anti-uromodulin (1:4000, Organon Teknika-Cappel, Turnhout, Belgium), rabbit polyclonal anti-aquaporin-2 (1:4000 Calbiochem, Amsterdam, The Netherlands), rabbit polyclonal anti-βcatenin (1:500, Santa Cruz sc-7199), rabbit monoclonal anti-active-βcatenin (1:800, Cell Signaling #8814), rabbit polyclonal anti-cadherin16 (1:300, Novus NBP1-59248), rabbit polyclonal anti-ATG7 (1:300, Santa Cruz sc-33211), rabbit monoclonal anti-Ki67 (ABCAM ab16667, clone SP6, 1:200), a rabbit polyclonal anti-PAX8 antibody (Proteintech, 10336-1-AP, 1:1000) and a mouse monoclonal anti-Cytokeratin 7 (Abcam, ab9021, 1:500). Secondary antibodies: anti-rabbit envision HRP (DakoCytomation, Glostrup, Denmark), rabbit-anti-goat HRP (1:100), power rabbit poly-HRP (Biocare Medical, M4U534L).

Quantitative histology:

Histomorphometric analysis was conducted on PAS and Ki67-stained sections and were performed in collaboration with Dr. Giovanni Bertalot at the European Institute of Oncology (IEO), Milan, Italy. For the cyst characterization, cyst number

and area was calculated on PAS sections from three animals per genotype and group. Cysts were hand-annotated and measured in the outer and inner cortex, and the outer and inner medulla. Finally, they were sub-divided according to their size. For the analyses performed on the drug- and vehicle-treated animals, the analysis was conducted on Ki67-stained sections. The number and size of the cysts were defined within the areas identified by the pathologist using ImageScope (Leica-Biosystems Nussloch GmbH). Using the same method, the number of papillae was counted and the proportion of Ki67 positive nuclei on the total number of nuclei within the papillae was calculated. For these analyses, a total of six *KSPcdh16/Tcfeb* vehicle (DMSO)-treated and six *KSPcdh16/Tcfeb* drug (PKF118-310)-treated animals were evaluated.

Antibodies and Western blotting:

Cells or tissues were lysed in ice-cold lysis buffer (50mM Tris at pH 7.9, 1% Triton X-100, 0,1% Tween 20, 150mM NaCl, 5mMMgCl2, 10% glycerol) containing phosphatase (Roche) and protease (Sigma) inhibitors. Tissue pieces were disrupted using a TissueLyser (Qiagen) whereas cells were collected by scraping the plates. Samples were lysed in lysis buffer for 1 hour in ice and then centrifuged at 14000 rpm for 15 minutes at 4°C to eliminate cells debris. Protein concentration was measured by using colorimetric Bradford method (Bio-rad). Samples were mixed with Laemmli lysis buffer containing β-mercaptoethanol, boiled and resolved by SDS-PAGE. Electrophoresis was run at 80V constant. Thereafter, proteins were blotted onto polyvinylidene fluoride (PVDF) membranes and blocked for 1 hour with non-fat 5% milk or 5% BSA diluted in 1X TBS, 0,1% Tween 20, according to the primary antibody protocol. Membranes were incubated with primary antibodies overnight at 4°C. The next day membranes were washed three

times in TBS/0,1%, Tween 20 and incubated with corresponding HRP-labelled secondary antibodies (Calbiochem). Finally, protein visualisation was performed using the enhanced chemiluminescence (ECL) (Perkin Elmer, Waltham, MA, USA). Membranes were developed using a Chemidoc UVP imaging system (Ultra-Violet Products Ltd) and densitometric quantification was performed in unsaturated images using ImageJ (NIH).

For Western blots, the following antibodies were used: anti-FLAG M2-HRP (Sigma, cat. A8592, 1:1000), anti-actin (Sigma, cat. A2066, 1:5000), anti-βtubulin (Sigma, cat. T8328, 1:1000), anti-Human/Mouse/Rat Pan-Akt (R&D, cat. MAB2055, 1:500), Phospho-Akt (Ser473) (D9E) (Cell Signaling, cat. #4060, 1:1000), anti-human, mouse, and rat ERK1/ERK2 (R&D, cat.216703, 1:2000), anti-Human/Mouse/Rat Phospho- ERK1(T202/Y204)/ERK2 (T185/Y187) (R&D, cat. AF1018, 1:1000), anti-βcatenin (BD, cat. 610154, 1:500), anti-non phospho active βcatenin (Cell Signaling, cat. #8814, 1:1000), anti-Cyclin D1 (Cell Signaling, cat. # 2978, 1:1000), anti-LRP6 (Cell Signaling, cat. #3395, 1:1000), anti-phospho-LRP6 (Ser1490) (Cell Signaling, cat. #2568, 1:1000), anti-GSK3β (Cell Signaling, cat. #9315, 1:1000), anti-phospho-GSK3β (Ser9) (Cell Signaling, cat. #9323, 1:1000).

Statistical Analysis:

GraphPad Prism (GraphPad Software, San Diego, CA) was used for all statistical analysis. Statistical analyses of data were performed using Student's t-test. One-way ANOVA and Tukey's post-hoc tests were performed when comparing more than two groups relative to a single factor (time or treatment/genotype). Two-way and three-way ANOVA and Tukey's post-hoc tests were performed when

comparing more than two groups relative to two or more factors. Mantel-Cox test was used for the survival analysis. $P<0.05$ was considered significant.

RESULTS

1. Generation of the transgenic mouse lines

To study the mechanisms underlying tumour development in *TFEB*-fusion *RCC,* we generated transgenic mouse lines that specifically overexpress *TFEB* in the kidney. We crossed a previously generated *Tcfeb* conditional overexpressing mouse line that carries *Tcfeb-3xFlag* under the control of a strong chicken beta-actin (CAG) promoter (Settembre *et al*, 2011), herein referred to as *CondTg-Tcfeb,* with the *KSPcdh16-CRE* mouse line, in which the *CRE* recombinase is specifically expressed in renal tubular epithelial cells starting from embryonic stage E12.5 (Shao, 2002). In addition, to assess the effects of *Tcfeb* overexpression during kidney development, we generated a second transgenic line by crossing the *CondTg-Tcfeb* mice with a mouse line that carries a tamoxifen-inducible *CRE-ER*^{T2} element under the control of a *KSPcdh16* promoter (*Ind*KSPcdh16CRE promoter) (Lantinga-van Leeuwen *et al*, 2006) (Fig. 11).

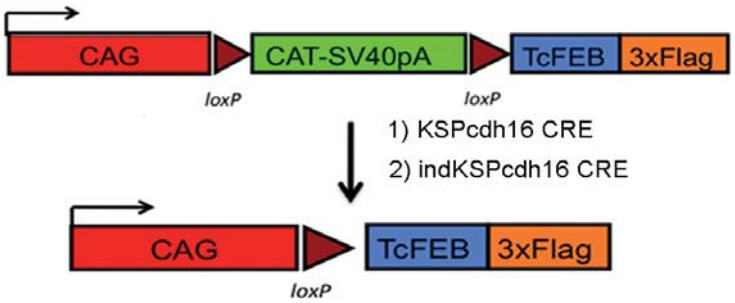

Figure 11. Map of the generation of the transgenic mouse lines with kidney-specific *Tcfeb* overexpression.

Map of the transgene: Tcfeb-3XFLAG was inserted after the chicken actin promoter (CAG) and the chloramphenicol acetyltransferase (CAT)-SV40pA flanked by loxP sites. The latter can be removed by CRE recombinase, resulting in the overexpression of the *Tcfeb* gene under the control of the

strong CAG promoter. Two different CRE lines were used: 1) a constitutive kidney-specific KSPcdh16 (Cadherin 16) CRE and 2) a tamoxifen-inducible indKSPcdh16.

KSPcdh16$^{+/-}$*/CondTg-Tcfeb*$^{+/-}$ and *indKSPcdh16*$^{+/-}$*/CondTg-Tcfeb*$^{+/-}$ double heterozygous mice, henceforth referred to as *KSPcdh16/Tcfeb* and *IndKSPcdh16/Tcfeb* mice, respectively, were generated from these crossings. We checked both the constitutive and inducible lines for renal *Tcfeb* overexpression and confirmed that *Tcfeb* mRNA levels were progressively increased over time (Fig. 12A). Consistently, immunoblot experiments revealed increased levels of Tcfeb-3xflag protein in kidneys from *KSPcdh16/Tcfeb* and *IndKSPcdh16/Tcfeb* mice (Fig. 12B).

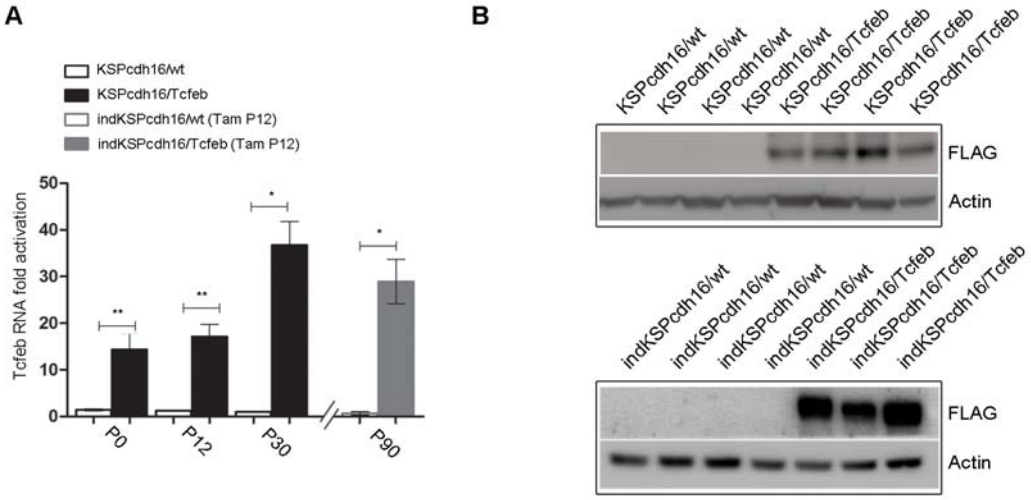

Figure 12. Assessment of Tcfeb overexpression in the transgenic mouse lines.

A) Real-time PCR analysis of *Tcfeb*-3xFLAG mRNA levels performed on *KSPcdh16/wt* and *KSPcdh16/Tcfeb* mice at different stages (P0, P12, P30) and on *indKSPcdh16/wt* and *indKSPcdh16/Tcfeb* mice induced with tamoxifen at P12 and sacrificed at P90. Values are shown as the average (± SEM) of three animals per time point and genotype (* P <0 .05, ** P < 0.01, two-sided, Student's t test). B) Immunoblot analysis using an anti-Flag antibody to determine the

expression of Tcfeb-3xFLAG protein in *KSPcdh16/Tcfeb* and Tam-treated *indKSPcdh16/Tcfeb* mice.

2. Progressive cystic pathology in transgenic mouse lines

At sacrifice, kidneys from adult KSPcdh16/*Tcfeb* and tamoxifen-treated *IndKSPcdh16/Tcfeb* mice completely filled the abdominal cavity (Fig. 13).

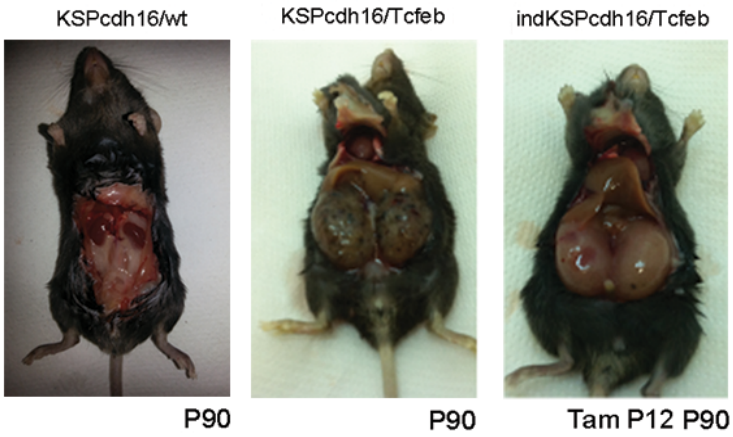

Figure 13. Renal Tcfeb overexpression results in a severe kidney enlargement.

Representative images of the abdominal cavity of *KSPcdh16/wt, KSPcdh16/Tcfeb* and Tam-treated *indKSPcdh16/Tcfeb* mice at P90.

KSPcdh16/*Tcfeb* mice started to enlarge at P12, but a sensible increase in size and Kidney to Body Weight (KW/BW) ratio was observable at P30 (Fig. 14A, B) and continued over time.

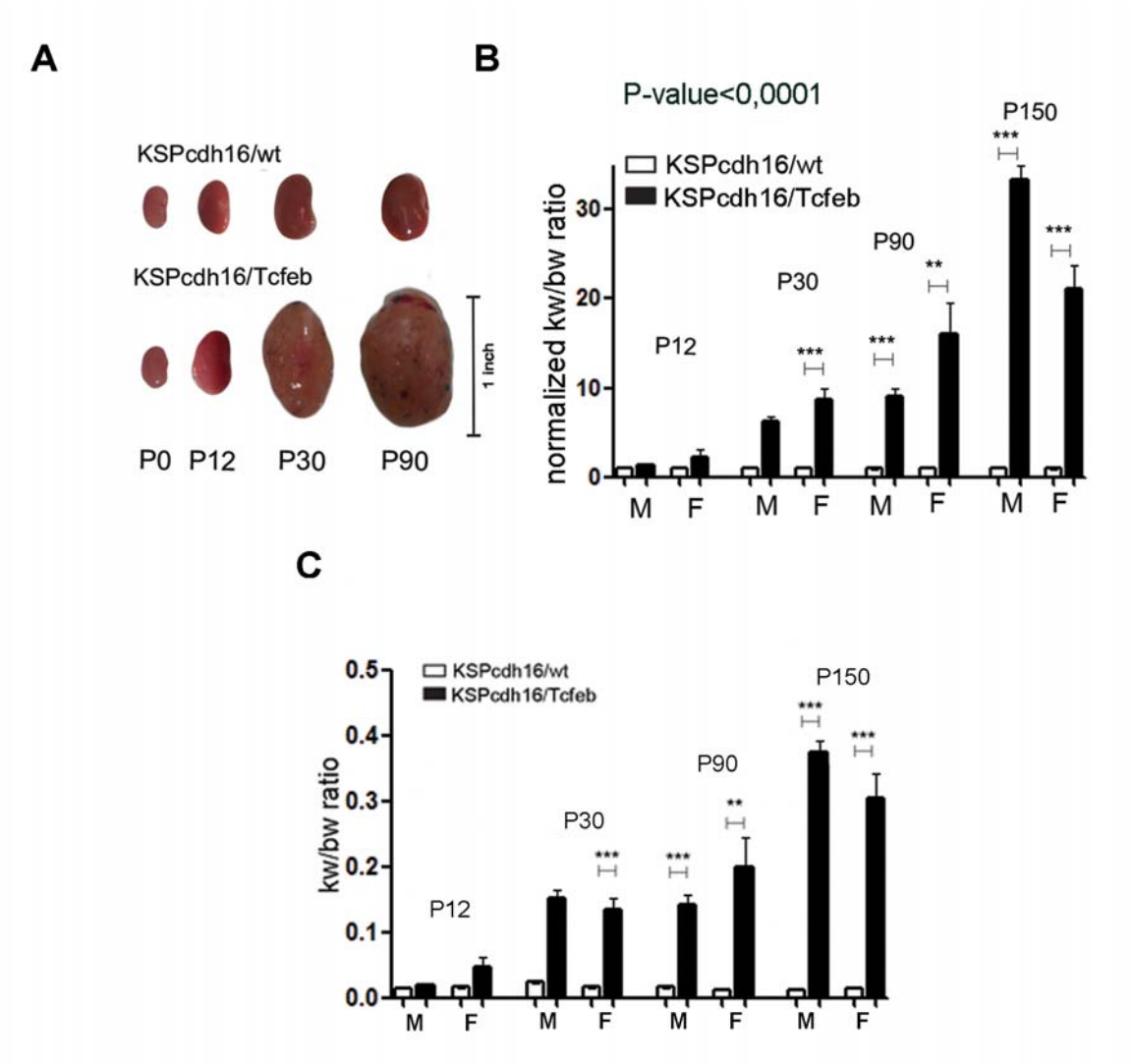

Figure 14. Quantification of kidney enlargement over time.

Kidney to body weight ratio (KW/BW) was calculated on *KSPcdh16/wt* and *KSPcdh16/Tcfeb* mice at different stages (P=days post-natal). A) Pictures of kidneys from *KSPcdh16/wt* and *KSPcdh16/Tcfeb* mice. B) Relative KW/BW ratio on P0, P12, P30 and P90 mice. Data from males (M) and females (F) are shown separately as means of *KSPcdh16/Tcfeb* to *KSPcdh16/wt* KW/BW ratio. C) KW/BW ratio of P0, P12, P30 and P90 mice. Three-way Anova was applied (factors: gender, time, genotype) (* P <0 .05, ** P < 0.01, *** P < 0.001). KW/BW data are relative to: 7 *KSPcdh16/wt* and 3 *KSPcdh16/Tcfeb* males at P12, 9 *KSPcdh16/wt* and 6 *KSPcdh16/Tcfeb* females at P12, 4 *KSPcdh16/wt* and 4 *KSPcdh16/Tcfeb* males at P30, 8 *KSPcdh16/wt* and 9 *KSPcdh16/Tcfeb* females at P30, 3 *KSPcdh16/wt* and 4 *KSPcdh16/Tcfeb* males at P90, 4 *KSPcdh16/wt* and 4 *KSPcdh16/Tcfeb* females at P90, 3 *KSPcdh16/wt* and 3 *KSPcdh16/Tcfeb* males at P150, 3 *KSPcdh16/wt* and 3 *KSPcdh16/Tcfeb* females at P150.

A severe enlargement of the kidneys and a significant increase in the Kidney to Body Weight (KW/BW) ratio were also observed in *IndKSPcdh16/Tcfeb* mice induced with tamoxifen at several developmental stages (P12, P14, P30) (Fig. 15A, B), even if a less severe increase in the KW/BW ratio was observed in mice induced at P30 (Fig. 15B, C).

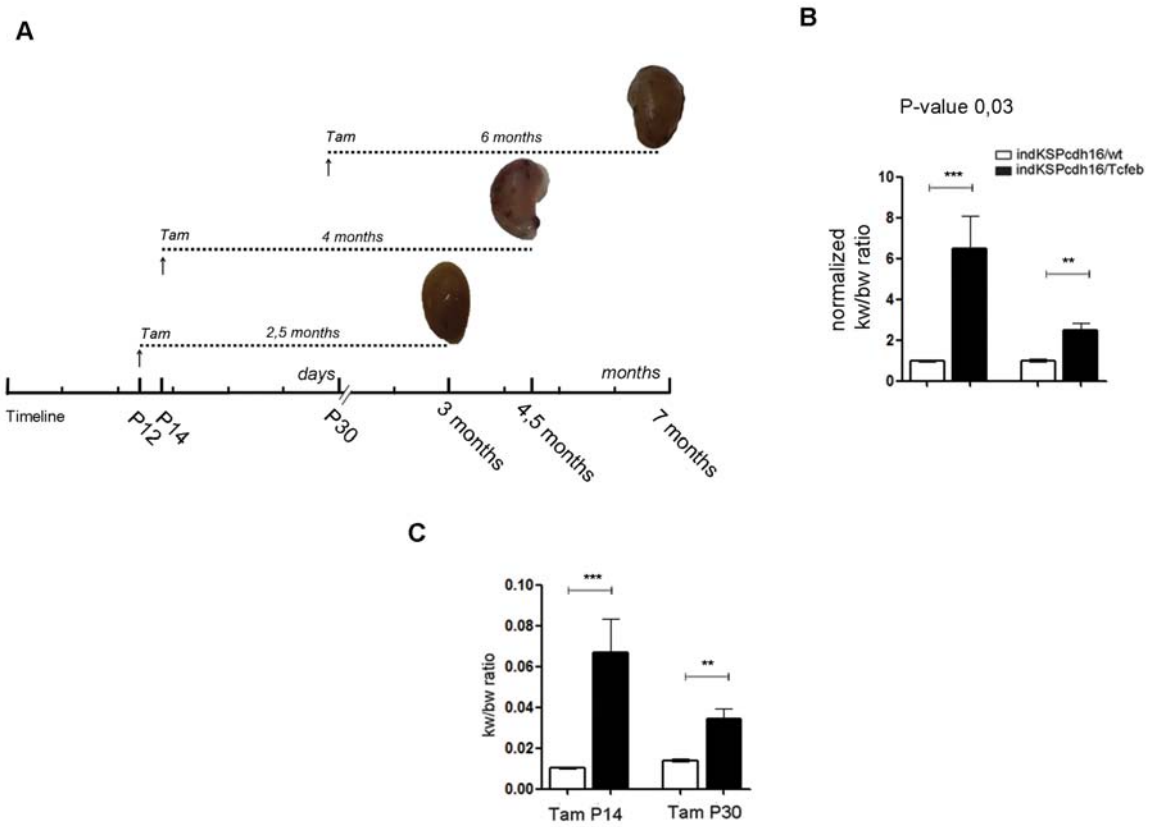

Figure 15. Quantification of renal enlargement in *IndKSPcdh16/Tcfeb* mice.

A) Tamoxifen injection of *IndKSPcdh16/Tcfeb* mice at P12, P14 and P30 with representative images at the time of sacrifice (Tam, tamoxifen). B) Relative ratio of kidney to body weight (KW/BW) evaluated in Tam-treated *IndKSPcdh16/Tcfeb* mice at P90. C) KW/BW ratio of Tam-treated *IndKSPcdh16/Tcfeb* mice at P90. Two-way Anova was applied (factors: treatment, genotype). KW/BW data are relative to: 6 *IndKSPcdh16/wt* and 5 *IndKSPcdh16/Tcfeb* mice injected with tamoxifen at P14 and sacrificed at P90, and 11 *IndKSPcdh16/wt* and 8 *IndKSPcdh16/Tcfeb* mice injected with tamoxifen at P30 and sacrificed at P90.

Survival time of *KSPcdh16/Tcfeb* mice was approximately 3 months (Fig. 16).

Interestingly, a late induction of *Tcfeb* overexpression in *IndKSPcdh16/Tcfeb* mice resulted in a slower development of the phenotype, with less severe kidney enlargement and an overall increase in the survival rate (Fig. 16).

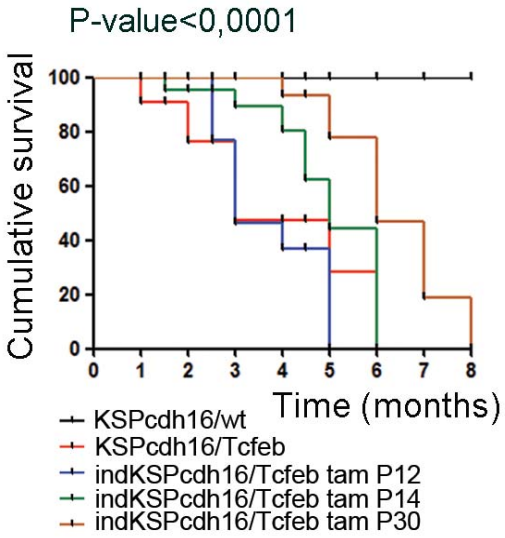

Figure 16. Evaluation of the survival time.

Evaluation of the survival of *KSPcdh16/Tcfeb* and Tam-treated *indKSPcdh16/Tcfeb* mice. Survival curves were calculated for a period of 8 months on a total of 15 *KSPcdh16/Tcfeb* mice, 10 *indKSPcdh16/Tcfeb* mice (Tam P12), 12 *indKSPcdh16/Tcfeb* mice (Tam P14) and 12 *indKSPcdh16/Tcfeb* mice (Tam P30). Mantel-Cox test was applied (*indKSPcdh16/Tcfeb* Tam P12/Tam P14 p-value 0.02; *indKSPcdh16/Tcfeb* Tam P12/P30 p-value <0.0001)

Renal function from *KSPcdh16/Tcfeb* and *IndKSPcdh16/Tcfeb* mice was severely affected, as observed by the strong increase in blood urea and albuminuria (Fig. 17).

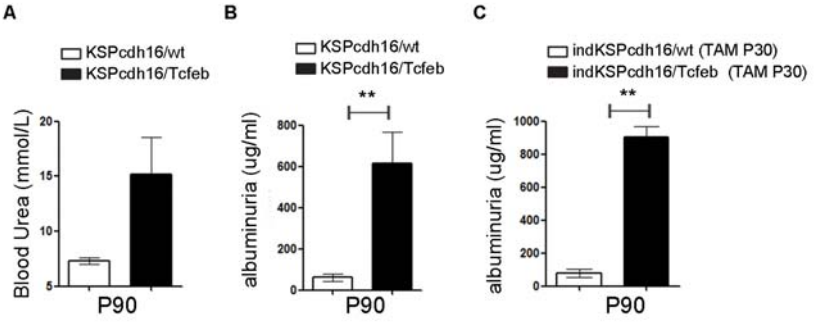

Figure 17. Renal-specific Tcfeb overexpression results in renal failure.

(A) Blood urea and albuminuria levels in (B) *KSPcdh16/Tcfeb* and (C) *indKSPcdh16/Tcfeb* mice. Values are shown as means (± SEM) of at least three *KSPcdh16/Tcfeb* and *indKSPcdh16/Tcfeb* mice and are normalized versus the control animals (*KSPcdh16/wt* and *indKSPcdh16/wt*). Blood urea was calculated on 3 *KSPcdh16/wt* and 4 *KSPcdh16/Tcfeb* animals, albuminuria was calculated on 8 *KSPcdh16/wt* and 6 *KSPcdh16/Tcfeb* animals and on 5 *indKSPcdh16/wt* and 3 *indKSPcdh16/Tcfeb* mice. These biochemical analyses were performed by Dr. Lotte Kors in the Amsterdam Medical Center.

High frequency ultrasound on transgenic animals revealed the presence of a severe cystic disease (Fig. 18).

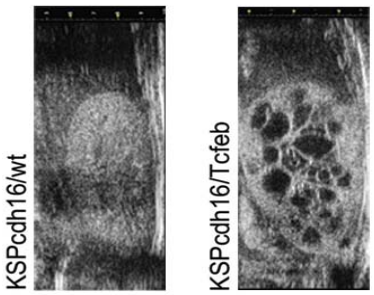

Figure 18. Ultrasound analysis shows the presence of cysts in kidneys.

High-frequency ultrasound (HFUS) images of kidneys from P30 *KSPcdh16/wt* and *KSPcdh16/Tcfeb* mice. This analysis was performed at CEINGE institute in collaboration with Prof. Marco Salvatore.

An extensive histological examination was performed on the animals to characterize the cystic disease. In *KSPcdh16/Tcfeb* mice small cysts arose mainly from the cortex and outer medulla at P12 and became significantly enlarged at P30. At P90 kidney architecture was completely disrupted by cysts (Fig. 19A, B). *IndKSPcdh16/Tcfeb* mice induced at P12 with tamoxifen and sacrificed at P90 showed a higher number of smaller cysts in both cortex and outer medulla (Fig. 19A, B)

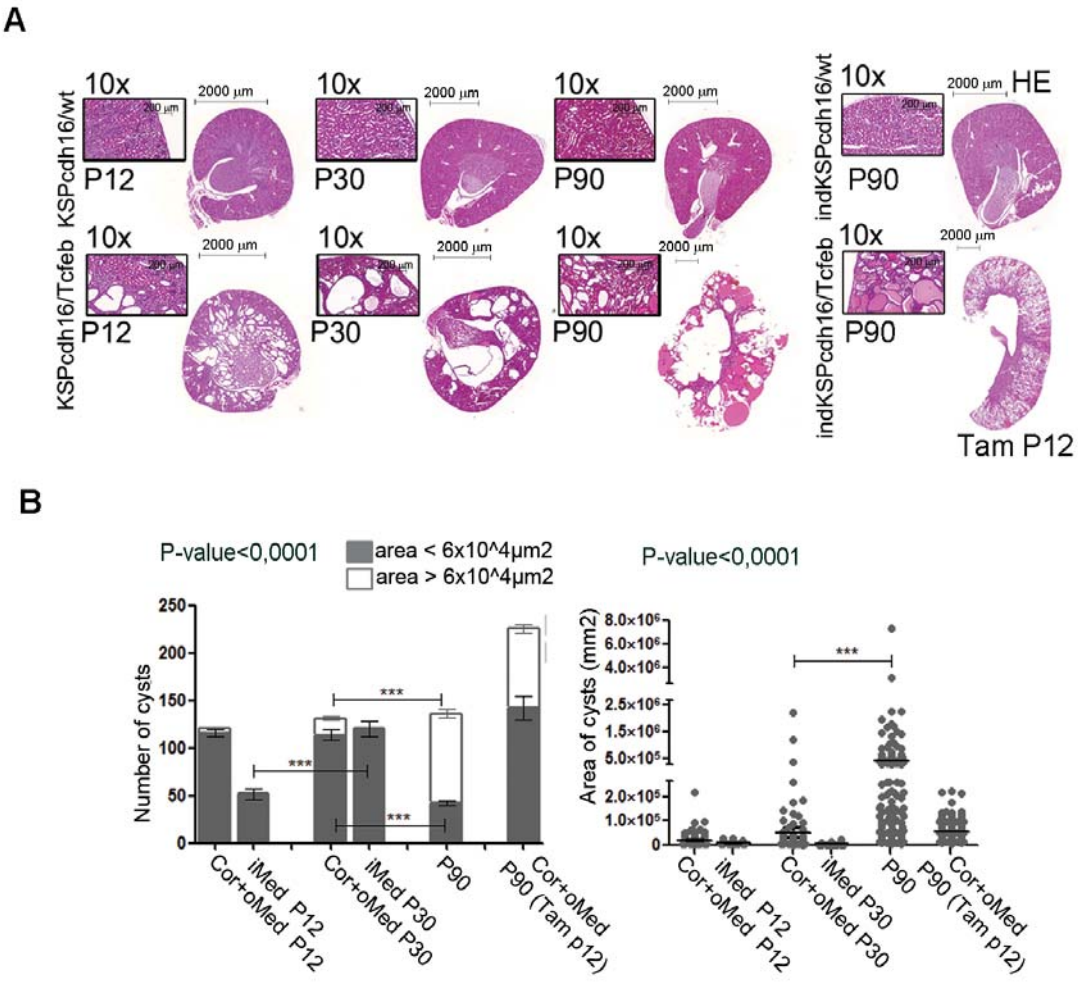

Figure 19. Histological characterization of the cystic disease.

A) Haematoxylin and Eosin (HE) staining of kidneys. Enlarged panels show cyst growth over time. B) Number (left graph) and area (right graph) of kidney cysts in *KSPcdh16/Tcfeb,* and

indKSPcdh16/Tcfeb mice. Number of cysts is shown as an average (±SEM) with bars sub-divided according to the dimension of the cysts. Cyst areas are presented as independent values (dots) with lines representing the means. Three-way (cyst number) and two-way (cyst area) Anova was applied. Cor, cortex; oMed, outer medulla; iMed, inner medulla. Data are shown as the average (± SEM) of three *KSPcdh16/Tcfeb* and *indKSPcdh16/Tcfeb* mice per time point (* P <0 .05, ** P < 0.01, *** P < 0.001).

Cysts were also observed in *IndKSPcdh16/Tcfeb* induced at P14 and, to a lesser extent, at P30 (Fig. 20).

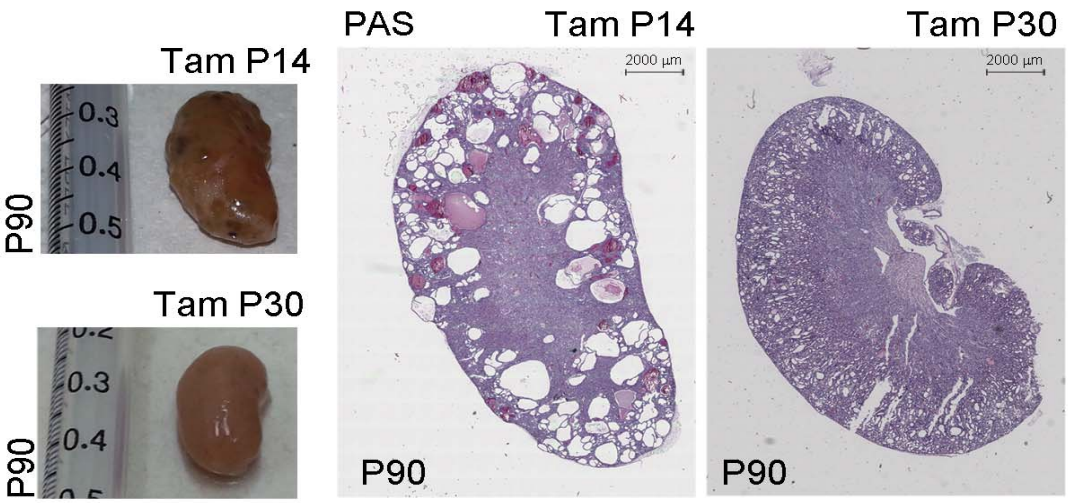

Figure 20. Severity of the cystic disease is dependent from the time of induction of Tcfeb overexpression.

Pictures and PAS stained section from Tam-treated *IndKSPcdh16/Tcfeb* mice at P90. In the Tam P14 group, 4 *IndKSPcdh16/wt and 3 IndKSPcdh16/Tcfeb* mice were analysed, in the Tam P30 group, 5 *IndKSPcdh16/wt and 3 IndKSPcdh16/Tcfeb* mice were analysed.

Tubular epithelial cells lining the cysts showed high levels of cadherin 16, indicating the presence of *KSPcdh16-CRE*-mediated *Tcfeb* overexpression in these cells (Fig. 21).

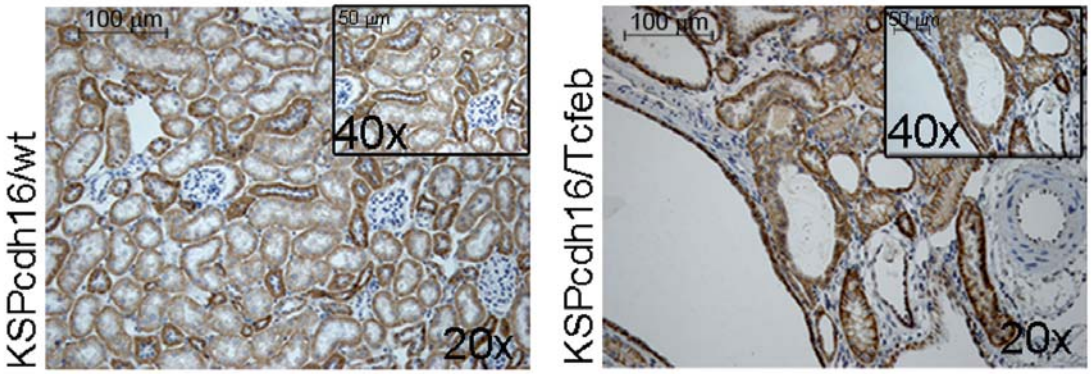

Figure 21. Cadherin16 (CDH16) staining of kidneys from Tcfeb overexpressing mice.

CDH16 immunohistochemistry (IHC) on kidneys from P30 *KSPcdh16/Tcfeb* mice. The staining was performed on 4 *KSPcdh16/wt* and 3 *KSPcdh16/Tcfeb* P30 mice

Histological analysis revealed that cysts from *KSPcdh16/Tcfeb* mice were positive for AQP2 and THP and negative for megalin, indicating that they originate from collecting ducts and distal tubules and not from proximal tubules. Notably, the largest cysts were almost completely negative to all tubular markers, suggesting that they became undifferentiated (Fig. 22).

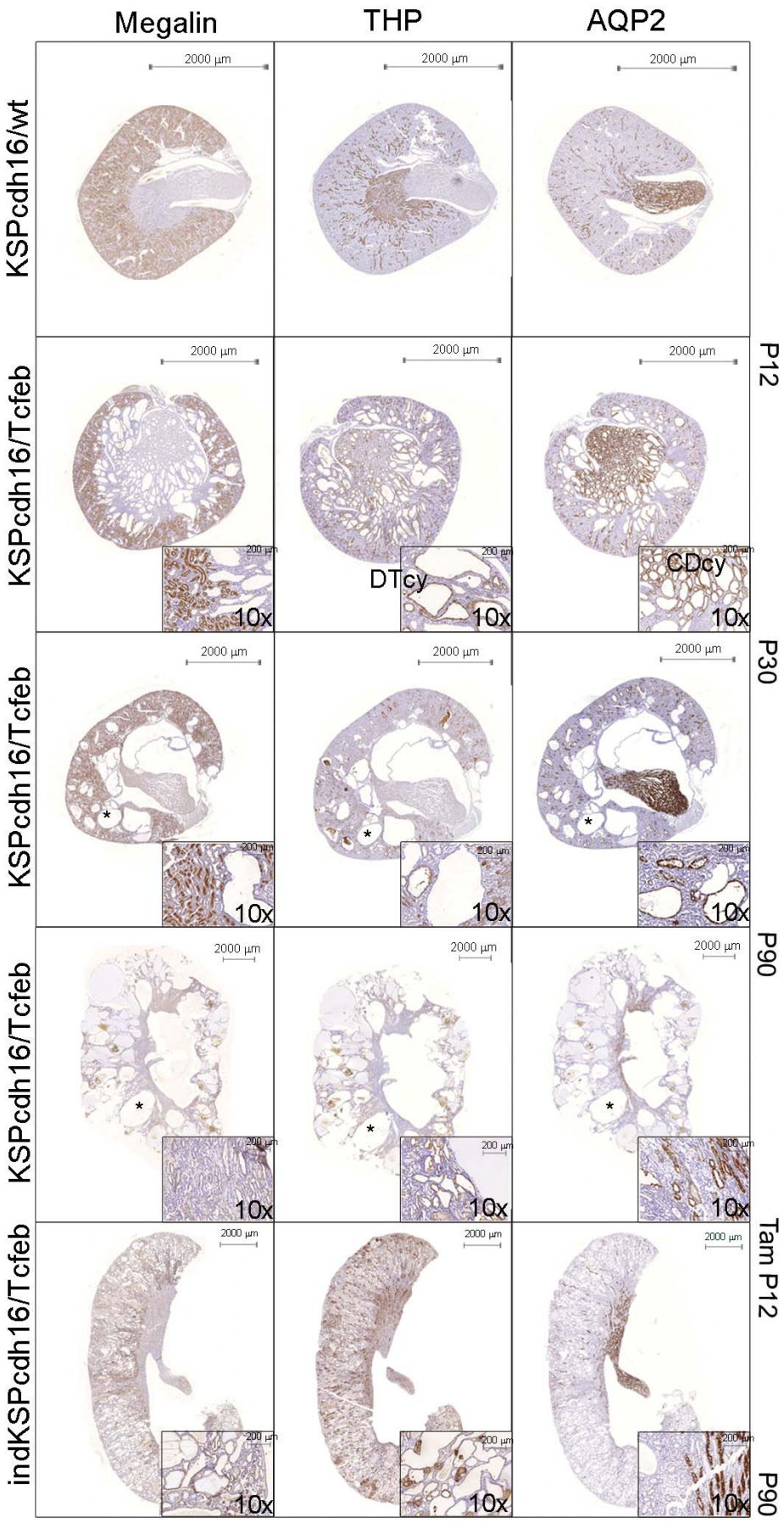
Megalin
THP
AQP2
KSPcdh16/wt
KSPcdh16/Tcfeb
KSPcdh16/Tcfeb
KSPcdh16/Tcfeb
indKSPcdh16/Tcfeb
P12
P30
P90
Tam P12
P90
2000 µm
200 µm
10x
DTcy
CDcy
*

Figure 22. Characterization of cyst origin in *KSPcdh16/Tcfeb* and *indKSPcdh16/Tcfeb* mice

IHC staining of megalin, THP and AQP2 at different time points. Insets are enlargements of representative areas of interest. Larger cysts (denoted by an asterisk) are negative for all the markers tested. DTcy=Distal Tubules cysts; CDcy=Collecting Ducts cysts. These IHC stainings were performed on 3 mice per time-point and genotype and were done in collaboration with Prof. Dorien Peters at Leiden University Medical Center.

Conversely, cysts from *IndKSPcdh16/Tcfeb* mice were positive to megalin and THP, indicating that they arose from proximal and distal tubules (Fig. 22, 23).

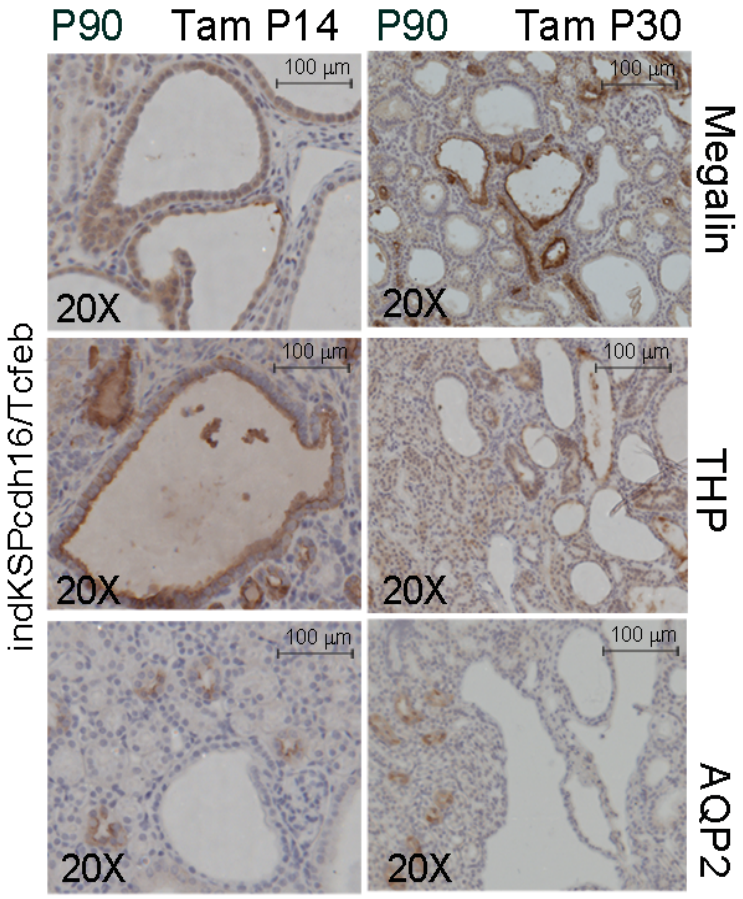

Figure 23. Characterization of cyst origin in *indKSPcdh16/Tcfeb* mice.

Megalin, THP and AQP2 stainings in P90 *indKSPcdh16/Tcfeb* mice. These stainings were performed on 4 *IndKSPcdh16/wt and 3 IndKSPcdh16/Tcfeb* mice (Tam P14), and on 5 *IndKSPcdh16/wt and 3 IndKSPcdh16/Tcfeb* mice (Tam P30).

Cysts were lined by either a single layer-flattened cuboidal epithelium (sCy), or by a multilayer epithelium (mCy), indicating a de-regulation of tubular cell proliferation (Fig. 24). We also noticed the presence of very enlarged cells with a clear cytoplasm, which are commonly known as Clear Cells (CCs) (Krishnan & Truong, 2002) (Fig. 24). Sirius Red staining showed the presence of fibrosis and protein casts and revealed a significant accumulation of collagen inside the affected kidneys, as well as the presence of regions surrounded by multi-layered basement membranes (mBM) (Fig. 24). Importantly, the presence of Clear Cells, fibrosis and mBMs are characteristic features of kidneys from human patients with *TFEB*-fusion *RCC* (Rao *et al*, 2012).

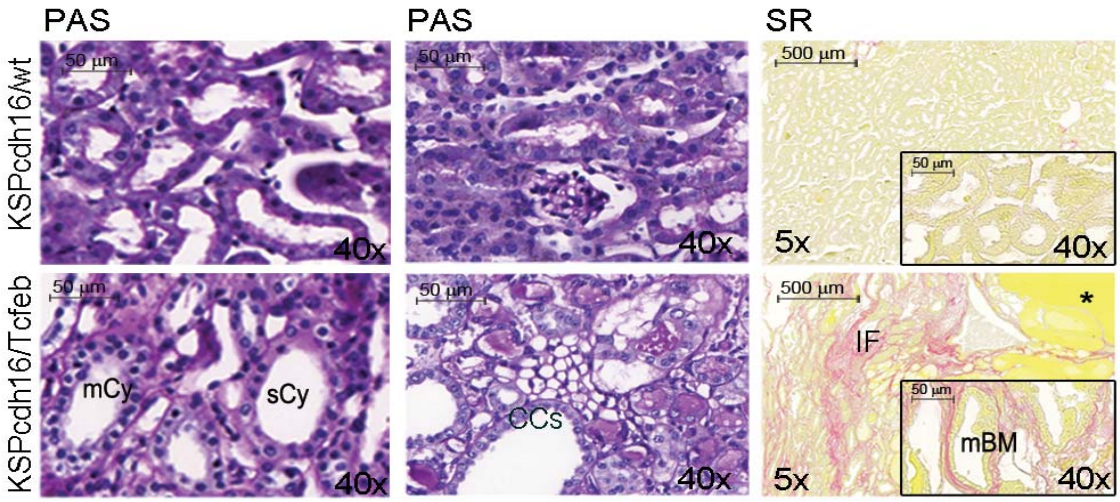

Figure 24. PAS and Sirius Red staining

PAS staining shows the presence of single-layered or multi-layered cysts, and the presence of Clear Cells (CCs). SR staining shows areas of interstitial fibrosis, multi-layered basement membrane and protein casts. These IHC stainings were performed in collaboration with Prof. Dorien Peters at Leiden University Medical Center. Asterisks, protein casts; sCy, simple Cysts; mCy, multilayered Cy; IF, Interstitial Fibrosis; mBM, multi-layered Basement Membrane.

3. Identification of papillary Renal Cell Carcinoma and of liver metastases

^{18}F-FDG PET analysis showed a higher glucose consumption in the kidneys of transgenic animals compared to controls, indicating a higher rate of glucose metabolism and suggesting a neoplastic transformation (Fig. 25).

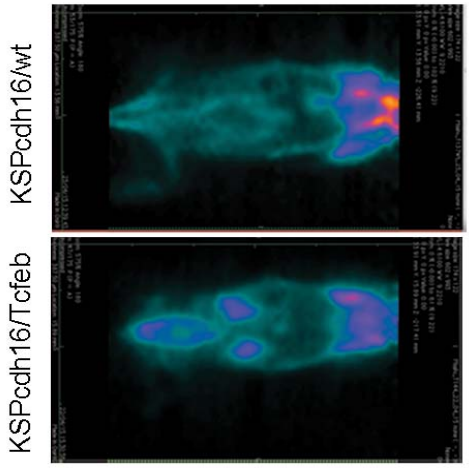

Figure 25. FDG-PET analysis on *KSPcdh16/Tcfeb* mice revealed an increased renal glucose consumption.

^{18}F-FDG PET/CT scan on P30 *KSPcdh16/Tcfeb* mice. This analysis was performed at CEINGE institute in collaboration with Prof. Marco Salvatore.

Similarly with PET analysis, HE and Ki67 stainings of the kidneys of *KSPcdh16/Tcfeb* mice revealed progressive cellular hyperproliferation, which evolved into Ki67-positive neoplastic papillae at 5 months (Fig. 26).

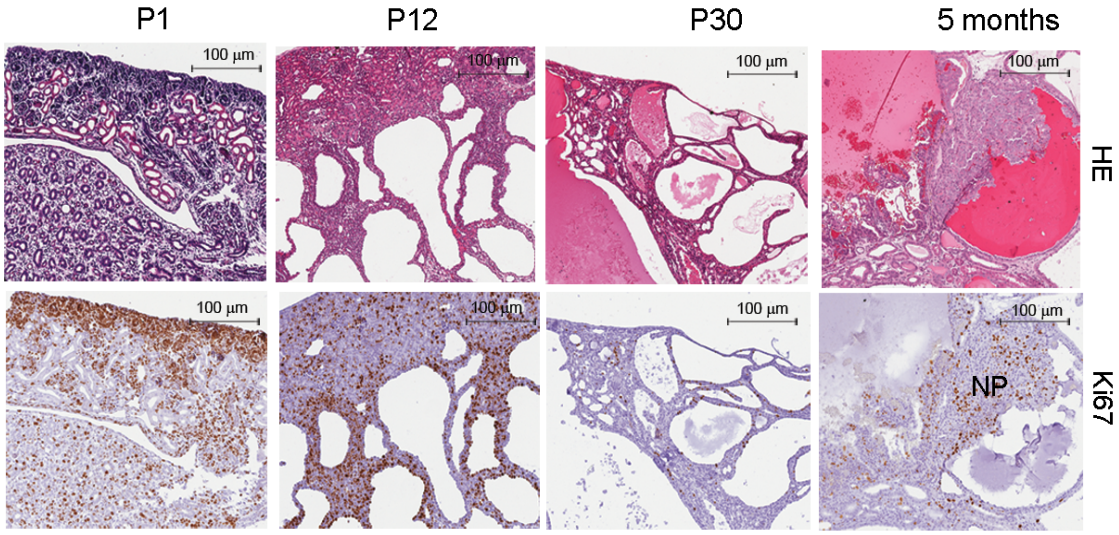

Figure 26. HE and Ki67 staining showed renal neoplastic lesions.

HE and Ki67 staining performed on *KSPcdh16/Tcfeb* mice at P1, P12, P30 and 5 months. Beginning at P12 the increase in cyst size is associated with an increase in papillary proliferation that becomes completely neoplastic by 5 months. NP, Neoplastic Papillae. This analysis was performed in collaboration with Prof. Di Fiore at IEO (European Institute of Oncology). The oncologic characterization was done in collaboration with Dott. Bertalot at IEO.

Neoplastic nodules, micropapillae and Hobnail-like cells, and mitotic spindles were detected at P12, 1 month, and 5 months, respectively (Fig. 27A-D). Focal microcalcifications (Fig. 27E), together with Clear Cells, and nests of neoplastic cells (Fig. 27F) were also detected in *IndKSPcdh16/Tcfeb* mice.

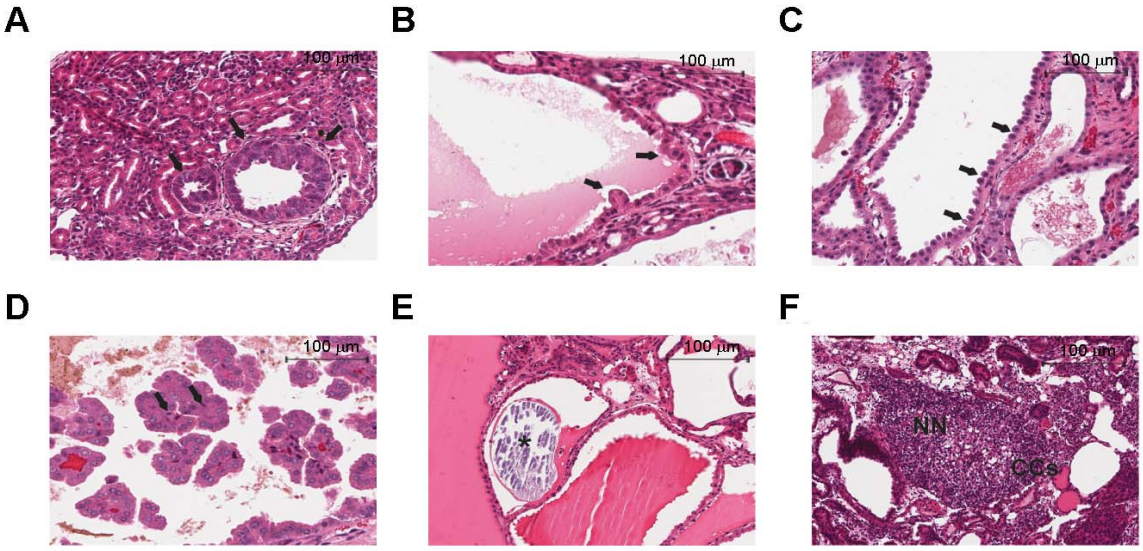

Figure 27. Histological characterization of the renal neoplasia.

A-F) Representative images of neoplastic lesions at different stages: A) neoplastic nodules (arrows) in P12 KSPcdh16/Tcfeb mice; (B) micropapillae (arrows) and (C) hobnail-like cells (arrows) in P30 KSPcdh16/Tcfeb mice; D) mitotic spindles (arrows) in 5 month-old KSPcdh16/Tcfeb mice; E) microcalcifications (asterisk) in Tam-treated indKSPcdh16/Tcfeb mice induced at P14 and sacrificed at 5 months; F) neoplastic nests (NN) and clear cells (CCs) in Tam-treated indKSPcdh16/Tcfeb mice induced at P12 and sacrificed at P90. This analysis was performed in collaboration with Prof. Di Fiore at IEO (European Institute of Oncology). The oncologic characterization was done in collaboration with Dott. Bertalot at IEO.

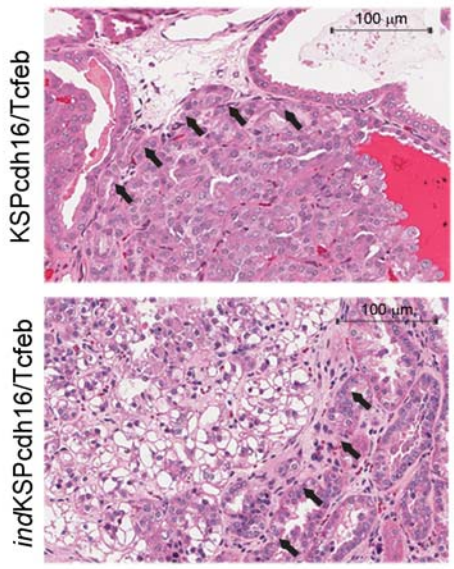

Figure 28. Invasion of the renal neoplasia

HE staining of neoplastic lesions invading the surrounding stroma (arrows) in *KSPcdh16/Tcfeb* and *indKSPcdh16/Tcfeb* mice. This analysis was performed in collaboration with Prof. Di Fiore at IEO (European Institute of Oncology). The oncologic characterization was done in collaboration with Dott. Bertalot at IEO.

Kidneys from both *KSPcdh16/Tcfeb* and ind*KSPcdh16/Tcfeb* mice presented numerous neoplastic lesions with both solid and cystic aspects, ranging from 0.102 to 2.93 mm and sometimes showing local invasion of the surrounding stroma (Figure 28). These features were observed on a total of 43 mice.

Most importantly, liver metastases ranging from 0.9 to 3.8 mm, were found in both *KSPcdh16/Tcfeb* and ind*KSPcdh16/Tcfeb* mice. In *KSPcdh16/Tcfeb* animals metastases were detected starting from P90 with an incidence of 23% (5 cases out of 21 *KSPcdh16/Tcfeb* mice older than three months). These metastases were positive for the renal markers PAX8 and CDH16, while they were negative for the cholangiocarcinoma marker Cytokeratin 7 (CK7), consistent with their renal origin (Fig. 29).

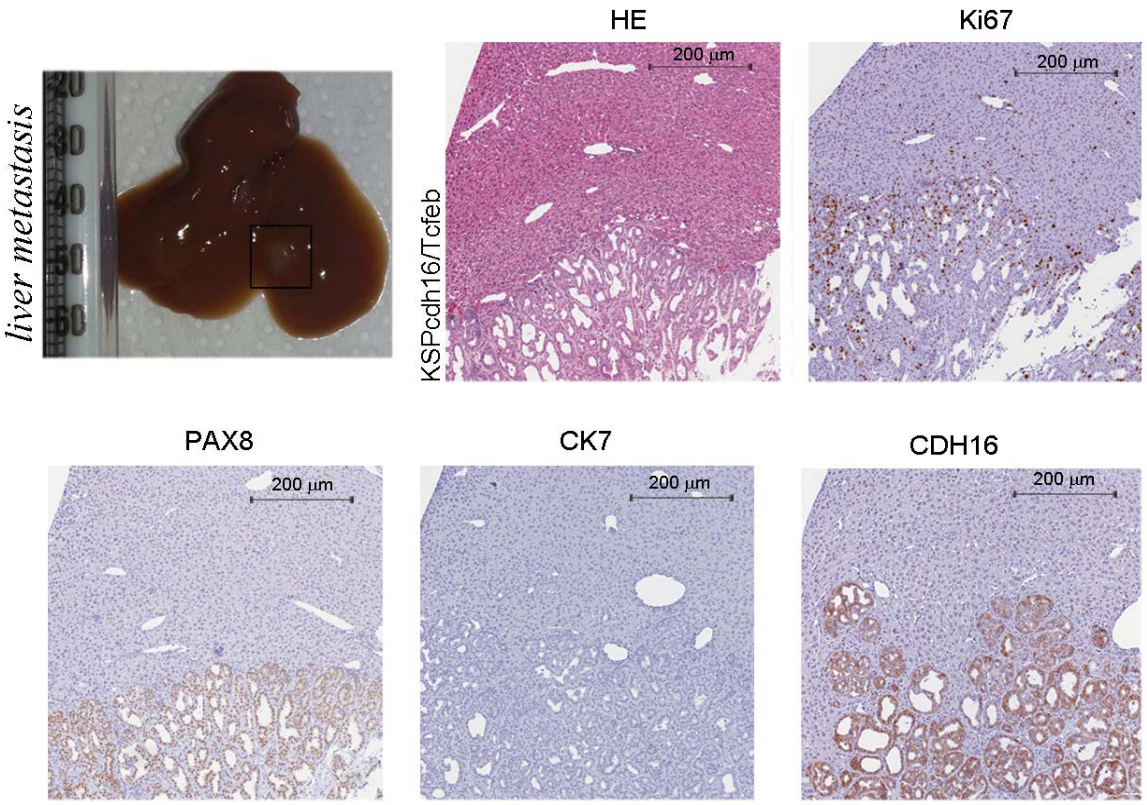

Figure 29. Liver metastases were observed in older animals.

Liver metastases in 5 month-old *KSPcdh16/Tcfeb* mice stained for HE, Ki67, PAX8 and CK7. Liver metastases were detected in 5 cases out of 21 *KSPcdh16/Tcfeb* mice older than three months. This analysis was performed in collaboration with Prof. Di Fiore at IEO (European Institute of Oncology). The oncologic characterization was done in collaboration with Dott. Bertalot at IEO.

4. TFEB overexpression results in the induction of the canonical WNT pathway

To characterize the molecular mechanisms and identify the relevant pathways necessary for tumour development, we performed transcriptome analysis on kidney samples from *KSPcdh16/Tcfeb* and *KSPcdh16/wt* mice at P0 (GSE62977-KSP_P0 dataset) and at P14 (GSE63376-KSP_P14 dataset) (see materials and methods) and found that *Tcfeb* overexpression perturbed the kidney transcriptome

in a statistically significant manner (see material and methods, “Microarray data processing” section).

Targeted analysis of the transcriptomic data revealed a significant induction of genes belonging to both ErbB and WNT signalling pathways (Table 3A, B).

A

Gene Symbol	signed_ratio (KSP_P0/CTL)
Hbegf	2,194808473
Tgfa	1,9286888
Areg	1,631011877
Cdkn1a	1,628361867
Crk	1,579433149
Pak1	1,507716537

Gene Symbol	signed_ratio (KSP_P0/CTL)
Areg	1,221605795

B

Gene Symbol	signed ratio (KSP_P0/CTL)
Rnf146	1,700903945
Fzd3	1,650328884
Kdm6a	1,565386988
Ccnd1	1,377411994

Gene Symbol	signed ratio (KSP_P14/CTL)
Rhou	1,639718601
Plcg2	1,601227563
Gata3	1,358534898
Fbxw2	1,262750602
Mark2	1,248332335
Axin1	1,21985179
Tab1	1,217280695
Psmb3	1,211737817
Ndrg2	1,193338279
Chd8	1,185904267

Table 3. List of ErbB and WNT-related genes belonging to the P0 and P14 microarray dataset.

A) List of 6 genes with a known role in ErbB signalling pathway which are significantly up-regulated (FDR≤0.05) following TFEB overexpression in KSP_P0 microarray dataset (GSE62977) (upper table). One gene with a known role in ErbB signalling pathway which is significantly up-regulated (FDR≤0.05) following TFEB overexpression in KSP_P14 microarray dataset (GSE62977) (lower table). B) List of 4 genes with a known role in WNT signalling pathway which are significantly up-regulated (FDR≤0.05) following TFEB overexpression in KSP_P0 microarray dataset (GSE62977) (upper table). List of 10 genes with a known role in WNT signalling pathway which are significantly up-regulated (FDR≤0.05) following TFEB overexpression in KSP_P14 microarray dataset (GSE63376) (lower table).

First, data from the targeted analysis performed on the KSP_P0 dataset were validated on *KSPcdh16/Tcfeb* mice at several developmental stages (P0, P12, P30) by real-time PCR (Fig. 30A, B). Moreover, considering the relevance of WNT pathway alteration in development of the renal cystic pathology, we assessed its activation status by looking at the transcriptional levels of c-Myc and Axin2 genes, which are, together with Ccnd1, well-established WNT direct gene targets (Clevers, 2006b). Real-time PCR performed on *KSPcdh16/Tcfeb* animals at different developmental stages also showed the induction of these genes (Fig. 30B).

A

Gene Symbol	signed ratio (KSP_P0/CTL)
Hbegf	2,194808473
Tgfa	1,9286888
Areg	1,631011877
Cdkn1a	1,628361867
Crk	1,579433149
Pak1	1,507716537

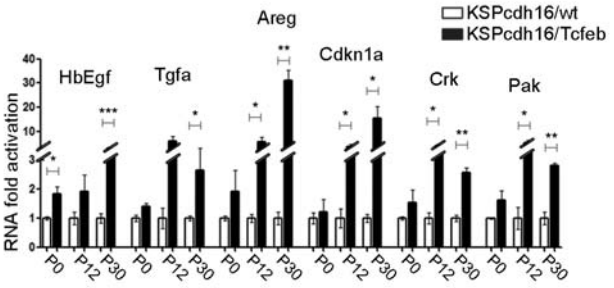

B

Gene Symbol	signed ratio (KSP_P0/CTL)
Rnf146	1,700903945
Fzd3	1,650328884
Kdm6a	1,565386988
Ccnd1	1,377411994

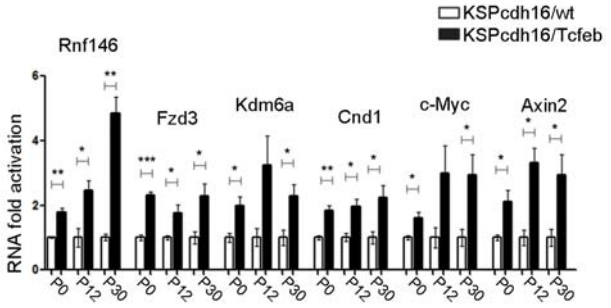

Figure 30. Transcriptional validation of the microarray data.

Transcriptional analyses were performed on *KSPcdh16/wt* and *KSPcdh16/Tcfeb* mice**.** A,B) Tables show the relative increase of genes related to the ErbB (A) and WNT (B) pathways in the microarray analyses performed on kidneys from P0 *KSPcdh16/Tcfeb* mice. Graphs show Real-time PCR validations performed on kidneys from *KSPcdh16/Tcfeb* mice at different stages (P0, P12, P30). Data are shown as the average (± SEM) of three *KSPcdh16/Tcfeb* mice normalized versus wild type mice (± SEM) (* P <0.05, ** P < 0.01, *** P < 0.001, two-sided, Student's t test).

Kidneys from Ind*KSPcdh16/Tcfeb* mice were also screened for their transcriptional profile, to check whether the same molecular alterations were also observed there. We validated the induction of all the genes belonging to the WNT pathway on Ind*KSPcdh16/Tcfeb* mice induced with tamoxifen at P14 and at P30 (Fig. 31A, B).

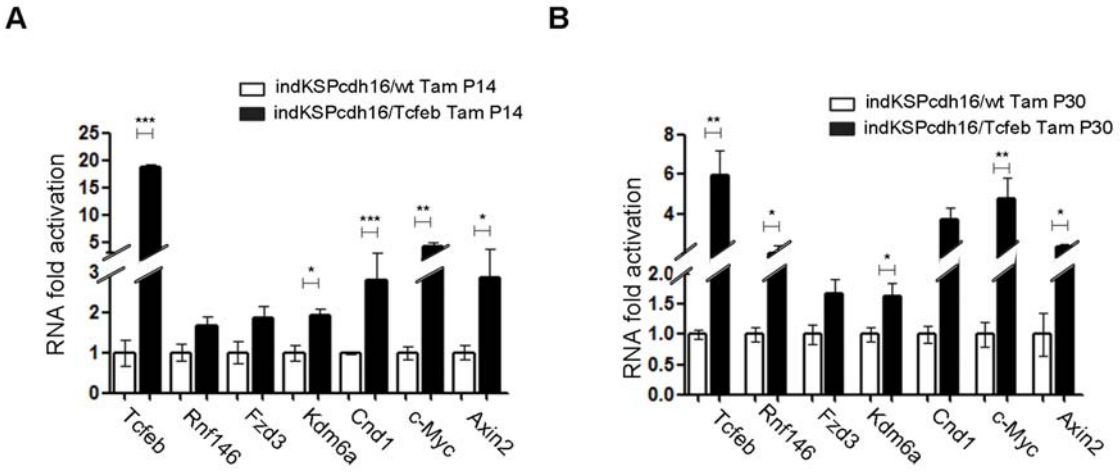

Figure 31. WNT transcriptional profile in indKSPcdh16/Tcfeb mice.

Transcriptional analysis of previously validated genes belonging to the WNT pathway on P90 *indKSPcdh16/Tcfeb* mice induced with tamoxifen respectively at P14 (A) and P30 (B). Data are shown as the average (± SEM) of three *indKSPcdh16/Tcfeb* mice and values are normalized to the wild type line. (* P <0.05, ** P < 0.01, *** P < 0.001, two-sided Student's t test).

Regarding the genes belonging to the ErbB pathway, the transcriptional response was more variable. We confirmed the induction of HbEgf, Tgfα, Areg and Cdkn1α, but not of Crk and Pak on Ind*KSPcdh16/Tcfeb* mice induced with tamoxifen at P14 (Fig. 32A), whereas we found an increase in HbEgf, Areg, Cdkn1α and Pak mRNA levels , but not of Tgfα and Crk on Ind*KSPcdh16/Tcfeb* mice induced with tamoxifen at P30 (Fig. 32B).

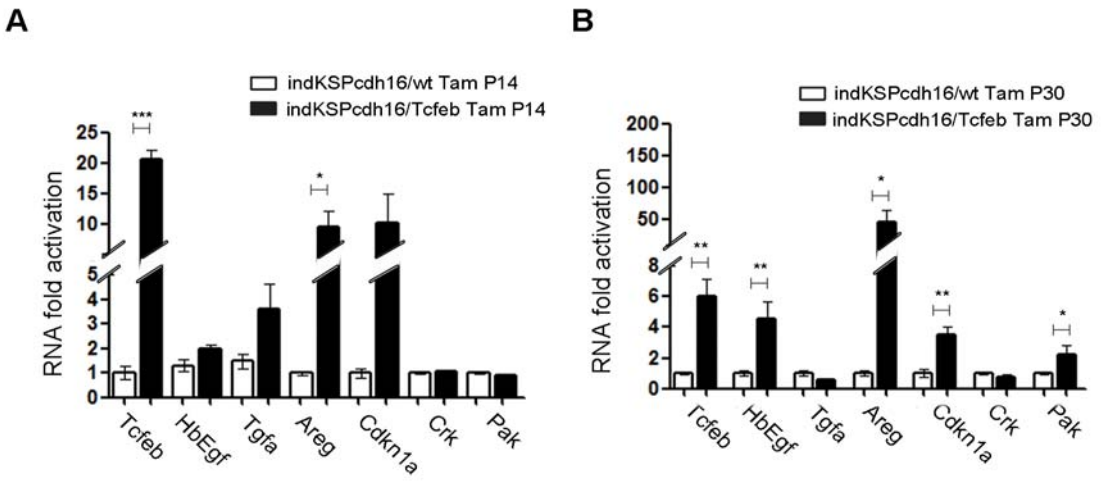

Figure 32. ErbB transcriptional profile in *indKSPcdh16/Tcfeb* mice.

Transcriptional analysis of previously validated genes belonging to the ErbB pathway on P90 *indKSPcdh16/Tcfeb* mice induced with tamoxifen respectively at P14 (A) and P30 (B). Data are shown as the average (± SEM) of three *indKSPcdh16/Tcfeb* mice and values are normalized to the wild type line. (* P <0.05, ** P < 0.01, *** P < 0.001, two-sided Student's *t* test).

Based on these results, we checked the activation of both ErbB and WNT signalling pathways. No evidence for an increase in the phosphorylation of AKT and ERK1/2 kinases (Arteaga & Engelman, 2014) was detected in P30 *KSPcdh16/Tcfeb* kidneys (Fig. 33) or in primary kidney cells obtained from transgenic mice (Fig. 34), indicating that the ErbB pathway was not induced.

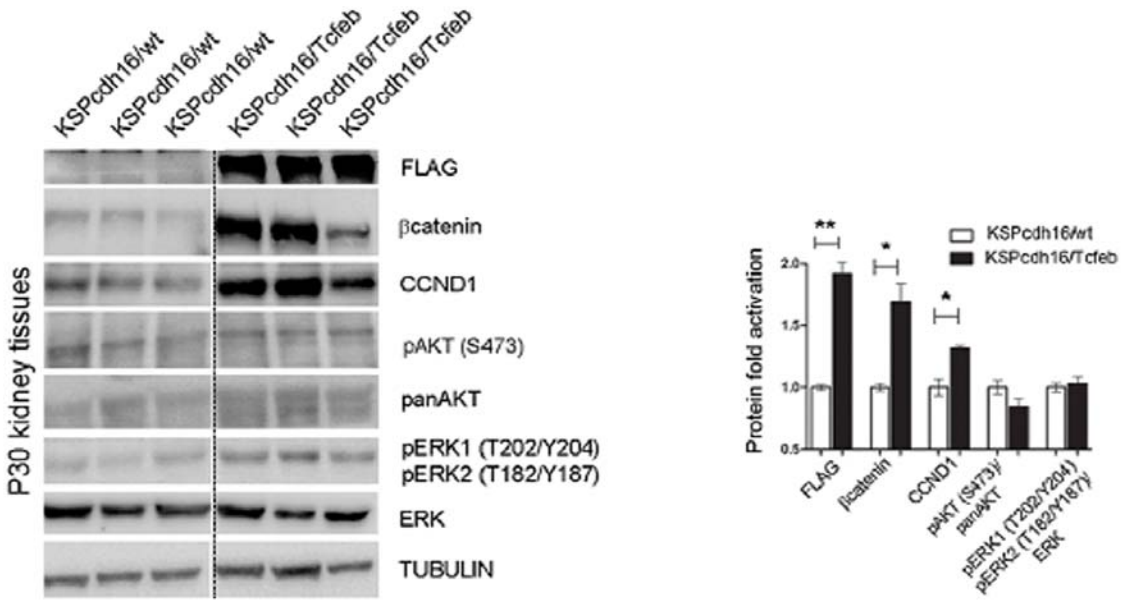

Figure 33. Activation of ErbB and WNT signalling pathways in kidneys from *KSPcdh16/Tcfeb* mice.

Immunoblot analyses performed on P30 kidney tissues derived from *KSPcdh16/Tcfeb* mice to evaluate ErbB and WNT activation status. Each replicate is a distinct biological sample. ErbB signalling was assessed by looking at phosphoAKT (Ser473) to total AKT ratio, and phosphoERK1 (T202/Y204)/ERK2(T185/Y187) to total ERK ratio; WNT signalling was assessed by quantifying βcatenin and CCND1 (Cyclin D1) protein levels. Graphs represent the densitometry quantification of Western blot bands. Values are normalized to tubulin when not specified, and are shown as an average (± SEM) (* P <0.05, ** P < 0.01, *** P < 0.001, two-sided, Student's t test) .

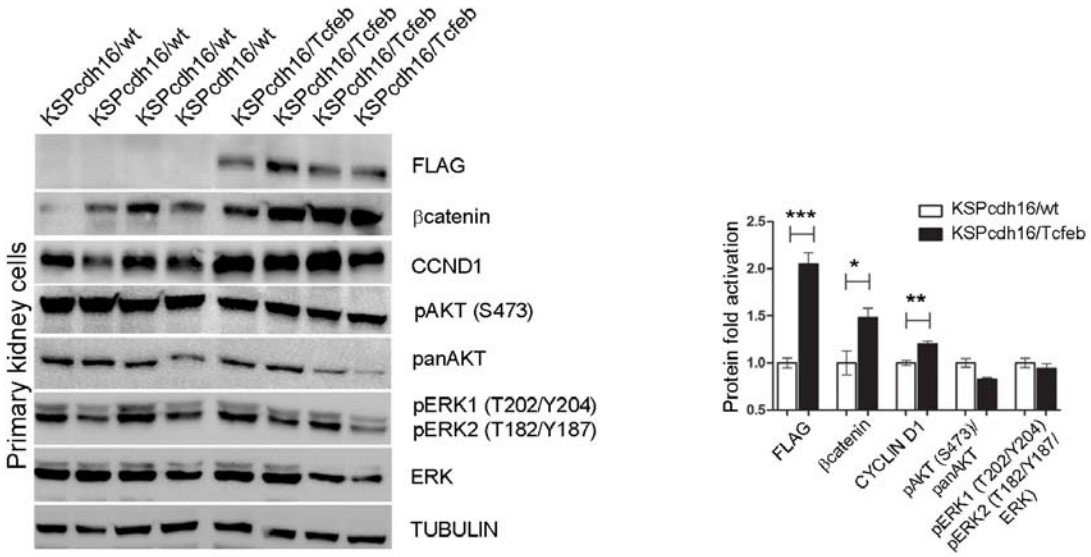

Figure 34. Activation of ErbB and WNT signalling pathways in primary kidney cells.

Immunoblot analyses performed on primary kidney cells isolated from KSPcdh16/Tcfeb to evaluate ErbB and WNT activation status. Each replicate is a distinct biological sample. The same antibodies described in figure 33 were used. Graphs represent the densitometry quantification of Western blot bands. Values are normalized to tubulin when not specified, and are shown as an average (± SEM) (* P <0.05, ** P < 0.01, *** P < 0.001, two-sided, Student's t test) .

Erk1/2 activation, as detected by pERK1/2, was observed only at later stages, while no pAKT activation was observed (Fig. 35).

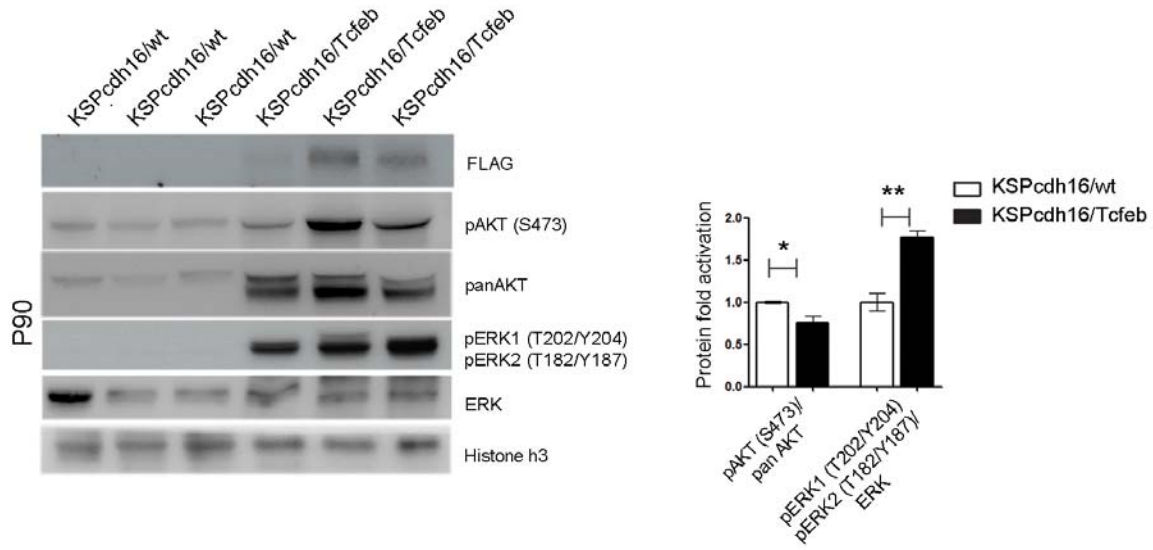

Figure 35. Biochemical analysis of ErbB signalling in older *KSPcdh16/Tcfeb mice*.

Immunoblot analysis performed on P90 kidneys from *KSPcdh16/Tcfeb*. Each replicate is a different biological sample. ErbB was analysed by quantifying phosphoAKT (Ser473) to total AKT, and phosphoERK1 (T202/Y204)/ERK2(T185/Y187) to total ERK; graphs are the densitometry quantifications of Western blot bands normalized to wild type line and are shown as an average (± SEM) (* P <0.05, ** P < 0.01, *** P < 0.001, two-sided Student's t test).

The same result was found in P90 *IndKSPcdh16/Tcfeb* mice induced with tamoxifen at P14 and at P30 (Fig. 36A, B).

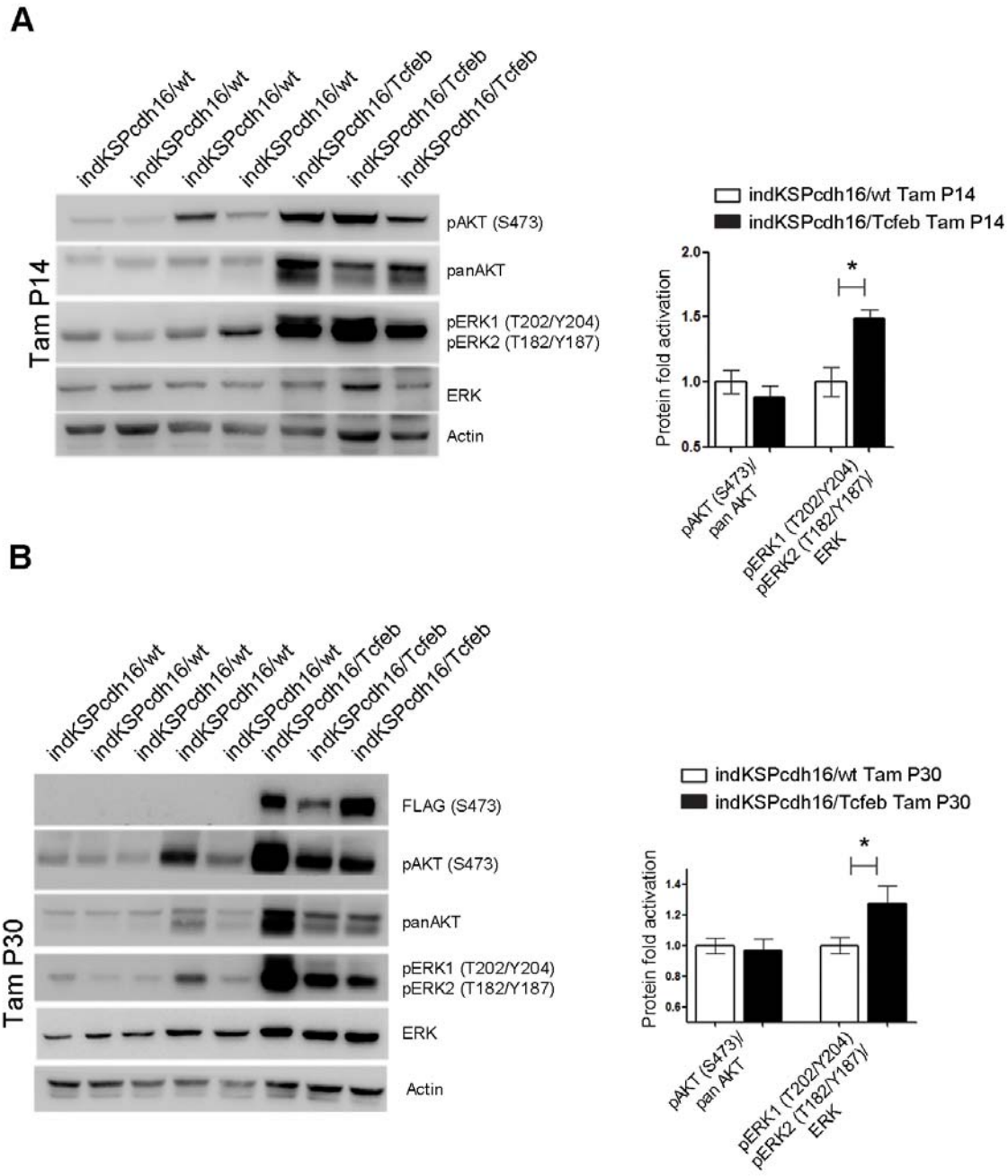

Figure 36. Biochemical analysis of ErbB signalling in *indKSPcdh16/Tcfeb* mice.

Immunoblot analysis performed on P90 *indKSPcdh16/Tcfeb* animals induced with tamoxifen at P14 (B) and at P30 (C), respectively. Each replicate is a different biological sample. The same antibodies described in figure 33 were used; graphs are the densitometry quantifications of Western blot bands normalized to wild type line and are shown as an average (± SEM) (* P <0.05, ** P < 0.01, *** P < 0.001, two-sided Student's t test).

Conversely, we detected increased levels of total βcatenin and CCND1 in P30 renal tissues (Fig. 32) and primary kidney cells (Fig. 33) and increased levels of non phospho active-βcatenin and of pLRP6 (Ser1490)/ LRP6 ratio in P30 and P90 renal tissues from *KSPcdh16/Tcfeb* mice (Fig. 37A, B).

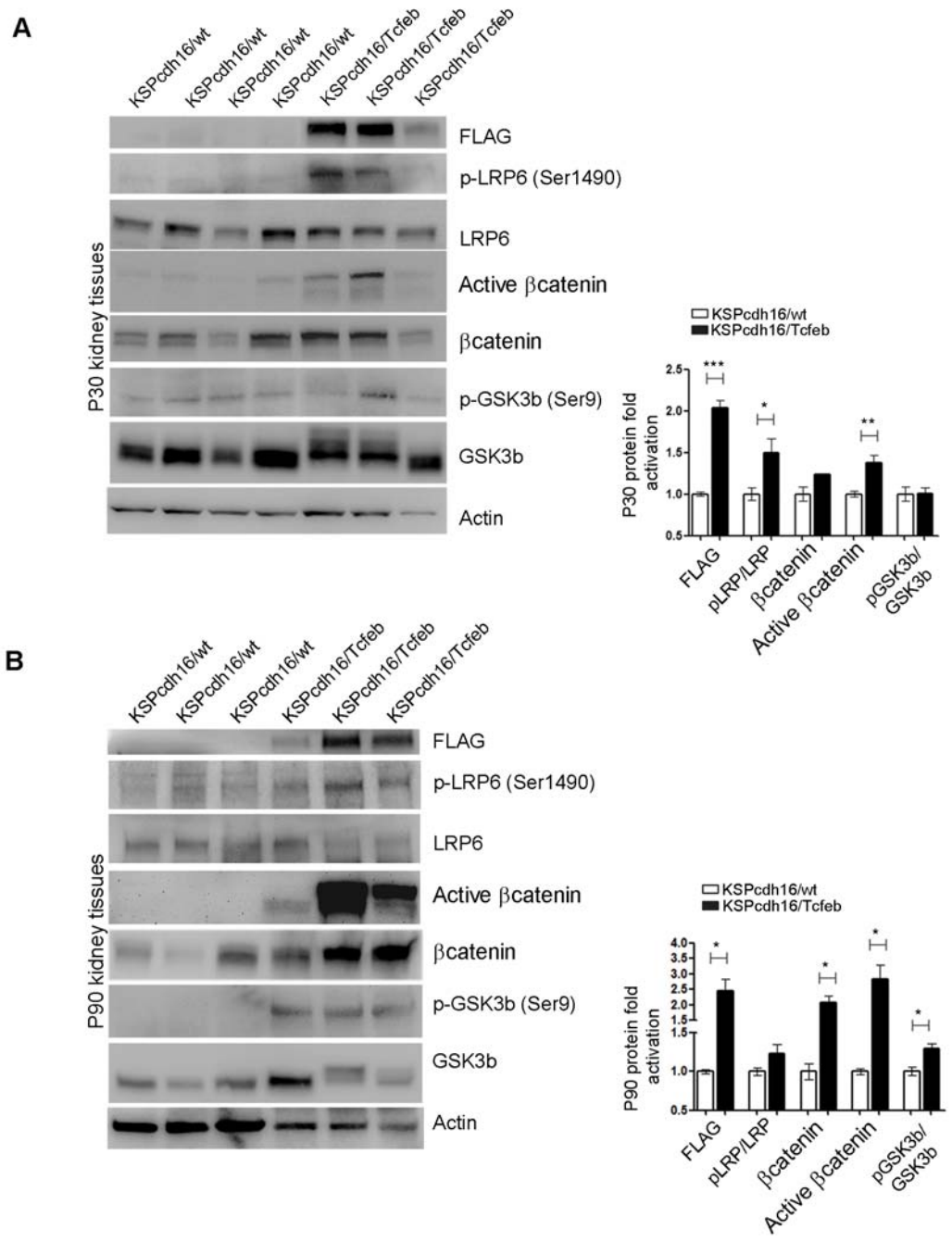

Figure 37. Molecular and analysis of WNT signalling.

Western blot analysis performed on (A) P30 and (B) P90 kidneys from *KSPcdh16/Tcfeb* mice to assess WNT signalling activation by looking at different proteins related to this pathway. Each

replicate is a distinct biological sample. p-LRP6 (Ser1490)/LRP6, active-βcatenin (non phospho), βcatenin and p-GSK3β (Ser9)/GSK3β protein levels were quantified by densitometry analysis of the Western blot bands. Values are normalized to actin when not specified, and are shown as an average (± SEM) (* P <0.05, ** P < 0.01, *** P < 0.001, two-sided Student's t test).

Moreover, also P90 *IndKSPcdh16/Tcfeb* mice induced with tamoxifen at P14 and at P30 displayed an increased WNT pathway activation (Fig. 38A, B) .

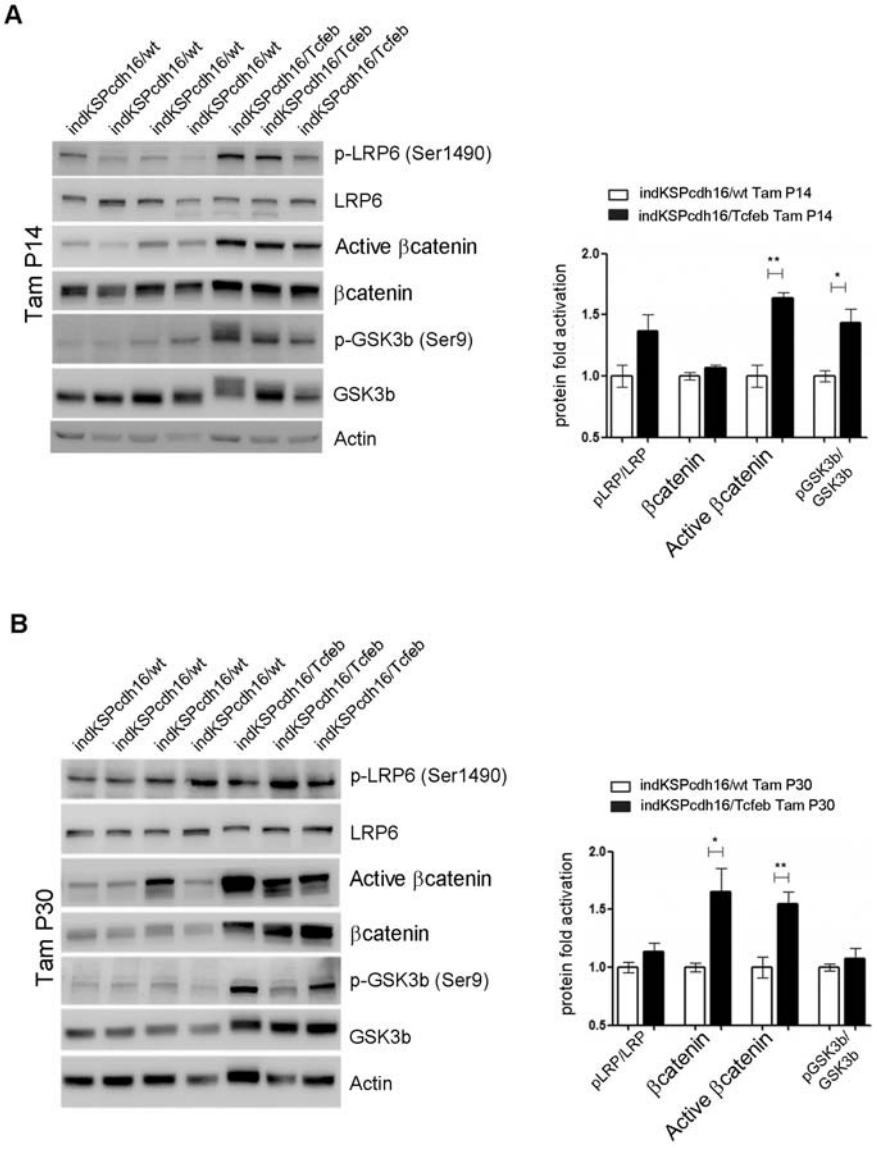

Figure 38. Molecular analysis of WNT signalling pathway in indKSPcdh16/Tcfeb animals.

A,B) Immunoblot analysis of WNT-related proteins performed on P90 *indKSPcdh16/Tcfeb* animals induced with tamoxifen at P14 (A) and at P30 (B). Each replicate is a different biological sample.

Graphs show densitometry analysis of the Western blot bands. Values are normalized to actin when not specified, and are shown as an average (± SEM) (* P <0.05, ** P < 0.01, *** P < 0.001, two-sided Student's t test).

Finally, immunohistochemistry showed that βcatenin and active-βcatenin staining of renal sections from *KSPcdh16/Tcfeb* mice were significantly enhanced around the cysts (Fig. 39).

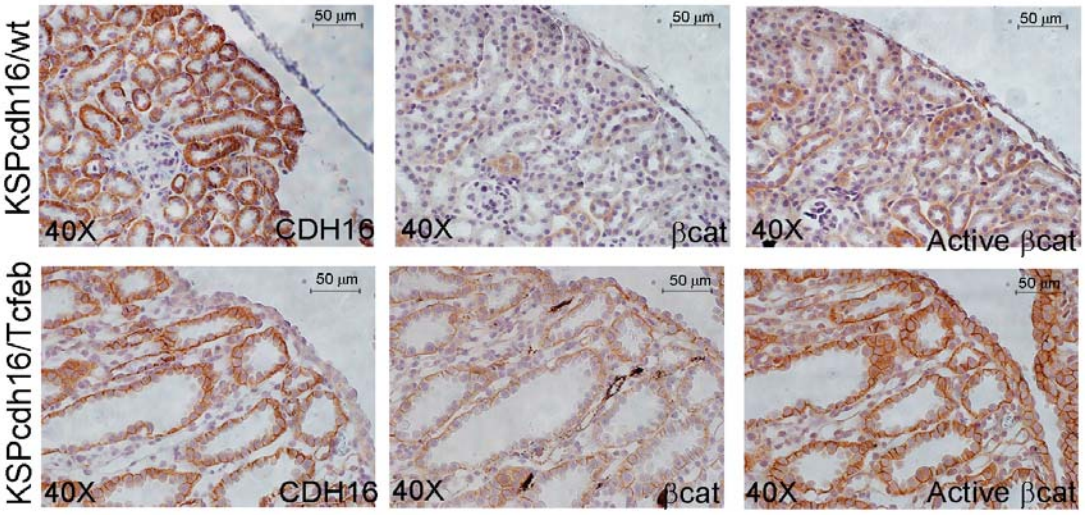

Figure 39. Histological analysis of WNT signalling.

Immunohistochemistry staining of CDH16, βcatenin and active-βcatenin proteins performed on P30 kidney tissues from *KSPcdh16/Tcfeb* mice. The staining was performed on 4 *KSPcdh16/wt* and 3 *KSPcdh16/Tcfeb* P30 mice.

These results indicate the presence of a strong activation of the WNT signalling pathway in TFEB-overexpressing mice. Interestingly, the WNT pathway is known to play a role in renal cyst development (Vainio & Uusitalo, 2000; Rodova *et al*, 2002) and renal tumour formation, such as in Wilm's tumor (Koesters *et al*, 1999; Zhu *et al*, 2000; Kim *et al*, 2000). To investigate the role of TFEB in WNT pathway

activation, we performed luciferase assays using a TOP-FLASH Luciferase WNT-reporter on immortalized kidney cell lines (HEK293 and HK2) co-transfected with *TFEB* and with both *βcatenin* and *TCF4* plasmids to stimulate WNT signalling. Luciferase activation was significantly higher in cells transfected with *TFEB* compared to controls without *TFEB*. No changes were observed when *TFEB* was transfected alone or only with *βcatenin* (Fig. 40) Together these data suggest that TFEB is able to enhance WNT pathway activation.

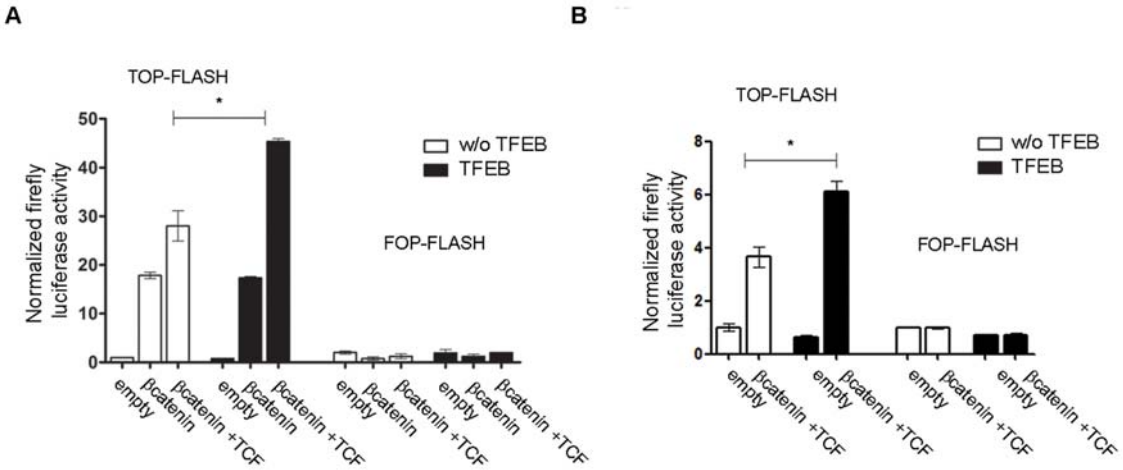

Figure 40. WNT-signalling activation assay.

Activity of the TCF/LEF reporter TOP-FLASH. Luciferase activity after co-transfection of *βcatenin-TCF* plasmids in HEK293 (A) and HK2 (B) cells with and without *TFEB* overexpression. Values are shown as an average (± SEM) of each point in duplicate, normalized to the Renilla values and to the basal condition. Data are representative of three independent experiments.

5. Treatment with WNT inhibitors ameliorates the disease phenotype

Primary kidney cells derived from the renal cortex and medulla of *KSPcdh16/Tcfeb* mice showed significantly higher levels of proliferation compared to wild type cells (Fig. 41).

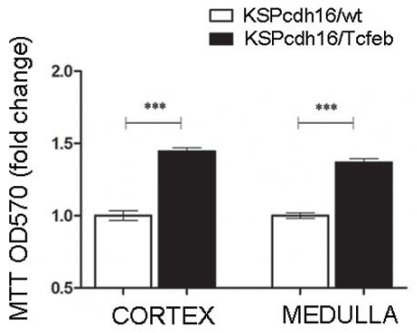

Figure 41. Primary kidney cells from KSPcdh16/Tcfeb mice show an hyper-proliferative phenotype.

MTT tetrazolium reduction assay (MTT) was used to evaluate proliferation of primary kidney cells derived from *KSPcdh16/Tcfeb* mice. Values are shown as an average (± SEM) of each point in triplicate and normalized versus wild type mice. Data are representative of three independent experiments performed on three *KSPcdh16/Tcfeb* and *KSPcdh16/wt* mice.

We tested whether this hyperproliferative phenotype was sensitive to WNT inhibition. Strikingly, cell proliferation was significantly dampened, in a dose-dependent way, by two small-molecules, PKF118-310 and CGP049090 that specifically inhibit the WNT pathway by disrupting the interaction between βcatenin and TCF4 (Avila *et al*, 2006) and are known to suppress cell proliferation in several types of cancers, both *in vitro* and *in vivo* (Wei *et al*, 2010; Wakita *et al*, 2001) (Fig. 42).

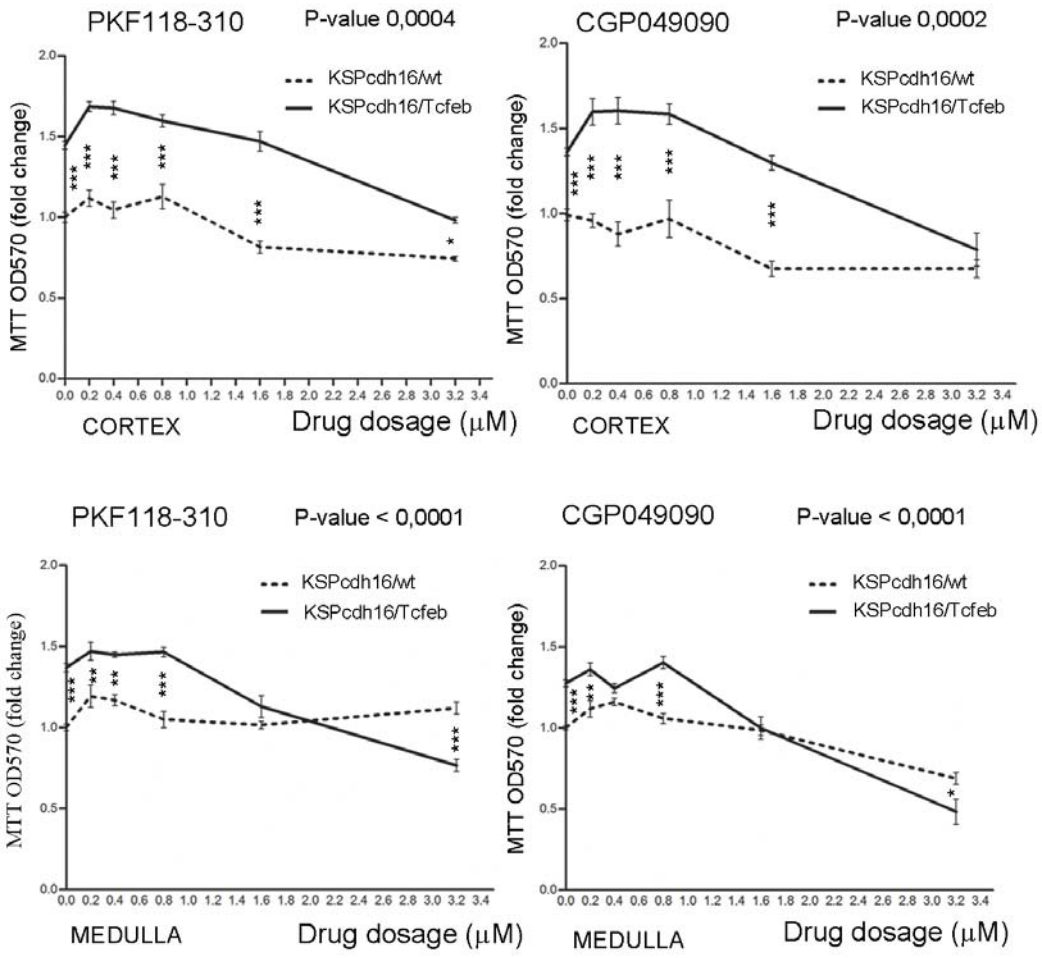

Figure 42. Inhibition of WNT signalling rescues the hyper-proliferative phenotype of kidney cells from *KSPcdh16/Tcfeb* mice.

MTT proliferation assays of primary kidney cells treated independently with two WNT signalling inhibitors, PKF118-310 and CGP049090, added at different dosages for 24 hours. 0 μm represents the basal proliferation of cells. Values are shown as means (± SEM) of three replicates per point normalized to the vehicle (DMSO), added at the same concentration, and versus the *KSPcdh16/wt* cells without drug treatment. Results are representative of three independent experiments performed on three *KSPcdh16/Tcfeb* and *KSPcdh16/wt* mice. Two-way Anova was applied (factors: cell genotype, treatment).

Moreover βcatenin and CCND1 protein levels were highly reduced after PKF118-310 treatment (Fig. 43).

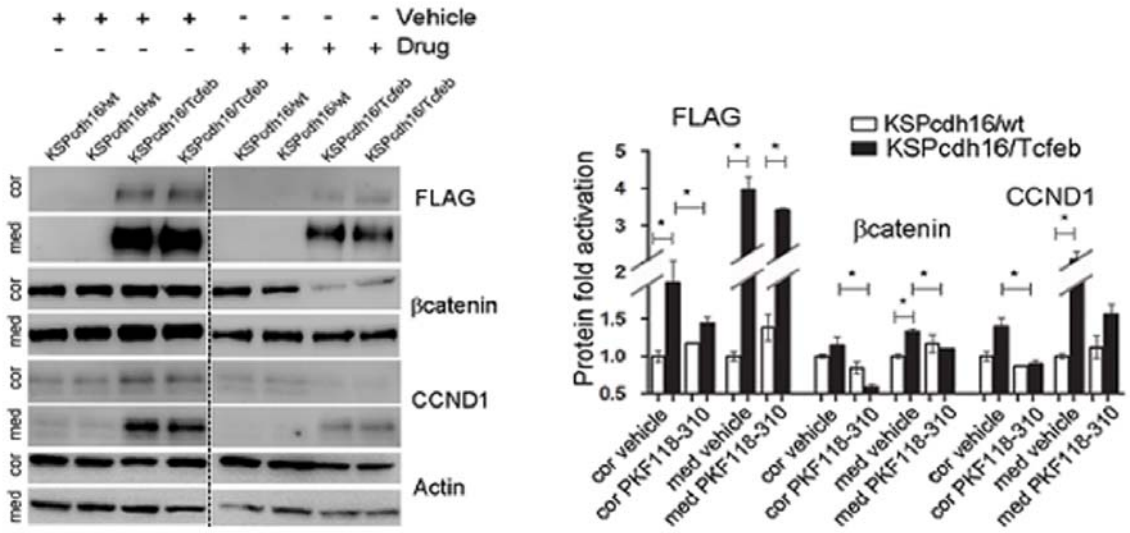

Figure 43. Molecular and analysis of WNT signalling after PKF118-310 treatment.

Immunoblot analysis on primary kidney cells treated with Drug (PKF118-310) or Vehicle (DMSO) for 24 hours at 1.6 μM. Graphs show the densitometry quantifications of Western blot bands. Values are normalized to actin and are shown as averages (± SEM) (Cor, cortex; Med, medulla). (* P <0.05, ** P < 0.01, *** P < 0.001).

Based on the results obtained in primary kidney cells, we tested whether WNT inhibition could ameliorate the disease phenotype *in vivo*. P21 *KSPcdh16/Tcfeb* transgenic animals were treated with daily IP injections of PKF118-310 for 30 days. At the end of the treatment they showed an almost complete rescue of the observable renal pathology (Fig.44A) and nearly normal KW/BW ratios (Fig. 44B, C).

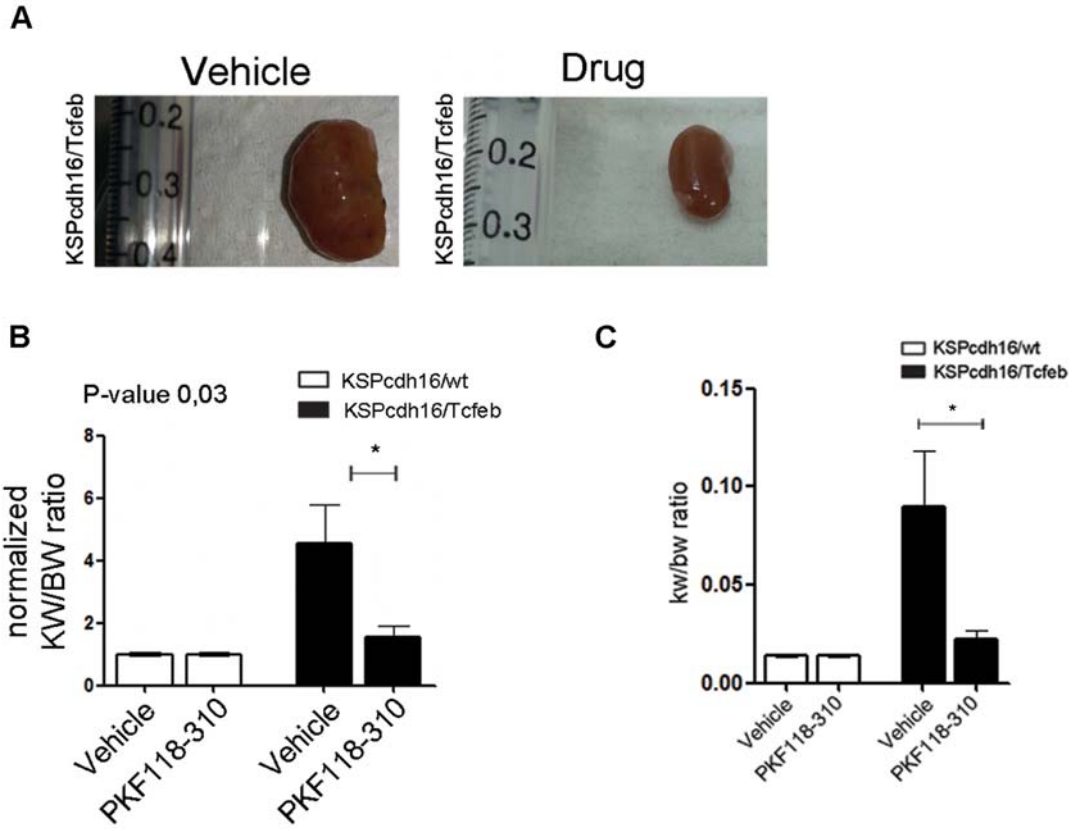

Figure 44. Treatment with WNT inhibitor reduces kidney size.

KSPcdh16/Tcfeb mice treated with Vehicle (DMSO) or Drug (PKF118-310). Pictures (A) and sizes (KW/BW) (B) of kidneys from *KSPcdh16/Tcfeb* mice injected Intraperitoneally (IP) either with vehicle or drug at 0.85mg/kg. KW/BW ratios are shown as means (± SEM) and values are normalized to the *KSPcdh16/wt* animals treated with vehicle. C) KW/BW ratio of Vehicle and Drug treated mice. Two-way Anova was applied (factors: treatment, genotype). KW/BW data are relative to: 3 Vehicle-treated *KSPcdh16/wt* mice, 5 Drug-treated *KSPcdh16/wt* mice*, 5* Vehicle-treated *KSPcdh16/Tcfeb mice* and 5 Drug-treated *KSPcdh16/Tcfeb* mice,

Moreover, we observed a significant reduction of many parameters of cystic and neoplastic pathology, such as the number and size of cysts and neoplastic papillae, and the levels of Ki67 (Fig. 45A, B, Fig. 46).

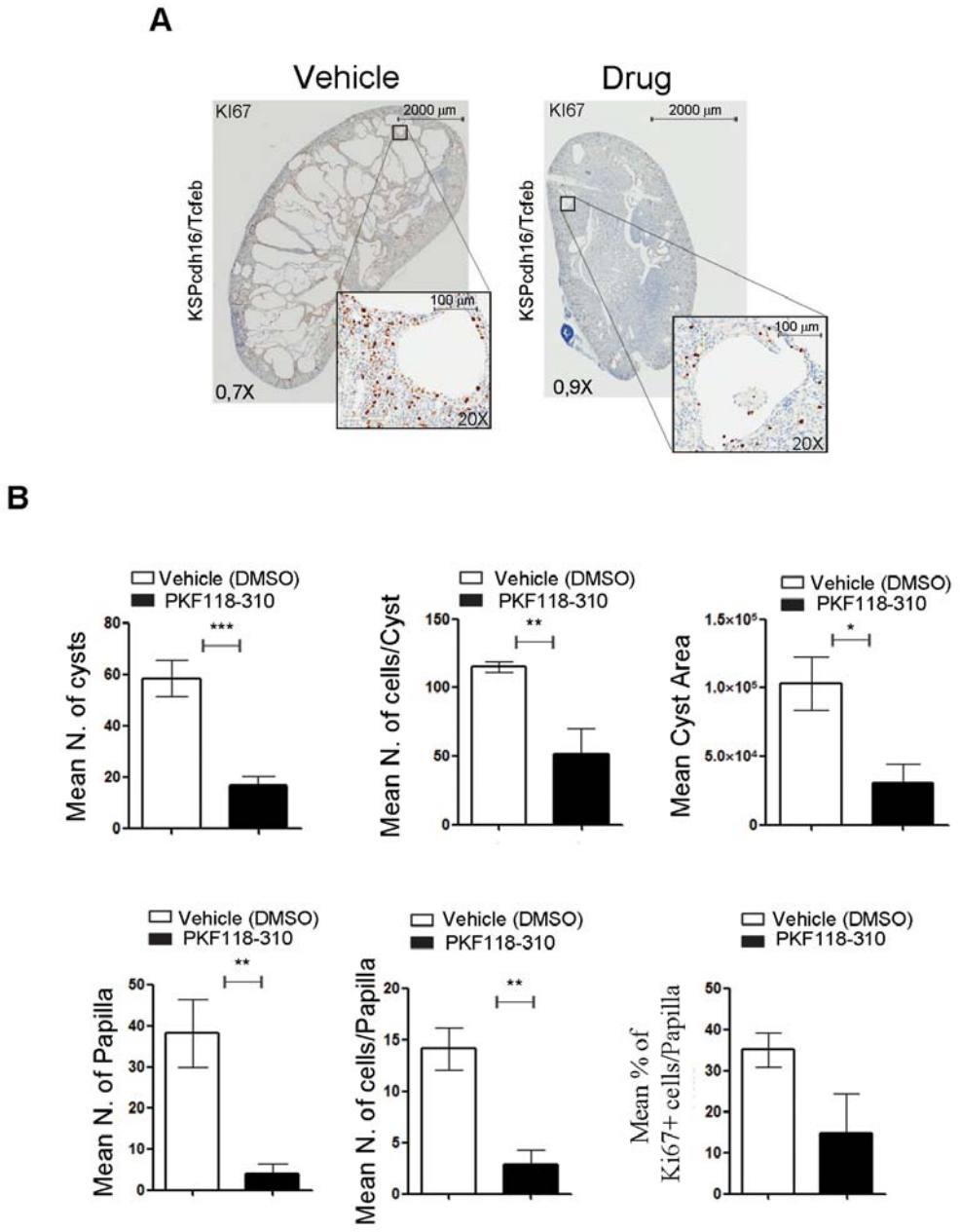

Figure 45. Treatment with WNT inhibitor attenuates cystic and neoplastic phenotypes.

A) Ki67 staining of kidneys from *KSPcdh16/Tcfeb* mice after treatment with vehicle or drug. Insets are enlargements of a single cyst. B) Quantification of several parameters related to cysts and papillae performed on kidney sections from vehicle- and PKF118-310-treated *KSPcdh16/Tcfeb* mice. Data are relative to 6 Vehicle- and Drug-treated *KSPcdh16/Tcfeb* mice. This analysis was done in collaboration with Prof. Di Fiore in IEO (European Institute of Oncology). The oncologic characterization was performed by Dott. Bertalot in IEO.

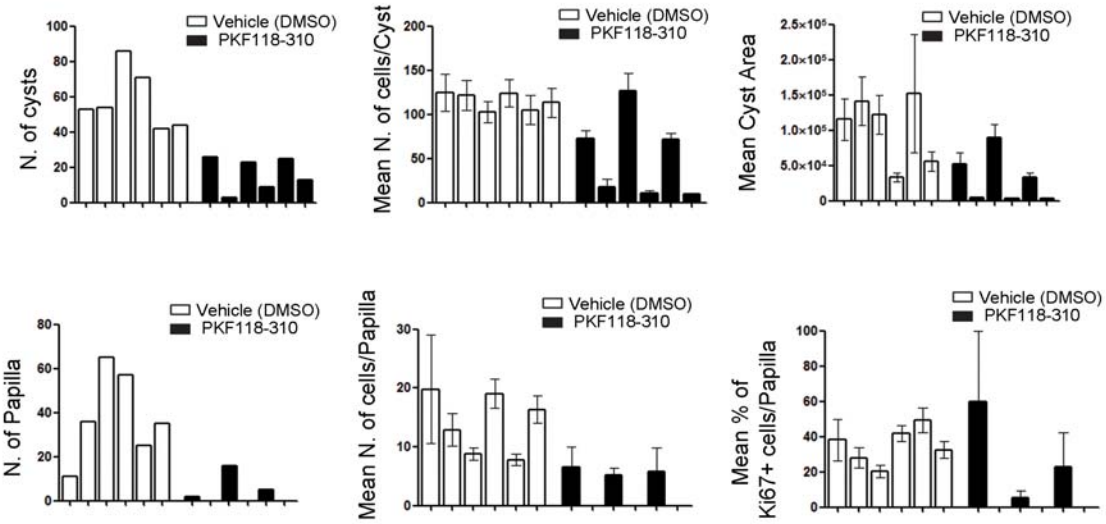

Figure 46. Treatment of *KSPcdh16/Tcfeb mice* with the WNT inhibitor PKF118-310 partially rescues cystic and neoplastic phenotypes.

Measurements of different parameters related to the cystic and papillary phenotype on 6 animals treated with Vehicle (DMSO) and 6 animals treated with Drug (PKF118-310). Values are shown as means (± SEM) when appropriate and are represented separately for each animal. This analysis was done in collaboration with Prof. Di Fiore in IEO (European Institute of Oncology). The oncologic characterization was performed by Dott. Bertalot in IEO.

We confirmed that drug-treatment in *KSPcdh16/Tcfeb* mice suppressed the WNT pathway both at the mRNA and protein levels, as shown by the reduction of the mRNA levels of the WNT direct gene targets Cyclin D1, c-Myc and Axin2 (Fig. 47), by the reduction of Cyclin D1 and c-MYC proteins (Fig. 48) and by the decrease of Cyclin D1-positive nuclei in *KSPcdh16/Tcfeb* drug-treated mice (Fig.49).

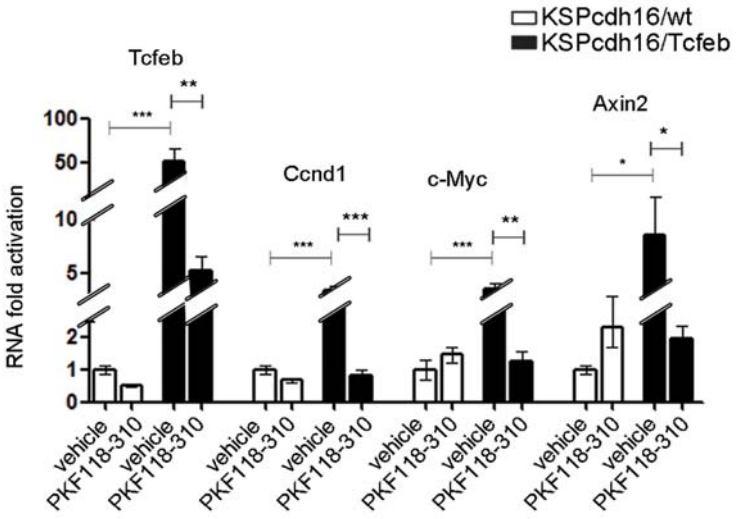

Figure 47. ***In vivo*** **treatment of *KSPcdh16/Tcfeb* mice with the PKF118-310 drug inhibits WNT target genes**

Tcfeb, Cyclin D1, *c-Myc* and *Axin2* mRNA levels in kidneys from *KSPcdh16/wt* and *KSPcdh16/Tcfeb* mice treated with vehicle or PKF118-310. Values are shown as the average (± SEM) of four animals per group, and are all normalized to the *KSPcdh16/wt* mice treated with vehicle. Two-way Anova was applied (factors: cell genotype, treatment) (* P <0.05, ** P < 0.01, *** P < 0.001).

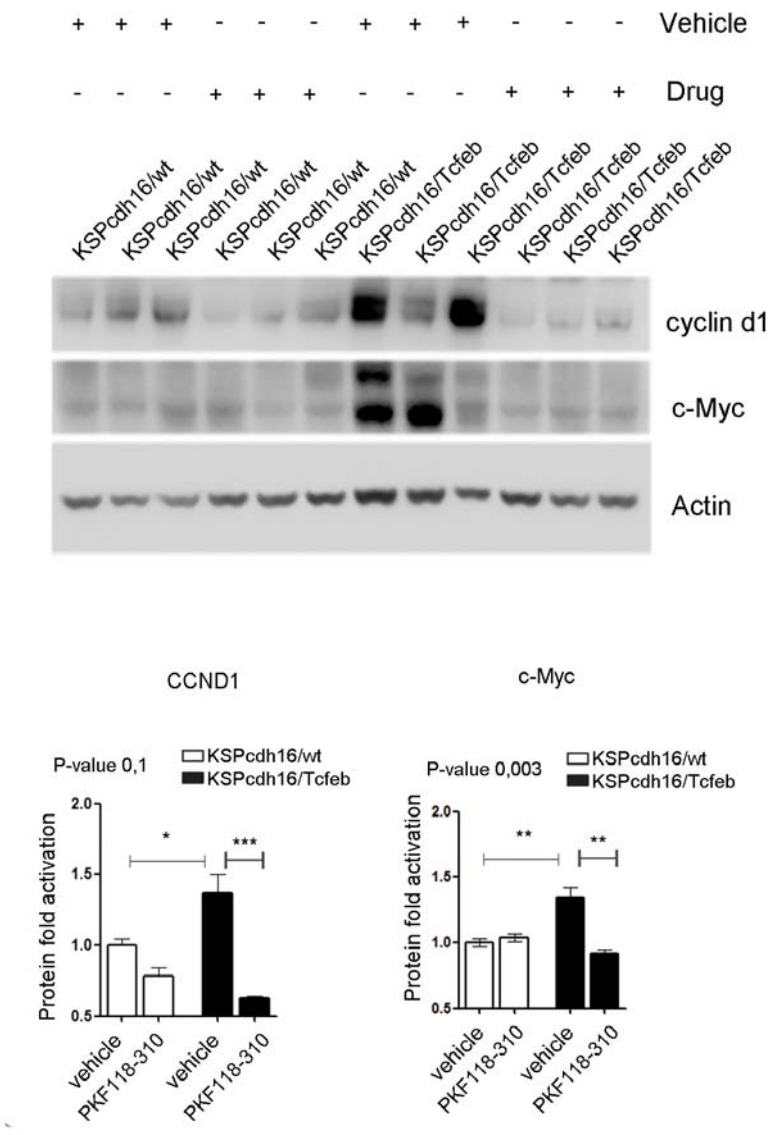

Figure 48. *In vivo* treatment of *KSPcdh16/Tcfeb* mice with the PKF118-310 drug inhibits WNT pathway overactivation

Biochemical analysis performed on *KSPcdh16/wt* and *KSPcdh16/Tcfeb* mice treated with vehicle or PKF118-310. Each replicate is a distinct biological sample. Cyclin D1 and c-MYC protein levels were quantified by densitometry analysis of Western blot bands. Values are normalized to actin when not specified, and are shown as an average (± SEM). Two-way Anova was applied (factors: cell genotype, treatment) (* P <0.05, ** P < 0.01, *** P < 0.001).

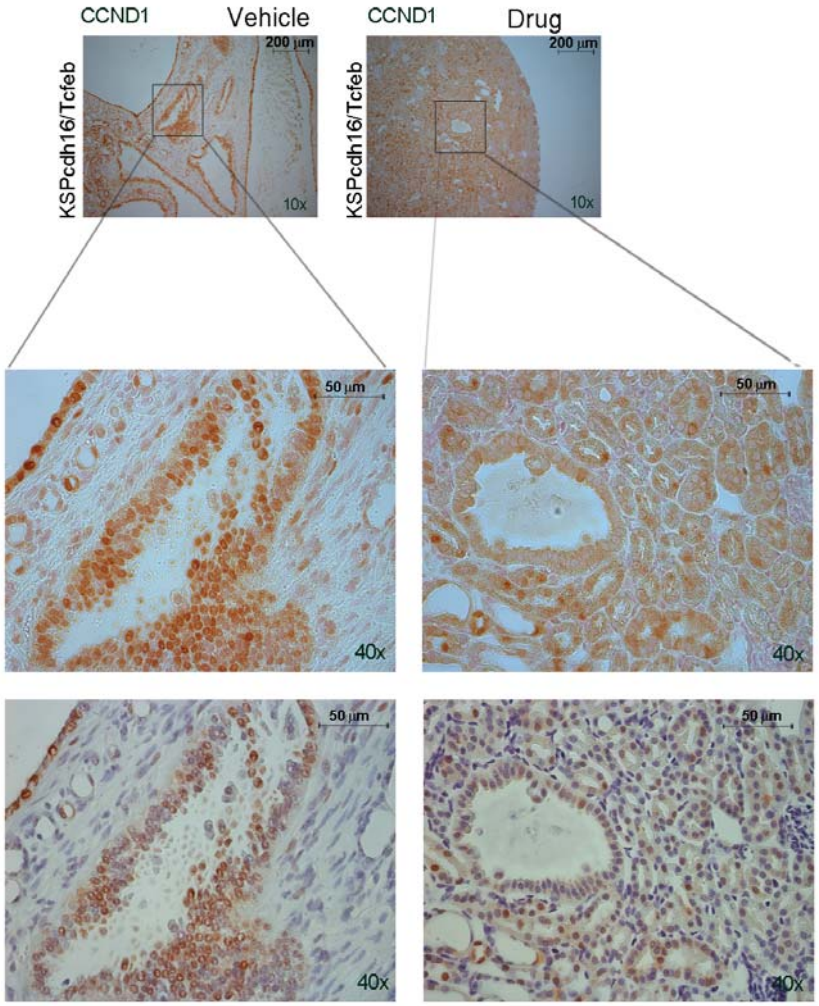

Figure 49. *In vivo* treatment of *KSPcdh16/Tcfeb* mice with the PKF118-310 drug inhibits Cyclin D1 nuclear accumulation

Cyclin D1 staining performed on Drug- and Vehicle- treated *KSPcdh16/Tcfeb* mice before and after the hematoxylin counterstaining. This IHC staining was performed on six Drug- and Vehicle-treated *KSPcdh16/Tcfeb* mice.

Furthermore, WNT inhibition resulted in normalization of expression levels of the gene encoding the transmembrane Glycoprotein NMB (*GPNMB*) (Fig. 50A, B), a known marker of melanomas, gliomas and breast cancers, which is also overexpressed in *TFE*-fusion *ccRCCs* (Malouf *et al*, 2014; Zhou *et al*, 2012).

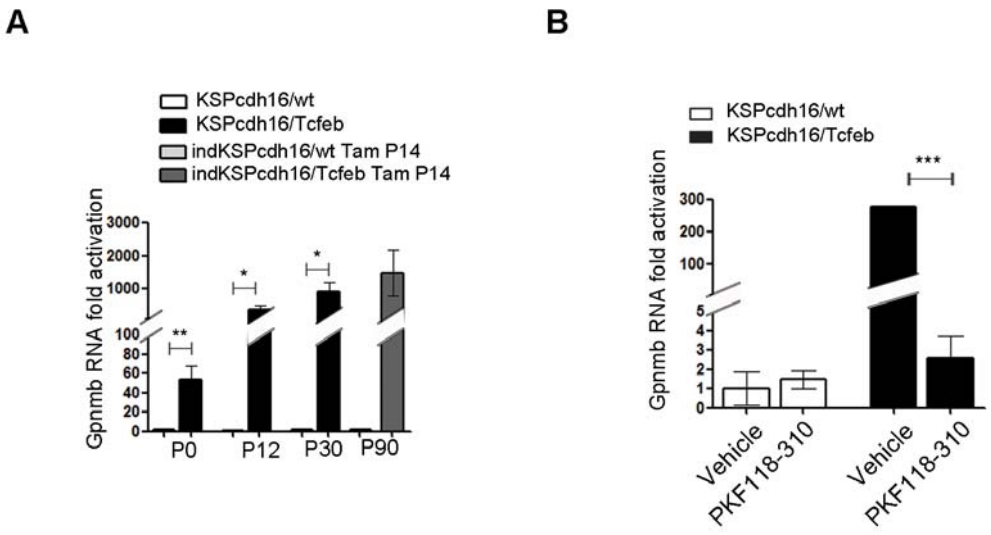

Figure 50. Gpnmb gene expression levels.

Gpnmb mRNA fold activation in kidneys from *KSPcdh16/Tcfeb* and Tam-treated *indKSPcdh16/Tcfeb* mice at different stages. Values are shown as means (± SEM) of at least three mice and each group is normalized to the proper control (respectively *KSPcdh16/wt* and tam-treated *indKSPcdh16/wt*). B) Gpnmb fold activation in kidneys from *KSPcdh16/Tcfeb* mice treated with vehicle or PKF118-310. Values are shown as means (± SEM). We analysed 4 *KSPcdh16/wt* vehicle-treated animals, 5 *KSPcdh16/wt* drug-treated animals, 4 *KSPcdh16/ Tcfeb* vehicle-treated animals and 4 *KSPcdh16/ Tcfeb* drug-treated animals., and all the values were normalized versus the *KSPcdh16/wt* mice treated with vehicle. (* P <0.05, ** P < 0.01, *** P < 0.001, two-sided Student's *t* test).

Interestingly, *GPNMB* gene resulted to be induced in both the microarray data set, as well as in *TFE3*-tRCC patients, and showed multiple CLEAR elements in its promoter (Table 4).

..

A

Probe Set ID	Gene Symbol	Gene Title	Representative Public ID	Ensembl	ratio (KSP_P0/CTL)	ratio (KSP_P14/CTL)	ratio (RCC/CTL)
1448303_at	Gpnmb	glycoprotein (transmembrane) nmb	NM_053110	ENSMUSG00000029816	10,61359	4,926016	141,4101

B

Gene	Score	Sequence	Chrom	ABS Start	ABS End	TSS_Position
Gpnmb	0,8731563	GGGGCAAGTGACTC	chr6	49036518	49036531	1
Gpnmb	0,803943	ACATCACATGATCT	chr6	49036587	49036600	70
GPNMB	0,8484716	CCATCACATGATCC	chr7	23286328	23286341	13

Table 4. GPNMB expression table.

Differentially expression of Gpnmb transcript in KSP_P0 (GSE62977), in KSP_P14 microarray dataset (GSE63376) and in RCC dataset. B) Sequence analysis of the CLEAR sites (i.e. the consensus TFEB binding sites) in the human and murine promoter region of Gpnmb.

Finally, the overlap of the KSP_P0 microarray dataset with a ChIP-Seq on HeLa TFEB-overexpressing cells (Sardiello *et al*, 2009), revealed that *GPNMB* was shared in both datasets, suggesting to act as a TFEB direct gene target (Table 5).

Gene Symbol	signed_ratio (KSP_P0/CTL)	chromosome	start	stop	peak tags	distance from 5' end of gene	RefSeq ID	symbol	ID	ABS distance
Elf3	1,881188134	chr1	201978496	201978977	8	-712	NM_001114309	ELF3	ETS-related transcription factor Elf-3	712
Gna13	1,504591673	chr17	63052978	63053379	8	-58	NM_006572	GNA13	guanine nucleotide-binding protein subunit	58
Ankrd12	1,599217835	chr18	9136350	9137025	15	0	NM_015208	ANKRD12	ankyrin repeat domain 12 isoform 1	0
Atp6v1c1	1,658752808	chr8	104033021	104033525	15	0	NM_001695	ATP6V1C1	V-type proton ATPase subunit C 1	0
Bhlhe40	2,03490115	chr3	5020679	5021164	10	0	NM_003670	BHLHE40	class E basic helix-loop-helix protein 40	0
Gpnmb	10,61358979	chr7	23286042	23286524	9	0	NM_002510	GPNMB	transmembrane glycoprotein NMB isoform b	0
Kdm6a	1,58385317	chrX	44732031	44732628	33	0	NM_021140	KDM6A	lysine-specific demethylase 6A	0
Lats2	1,761917857	chr13	21635470	21636098	22	0	NM_014572	LATS2	serine/threonine-protein kinase LATS2	0
Ppargc1a	2,713649997	chr4	23891451	23891989	11	0	NM_013261	PPARGC1A	peroxisome proliferator-activated receptor gamma	0
Rnf146	1,700903945	chr6	127587589	127588198	14	0	NM_030963	RNF146	ring finger protein 146	0
Usp2	2,284889961	chr11	119252322	119252760	8	0	NM_004205	USP2	ubiquitin specific peptidase 2 isoform a	0

Table 5. Microarray and ChIP-Seq overlap.

List of 11 genes shared between the KSP_P0 dataset and from an HeLA TFEB-overexpressing ChIP-Seq dataset.

6. Autophagy is not required for disease progression

Considering the known role of TFEB as a master regulator of the lysosomal-autophagy pathway (Argani *et al*, 2001, 2005; Camparo *et al*, 2008; Davis *et al*, 2003), and the recent evidence indicating that activation of autophagy driven by MiT/TFE genes plays an important role in pancreatic cancer (Perera *et al*, 2015), we tested whether autophagy plays a role in *TFE*-tRCC development. We analysed the expression levels of a well-characterized panel of TFEB target genes known to be involved in lysosomal biogenesis and autophagy in *KSPcdh16/Tcfeb* mice. Surprisingly, no significant changes in the expression levels of these genes

were detected in *KSPcdh16/Tcfeb* compared to wild type mice, with a few exceptions (Fig. 51).

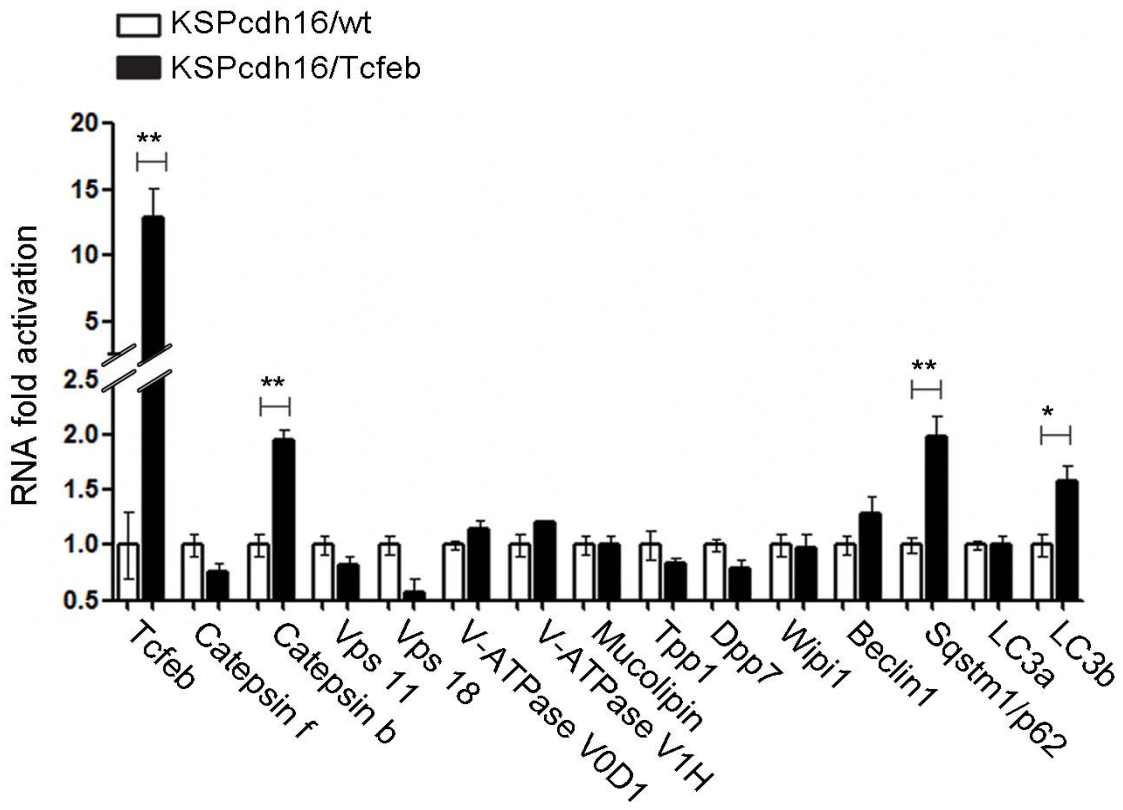

Figure 51. Expression analysis of lysosomal and autophagy genes in Tcfeb overexpressing mice.

Real-time PCR validation of well-known TFEB direct gene targets whose function is related to the lysosomal and autophagic pathways performed on P30 *KSPcdh16/Tcfeb* mice. Values are shown as the average (± SEM) of three *KSPcdh16/Tcfeb* mice and are normalized to wild type mice (* P <0.05, ** P < 0.01, *** P < 0.001, two-sided Student's *t* test).

Consistently, immunoblot analysis of the autophagy marker LC3 in kidneys from transgenic mice did not reveal any significant changes compared to control littermates until P90, where we could detect a reduction of the LC3-II band consistent both with an increase or a reduction of the autophagic flux (Fig. 52).

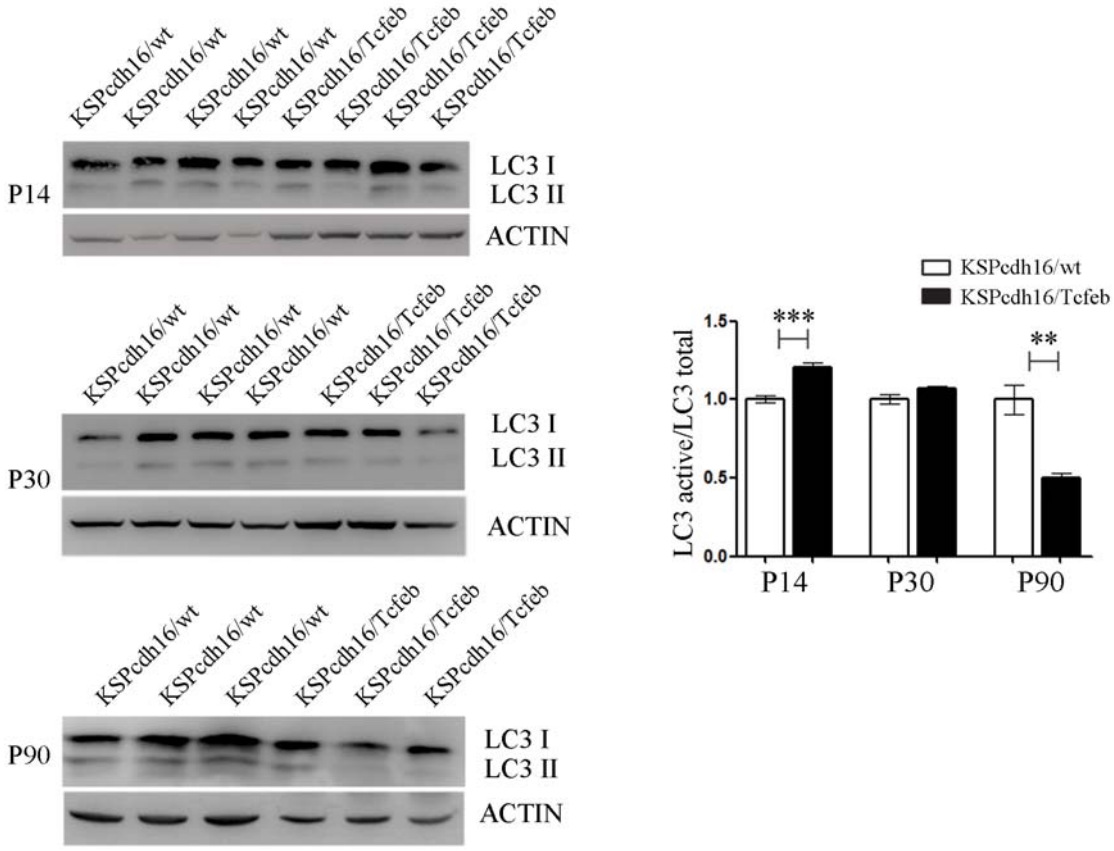

Figure 52. Biochemical analysis of LC3I/II protein.

P14 and P30 kidney lysates from *KSPcdh16/Tcfeb* animals were evaluated by LC3I/II immunoblot. LC3 active / LC3 total ratios were quantified via densitometry of the Western blot bands (graph). Each replicate is a different biological sample. Values are shown as the average (± SEM) of at least three *KSPcdh16/Tcfeb* mice and are normalized to wild type lines. (* P <0.05, ** P < 0.01, *** P < 0.001, two-sided, Student's *t* test).

Consequently, to test the role of autophagy in the pathogenesis of *TFE*-tRCC we crossed *KSPcdh16/Tcfeb* mice with autophagy-deficient *ATG7*$^{flox/flox}$ mice. *ATG7-/-;KSPcdh16 and ATG7-/-;KSPcdh16/Tcfeb* animals, as expected, didn't show ATG7 protein expression in the kidneys (Fig. 53A), but LC3 staining resulted to be highly enhanced in *ATG7-/-;KSPcdh16/Tcfeb* animals (Fig. 53B), suggesting that TFEB-overexpressing mice had an increased autophagic flux.

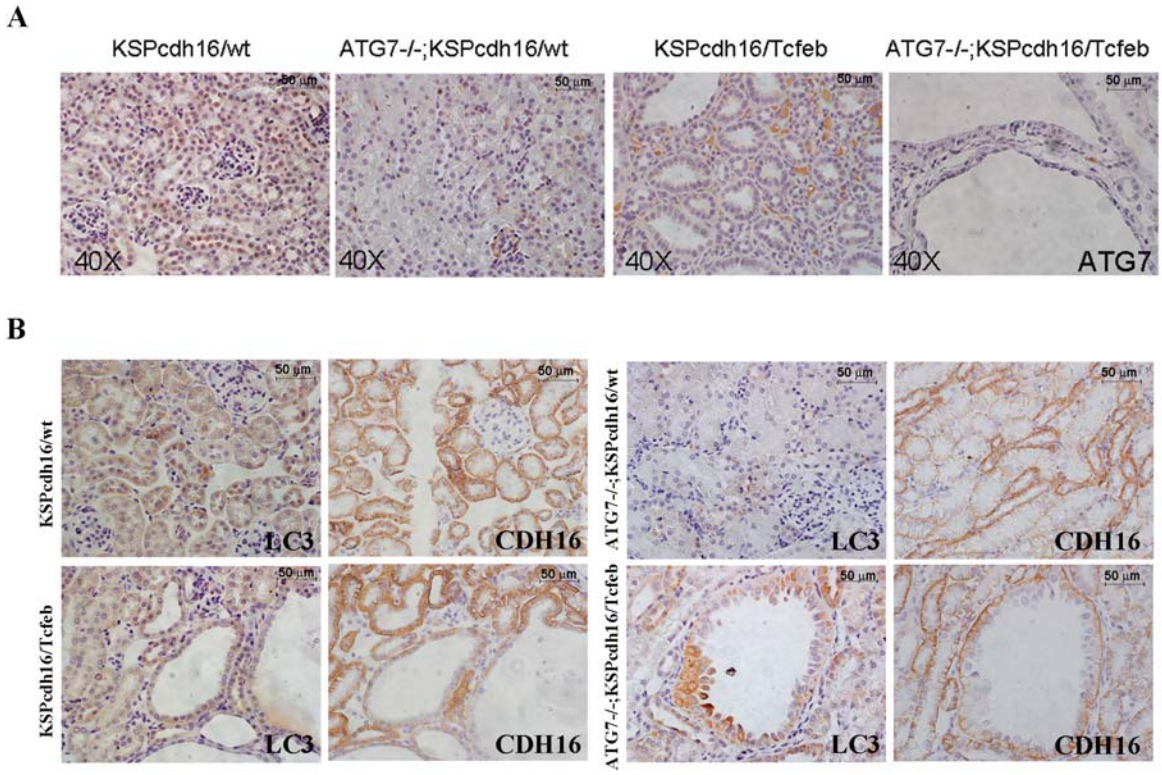

Figure 53. ATG7 and LC3 immunohistochemistry in ATG7-/-;KSPcdh16/Tcfeb mice.

ATG7 (A) and LC3 (B) staining of kidneys from *KSPcdh16/Tcfeb* and *ATG7-/-;KSPcdh16/Tcfeb* mice.

Despite this, no changes in kidney size or in the cystic phenotype were observed in TFEB overexpressing/autophagy-deficient double transgenic mice (*ATG7-/-;KSPcdh16/Tcfeb)* compared to *KSPcdh16/Tcfeb* mice (Fig. 54A, B, C).

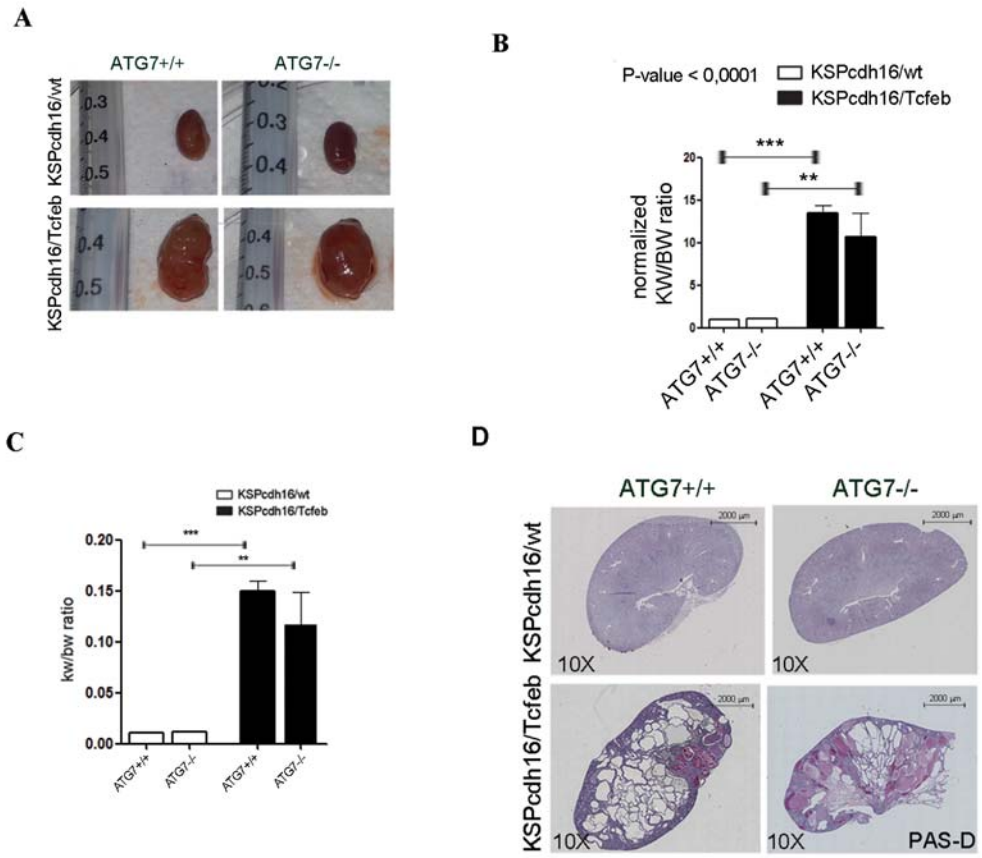

Figure 54. Inhibition of autophagy in Tcfeb overexpressing mice does not affect the cystic phenotype.

A) Renal images of (*ATG7-/-;KSPcdh16/Tcfeb)* double transgenic mice and controls at P30. B) Kidney-to-body weight ratio (KW/BW) from the different genotypes obtained. We analysed 5 *ATG7+/+;KSPcdh16/wt* mice, 3 *ATG7-/-;KSPcdh16/wt mice,* 12 *ATG7+/+;KSPcdh16/Tcfeb* mice and 5 *ATG7-/-;KSPcdh16/Tcfeb* mice. Values are normalized to the *ATG7+/+;KSPcdh16/wt* line and are shown as an average (± SEM). One-way Anova was applied (factors: genotype) (* P <0.05, ** P < 0.01, *** P < 0.001). C) PAS staining of kidneys from the different mouse lines.

These results suggest that autophagy does not play a critical role in the development of *TFE*-tRCC phenotype.

DISCUSSION

Kidney cancers associated with translocations of *TFE* genes represent a major unmet medical need (Argani & Ladanyi, 2005; Komai *et al*, 2009; Malouf *et al*, 2014). Unfortunately, little is known about the mechanisms underlying this type of tumours.

In most cases *TFEB*-tRCCs are associated to a well-characterized chromosomal translocation involving the TFEB gene and the non-coding Alpha gene, generating the alpha-*TFEB* fusion (t(6;11)(p21.2;q13) (Davis *et al*, 2003; Kuiper, 2003). Until recent reports, *TFEB* breakpoints were in all cases located upstream exon 3, allowing the retention of the entire TFEB coding sequence (Davis *et al*, 2003; Argani *et al*, 2005; Inamura *et al*, 2012) and leading to a promoter substitution event resulting in a strong up-regulation of the *TFEB* transcript and protein up to 60-times (Kuiper, 2003). Only recently a new breakpoint was identified within exon 4, but the protein size appears to be the same as the wild-type protein (Inamura *et al*, 2012). Rarely, *TFEB* translocation partners were the *KHDBRS2* (*inv(6)(p21;q11)*) (Malouf *et al*, 2014) and the *CLTC* (*t(6;17)(p21;q23)*) genes (Durinck *et al*, 2015). Regarding *TFE3*-tRCCs, *TFE3* gene can translocate with 5 known gene partners (i.e. *PRCC*, *ASPSCR1*, *SFQP*, *NONO*, *CLTC*), thus generating different fusion proteins. The identification of multiple *TFE3*-gene partners and the characterization of some of them (Clark *et al*, 1997) strongly suggested that RCC is caused by *TFE3*, rather than by its partners (Kauffman *et al*, 2014). Indeed, *TFE3* fusion protein resulted to be much more stable and transcriptionally active than the wild-type protein (Weterman *et al*, 2000). Together, these data suggest that the first step, and driving force, of the disease pathological cascade is the

overexpression of active TFEB and TFE3 proteins, which is likely associated to an increase of their transcriptional activity.

Currently, there are no model systems to study the mechanisms underlying *TFE*-tRCC kidney tumours and to identify and test new therapeutic strategies. Moreover, there are very limited data available on the biological pathways involved in these tumours. The mTOR pathway (Argani *et al*, 2010) and the MET-tyrosine kinase receptor (Tsuda *et al*, 2007) were found up-regulated in *TFE*-tRCC patients, but targeting of these pathways failed to be effective in therapy (Malouf *et al*, 2010; Wagner *et al*, 2012; Kauffman *et al*, 2014). The lack of mechanistic insights in *TFE*-t*RCCs* has hampered the identification of effective therapeutic strategies (Kauffman *et al*, 2014). Some patients with metastatic *TFE3*-tRCC have been treated with inhibitors of ErbB receptors and of the mTOR pathway. Unfortunately, most of these patients relapsed after an initial period of remission (Parikh *et al*, 2009; Wu *et al*, 2008).

The lack of knowledge of the mechanisms underlying *TFE*-t*RCCs* prompted us to generate transgenic mouse models that overexpress *TFEB* in the kidney, thus mimicking the human disease. We generated two transgenic mouse models overexpressing *TFEB* in the epithelial cells of the kidney in either a constitutive (*KSPcdh16/Tcfeb*) or an inducible (*IndKSPcdh16/Tcfeb*) manner. A severe renal cystic pathology associated with a significant increase in renal size was observed in these mice. In the constitutive model, cysts arose from the collecting ducts and distal tubules, whereas in the inducible one they derived from proximal and distal tubules. Our results were in line with previous studies on mouse models of polycystic kidney disease, showing that cysts may originate from different cell types (Lantinga-van Leeuwen et al. 2007) (Happé et al. 2009) (Leonhard et al. 2016). These differences were explained considering that different renal segments

showed different sensitivity to external stimuli thus leading to different cellular responses over time (Lantinga-van Leeuwen et al. 2007) (Happé et al. 2009) (Leonhard et al. 2016) (Piontek et al. 2007).

We observed that cysts were either single- or multi-layered. Epithelial cells lining the mono-layered cysts often lost their cuboidal shape, becoming flattened. Further analyses revealed the presence of protein casts inside the cysts and multi-layered basal membranes in the regions surrounding the cysts, due to collagen deposition. Interestingly, the presence of fibrosis, mBMs and tubular or cystic structures covered by a single layer of flattened, cuboidal, and columnar cells is also observed in human patients affected by *TFEB*-tRCCs (Rao *et al*, 2012, 2013). Finally, in both types of transgenic lines we observed the presence of highly enlarged cells with a clear cytoplasm, that closely resemble the “Clear Cells” found in human patients with RCC (Rao *et al*, 2012).

Transgenic mice also displayed a higher glucose metabolism, as shown by PET-scan performed in P30 animals suggesting the presence of renal cancer. At P12, *KSPcdh16/Tcfeb* mice already presented cystic changes together with neoplastic nodules that were Ki67-positive. The progressive hyper-proliferation of these nodules resulted in the development of numerous neoplastic lesions with both solid and cystic appearance, ranging from 0.102 to 2.93 mm and sometimes showing local invasion of the surrounding stroma. Additionally, liver metastases ranging from 0.9 to 3.8 mm, were found in both *KSPcdh16/Tcfeb* and ind*KSPcdh16/Tcfeb* mice. In *KSPcdh16/Tcfeb* animals they were detected starting from P90 with an incidence of 23%. Liver metastases were positive for Ki67, PAX8 and CDH16, and were negative for cytokeratin 7, consistent with the renal origin of the lesions. These data indicate that the newly-generated transgenic lines bear all major histological and phenotypic features of human *TFE*-tRCC (Kauffman *et al*,

2014; Rao *et al*, 2012, 2013), thus representing excellent models to study this disease.

To identify the effect of TFEB overexpression on the kidney transcriptome we performed microarray analysis on kidney samples from P0 *KSPcdh16/Tcfeb* mice. Unexpectedly, transgenic mice did not show a significant induction of the autophagy machinery. We checked by Real-Time PCR the expression levels of some of the well-characterized lysosomal and autophagy TFEB gene targets, and we could detect the induction of only a few of them. Moreover, crossing of these animals with an autophagy deficient *ATG7*$^{flox/flox}$ mouse line failed to revert the disease phenotype. In conclusion, we couldn't find the presence of a strong transcriptional program activating autophagy in the kidney and the specific block of this pathway didn't show effects on the disease phenotype. We believe that the overexpression of TFEB in this specific tissue during embryogenesis prompted the induction of a different pool of genes. Indeed, transcriptome analysis revealed a significant induction of genes involved in the WNT pathway, such as WNT direct target genes *Ccnd1*, *c-Myc* and *Axin2* and WNT-related genes *Fzd3*, *Rnf146* and *Kdm6a*. This transcriptional induction was consistent with increased protein levels of total βcatenin, active-βcatenin, CCND1 and pLRP6 (Ser1490)/ LRP6 ratio. Furthermore, an induction of the phospho-GSK3β (Ser9)/ GSK3β ratio, an inactive form of the GSK3β kinase, was detected at later stages. Hyper-activation of the WNT pathway was also observed in cortical and medullary primary kidney cells derived from *KSPcdh16/Tcfeb* mice. Most importantly, luciferase assays performed on HEK-293 and HK-2 cells revealed that TFEB overexpression resulted in a significant enhancement of WNT pathway activation.

WNT signalling is of central importance for the development of many organs and has been implicated in tumour pathogenesis at different sites. Its activation

requires the formation of the WNT signalosome, resulting from the binding of WNT ligands to Frizzled (Fzd) receptors. This mediates the interaction of Fzd with LRP5/6 proteins. Fzd-LRP5/6 hetero-oligomerization is required to sequester the βCatenin degradation complex, containing several kinases such as GSK3 and CK1. GSK3 is then able to phosphorylate LRP but not βCatenin. Active-βCatenin, which is the non-phosphorylated form of βCatenin, translocates into the nucleus and activates its target genes, such as *C-MYC*, *AXIN2* and *CCND1* (Clevers, 2006b), by interacting with the TCF4/LEF1 transcription factors (Voronkov & Krauss, 2013).

Interestingly, hyper-activation of the WNT pathway was recently detected in a melanoma cell line in which MITF, another member of the MiT/TFE family, was overexpressed, leading to an expansion of the endo-lysosomal compartment that in turn was able to concentrate and relocate the WNT signalosome/destruction complex and consequently to enhance WNT signalling (Ploper *et al*, 2015). In addition, several studies have linked alterations in the regulation of the βcatenin pathway to abnormalities of kidney development and function (Vainio & Uusitalo, 2000). Indeed, βcatenin is necessary for proper regulation of the *PKD1* promoter (Rodova *et al*, 2002), that is mutated in 85% of patients with Autosomal Dominant Polycystic Kidney Disease (ADPKD). Unlikely, the role of WNT pathway in cyst pathogenesis is still controversial. Mice with overexpression of the Pkd1 transgene developed high levels of MYC protein and cystogenesis (Thivierge et al, 2006). Conversely, it was recently shown that WNTs can bind the extracellular portion of PKD1, thus resulting in whole cell current and Calcium influx, and mutations of PKD1 or PKD2 genes suppress the WNT-induced Calcium currents and led to cystogenesis (Kim et al. 2016). Furthermore, the WNT pathway is also known to play a role in renal tumour formation, such as Wilm's tumour (Koesters *et al*, 1999;

Zhu *et al*, 2000; Kim *et al*, 2000). Mice lacking the *Apc* gene specifically in the kidney are prone to the development of cystic renal cell carcinomas (Sansom *et al*, 2005). Finally, cytoplasmic accumulation of βcatenin was observed in patients with *TFE3*-tRCC, suggesting the presence of a possible link between *TFE*-factors and WNT-signaling components (Bruder *et al*, 2007). Together these studies reveal a strong link between hyper-activation of WNT signalling and tumorigenesis in the kidney and reinforce our finding of WNT hyper-activation in TFEB transgenic mice as a critical step of the disease pathogenesis.

Based on this evidence, we postulated that treatment with WNT inhibitors had beneficial effects on *TFE*-tRCCs. To test this hypothesis, we treated primary kidney cells from *KSPcdh16/Tcfeb* mice with two small molecules, PKF118-310 and CGP049090, able to inhibit the WNT pathway by disrupting the interaction between βcatenin and TCF-4 (Avila *et al*, 2006). Drug treatments significantly reduced the hyper-proliferation rate observed in cells from transgenic mice, bringing it to normal levels. Therefore, we sought to reproduce these data *in vivo* by treating *KSPcdh16/Tcfeb* mice with WNT inhibitors. Administration of the PKF118-310 molecule or vehicle for 30 days resulted in a substantial reduction of several important parameters, such as kidney size, cyst number and size, Ki67 index and the number of neoplastic papillae. Moreover, drug-treated *KSPcdh16/Tcfeb* animals showed a significant decrease in the mRNA levels of Gpnmb, a known marker of melanomas, gliomas and breast cancer, which was reported to be overexpressed in *TFE*-fusion *ccRCCs* (Malouf *et al*, 2014; Zhou *et al*, 2012). Interestingly, we also found that Gpnmb is a direct transcriptional target of TFEB (Sardiello *et al*, 2009).

This study provides direct evidence that overexpression of *TFEB* in the kidney is able to generate a severe cystic pathology associated with the development of

kidney cancer and liver metastases, thus mimicking the cancer phenotype associated with human *TFE*-fusion *ccRCCs* chromosomal translocations. Thus, the transgenic mouse lines that we generated represent the first genetic animal models of renal cell carcinoma. The study of these mice revealed that WNT activation plays a crucial role in *TFE*-t*RCCs* and that WNT inhibitors can be used to rescue the phenotype of our transgenic mouse models, suggesting that targeting WNT signalling could be a promising therapeutic approach for the treatment of *TFE*-t*RCC* patients.

BIBLIOGRAPHY

Aberle H, Bauer A, Stappert J, Kispert A & Kemler R (1997) beta-catenin is a target for the ubiquitin-proteasome pathway. *The EMBO journal* **16:** 3797–804

Aksan I & Goding CR (1998) Targeting the microphthalmia basic helix-loop-helix-leucine zipper transcription factor to a subset of E-box elements in vitro and in vivo. *Molecular and cellular biology* **18:** 6930–8 Available at:

Amin MB, Amin MB, Tamboli P, Javidan J, Stricker H, de-Peralta Venturina M, Deshpande A & Menon M (2002) Prognostic impact of histologic subtyping of adult renal epithelial neoplasms: an experience of 405 cases. *The American journal of surgical pathology* **26:** 281–91

Anastas JN & Moon RT (2013) WNT signalling pathways as therapeutic targets in cancer. *Nature reviews. Cancer* **13:** 11–26

Arce L, Yokoyama NN & Waterman ML (2006) Diversity of LEF/TCF action in development and disease. *Oncogene* **25:** 7492–504

Argani P, Antonescu CR, Illei PB, Lui MY, Timmons CF, Newbury R, Reuter VE, Garvin AJ, Perez-Atayde AR, Fletcher JA, Beckwith JB, Bridge JA & Ladanyi M (2001) Primary renal neoplasms with the ASPL-TFE3 gene fusion of alveolar soft part sarcoma: a distinctive tumor entity previously included among renal cell carcinomas of children and adolescents. *The American journal of pathology* **159:** 179–192

Argani P, Hicks J, De Marzo AM, Albadine R, Illei PB, Ladanyi M, Reuter VE & Netto GJ (2010) Xp11 translocation renal cell carcinoma (RCC): extended immunohistochemical profile emphasizing novel RCC markers. *The American journal of surgical pathology* **34:** 1295–1303

Argani P & Ladanyi M (2005) Translocation carcinomas of the kidney. *Clinics in Laboratory Medicine* **25:** 363–378

Argani P, Laé M, Ballard ET, Amin M, Manivel C, Hutchinson B, Reuter VE & Ladanyi M (2006) Translocation carcinomas of the kidney after chemotherapy in childhood. *Journal of Clinical Oncology* **24:** 1529–1534

Argani P, Laé M, Hutchinson B, Reuter VE, Collins MH, Perentesis J, Tomaszewski JE, Brooks JSJ, Acs G, Bridge JA, Vargas SO, Davis IJ, Fisher DE & Ladanyi M (2005) Renal carcinomas with the t(6;11)(p21;q12):

clinicopathologic features and demonstration of the specific alpha-TFEB gene fusion by immunohistochemistry, RT-PCR, and DNA PCR. *The American journal of surgical pathology* **29:** 230–240

Argani P, Lui MY, Couturier J, Bouvier R, Fournet J-C & Ladanyi M (2003) A novel CLTC-TFE3 gene fusion in pediatric renal adenocarcinoma with t(X;17)(p11.2;q23). *Oncogene* **22:** 5374–5378

Arteaga CL & Engelman JA (2014) ERBB receptors: from oncogene discovery to basic science to mechanism-based cancer therapeutics. *Cancer cell* **25:** 282–303

Avila MA, Berasain C, Sangro B & Prieto J (2006) New therapies for hepatocellular carcinoma. *Oncogene* **25:** 3866–84

Baldi P & Long AD (2001) A Bayesian framework for the analysis of microarray expression data: regularized t -test and statistical inferences of gene changes. *Bioinformatics* **17:** 509–519

Ballabio A (2016) The awesome lysosome. *EMBO Molecular Medicine* **8:** 1–4

Bänziger C, Soldini D, Schütt C, Zipperlen P, Hausmann G & Basler K (2006) Wntless, a conserved membrane protein dedicated to the secretion of Wnt proteins from signaling cells. *Cell* **125:** 509–22

Barolo S (2006) Transgenic Wnt/TCF pathway reporters: all you need is Lef? *Oncogene* **25:** 7505–11

Beckmann H, Su LK & Kadesch T (1990) TFE3: a helix-loop-helix protein that activates transcription through the immunoglobulin enhancer muE3 motif. *Genes & development* **4:** 167–79

Belenkaya TY, Wu Y, Tang X, Zhou B, Cheng L, Sharma Y V, Yan D, Selva EM & Lin X (2008) The retromer complex influences Wnt secretion by recycling wntless from endosomes to the trans-Golgi network. *Developmental cell* **14:** 120–31

Bertolotto C, Lesueur F, Giuliano S, Strub T, de Lichy M, Bille K, Dessen P, d'Hayer B, Mohamdi H, Remenieras A, Maubec E, de la Fouchardière A, Molinié V, Vabres P, Dalle S, Poulalhon N, Martin-Denavit T, Thomas L, Andry-Benzaquen P, Dupin N, et al (2011) A SUMOylation-defective MITF germline mutation predisposes to melanoma and renal carcinoma. *Nature* **480:** 94–8

Boletta A & Germino GG (2003) Role of polycystins in renal tubulogenesis. *Trends*

in cell biology **13:** 484–92

Bovolenta P, Esteve P, Ruiz JM, Cisneros E & Lopez-Rios J (2008) Beyond Wnt inhibition: new functions of secreted Frizzled-related proteins in development and disease. *Journal of cell science* **121:** 737–46

Brembeck FH, Rosário M & Birchmeier W (2006) Balancing cell adhesion and Wnt signaling, the key role of beta-catenin. *Current opinion in genetics & development* **16:** 51–9

Brooke MA, Nitoiu D & Kelsell DP (2012) Cell-cell connectivity: desmosomes and disease. *The Journal of pathology* **226:** 158–71

Bruder E, Moch H, Ehrlich D, Leuschner I, Harms D, Argani P, Briner J, Graf N, Selle B, Rufle A, Paulussen M & Koesters R (2007) Wnt signaling pathway analysis in renal cell carcinoma in young patients. *Modern pathology : an official journal of the United States and Canadian Academy of Pathology, Inc* **20:** 1217–29

Bumsted KM & Barnstable CJ (2000) Dorsal Retinal Pigment Epithelium Differentiates as Neural Retina in the Microphthalmia (mi/mi) Mouse. *Investigative Ophthalmology & Visual Science* **41:** 903–908

Camparo P, Vasiliu V, Molinie V, Couturier J, Dykema KJ, Petillo D, Furge KA, Comperat EM, Lae M, Bouvier R, Boccon-Gibod L, Denoux Y, Ferlicot S, Forest E, Fromont G, Hintzy MC, Laghouati M, Sibony M, Tucker ML, Weber N, et al (2008) Renal translocation carcinomas: clinicopathologic, immunohistochemical, and gene expression profiling analysis of 31 cases with a review of the literature. *Am J Surg Pathol* **32:** 656–670

Cancer Genome Atlas Research Network, Linehan WM, Spellman PT, Ricketts CJ, Creighton CJ, Fei SS, Davis C, Wheeler DA, Murray BA, Schmidt L, Vocke CD, Peto M, Al Mamun AAM, Shinbrot E, Sethi A, Brooks S, Rathmell WK, Brooks AN, Hoadley KA, Robertson AG, et al (2016) Comprehensive Molecular Characterization of Papillary Renal-Cell Carcinoma. *The New England journal of medicine* **374:** 135–45

Cang C, Zhou Y, Navarro B, Seo Y-J, Aranda K, Shi L, Battaglia-Hsu S, Nissim I, Clapham DE & Ren D (2013) mTOR regulates lysosomal ATP-sensitive two-pore Na(+) channels to adapt to metabolic state. *Cell* **152:** 778–90

Carroll TJ, Park J-S, Hayashi S, Majumdar A & McMahon AP (2005) Wnt9b plays a central role in the regulation of mesenchymal to epithelial transitions

underlying organogenesis of the mammalian urogenital system. *Developmental cell* **9:** 283–92

Choueiri TK, Vaishampayan U, Rosenberg JE, Logan TF, Harzstark AL, Bukowski RM, Rini BI, Srinivas S, Stein MN, Adams LM, Ottesen LH, Laubscher KH, Sherman L, McDermott DF, Haas NB, Flaherty KT, Ross R, Eisenberg P, Meltzer PS, Merino MJ, et al (2013) Phase II and biomarker study of the dual MET/VEGFR2 inhibitor foretinib in patients with papillary renal cell carcinoma. *Journal of clinical oncology : official journal of the American Society of Clinical Oncology* **31:** 181–6

Clark J, Lu YJ, Sidhar SK, Parker C, Gill S, Smedley D, Hamoudi R, Linehan WM, Shipley J & Cooper CS (1997a) Fusion of splicing factor genes PSF and NonO (p54nrb) to the TFE3 gene in papillary renal cell carcinoma. *Oncogene* **15:** 2233–2239

Clevers H (2006) Wnt/beta-catenin signaling in development and disease. *Cell* **127:** 469–80

Clevers H & Nusse R (2012) Wnt/β-catenin signaling and disease. *Cell* **149:** 1192–205

Cong F & Varmus H (2004) Nuclear-cytoplasmic shuttling of Axin regulates subcellular localization of beta-catenin. *Proceedings of the National Academy of Sciences of the United States of America* **101:** 2882–7

Coudreuse DYM, Roël G, Betist MC, Destrée O & Korswagen HC (2006) Wnt gradient formation requires retromer function in Wnt-producing cells. *Science (New York, N.Y.)* **312:** 921–4

Cronin JC, Wunderlich J, Loftus SK, Prickett TD, Wei X, Ridd K, Vemula S, Burrell AS, Agrawal NS, Lin JC, Banister CE, Buckhaults P, Rosenberg SA, Bastian BC, Pavan WJ & Samuels Y (2009) Frequent mutations in the MITF pathway in melanoma. *Pigment cell & melanoma research* **22:** 435–44

Cselenyi CS, Jernigan KK, Tahinci E, Thorne CA, Lee LA & Lee E (2008) LRP6 transduces a canonical Wnt signal independently of Axin degradation by inhibiting GSK3's phosphorylation of beta-catenin. *Proceedings of the National Academy of Sciences of the United States of America* **105:** 8032–7

Dalgliesh GL, Furge K, Greenman C, Chen L, Bignell G, Butler A, Davies H, Edkins S, Hardy C, Latimer C, Teague J, Andrews J, Barthorpe S, Beare D, Buck G, Campbell PJ, Forbes S, Jia M, Jones D, Knott H, et al (2010)

Systematic sequencing of renal carcinoma reveals inactivation of histone modifying genes. *Nature* **463:** 360–3

Davis IJ, Hsi B-L, Arroyo JD, Vargas SO, Yeh YA, Motyckova G, Valencia P, Perez-Atayde AR, Argani P, Ladanyi M, Fletcher JA & Fisher DE (2003) Cloning of an Alpha-TFEB fusion in renal tumors harboring the t(6;11)(p21;q13) chromosome translocation. *Proceedings of the National Academy of Sciences of the United States of America* **100:** 6051–6056

Davis IJ, Kim JJ, Ozsolak F, Widlund HR, Rozenblatt-Rosen O, Granter SR, Du J, Fletcher JA, Denny CT, Lessnick SL, Linehan WM, Kung AL & Fisher DE (2006) Oncogenic MITF dysregulation in clear cell sarcoma: Defining the MiT family of human cancers. *Cancer Cell* **9:** 473–484

Durinck S, Stawiski EW, Pavía-Jiménez A, Modrusan Z, Kapur P, Jaiswal BS, Zhang N, Toffessi-Tcheuyap V, Nguyen TT, Pahuja KB, Chen Y-J, Saleem S, Chaudhuri S, Heldens S, Jackson M, Peña-Llopis S, Guillory J, Toy K, Ha C, Harris CJ, et al (2015) Spectrum of diverse genomic alterations define non-clear cell renal carcinoma subtypes. *Nature genetics* **47:** 13–21

Edgar R, Domrachev M & Lash AE (2002) Gene Expression Omnibus: NCBI gene expression and hybridization array data repository. *Nucleic acids research* **30:** 207–10

Ferron M, Settembre C, Shimazu J, Lacombe J, Kato S, Rawlings DJ, Ballabio A & Karsenty G (2013) A RANKL-PKCβ-TFEB signaling cascade is necessary for lysosomal biogenesis in osteoclasts. *Genes & development* **27:** 955–69

Fiedler M, Mendoza-Topaz C, Rutherford TJ, Mieszczanek J & Bienz M (2011) Dishevelled interacts with the DIX domain polymerization interface of Axin to interfere with its function in down-regulating β-catenin. *Proceedings of the National Academy of Sciences of the United States of America* **108:** 1937–42

Garraway LA, Widlund HR, Rubin MA, Getz G, Berger AJ, Ramaswamy S, Beroukhim R, Milner DA, Granter SR, Du J, Lee C, Wagner SN, Li C, Golub TR, Rimm DL, Meyerson ML, Fisher DE & Sellers WR (2005) Integrative genomic analyses identify MITF as a lineage survival oncogene amplified in malignant melanoma. *Nature* **436:** 117–22

Gentleman RC, Carey VJ, Bates DM, Bolstad B, Dettling M, Dudoit S, Ellis B, Gautier L, Ge Y, Gentry J, Hornik K, Hothorn T, Huber W, Iacus S, Irizarry R, Leisch F, Li C, Maechler M, Rossini AJ, Sawitzki G, et al (2004) Bioconductor:

open software development for computational biology and bioinformatics. *Genome biology* **5:** R80

Guo T, Zhu Y, Gan CS, Lee SS, Zhu J, Wang H, Li X, Christensen J, Huang S, Kon OL & Sze SK (2010) Quantitative proteomics discloses MET expression in mitochondria as a direct target of MET kinase inhibitor in cancer cells. *Molecular & cellular proteomics : MCP* **9:** 2629–41

Hallett RM, Kondratyev MK, Giacomelli AO, Nixon AML, Girgis-Gabardo A, Ilieva D & Hassell JA (2012) Small molecule antagonists of the Wnt/β-catenin signaling pathway target breast tumor-initiating cells in a Her2/Neu mouse model of breast cancer. *PloS one* **7:** e33976

Halt K & Vainio S (2014) Coordination of kidney organogenesis by Wnt signaling. *Pediatric nephrology (Berlin, Germany)* **29:** 737–44

Harris PC & Torres VE (2009) Polycystic kidney disease. *Annual review of medicine* **60:** 321–37

Hausmann G, Bänziger C & Basler K (2007) Helping Wingless take flight: how WNT proteins are secreted. *Nature reviews. Molecular cell biology* **8:** 331–6

Hemesath TJ, Steingrímsson E, McGill G, Hansen MJ, Vaught J, Hodgkinson CA, Arnheiter H, Copeland NG, Jenkins NA & Fisher DE (1994) microphthalmia, A critical factor in melanocyte development, defines a discrete transcription factor family. *Genes and Development* **8:** 2770–2780

Herring JC, Enquist EG, Chernoff A, Linehan WM, Choyke PL & Walther MM (2001) Parenchymal sparing surgery in patients with hereditary renal cell carcinoma: 10-year experience. *The Journal of urology* **165:** 777–81

Hershey CL & Fisher DE (2004) Mitf and Tfe3: members of a b-HLH-ZIP transcription factor family essential for osteoclast development and function. *Bone* **34:** 689–96

Hino S, Tanji C, Nakayama KI & Kikuchi A (2005) Phosphorylation of beta-catenin by cyclic AMP-dependent protein kinase stabilizes beta-catenin through inhibition of its ubiquitination. *Molecular and cellular biology* **25:** 9063–72

Hofmann K (2000) A superfamily of membrane-bound O-acyltransferases with implications for wnt signaling. *Trends in biochemical sciences* **25:** 111–2

Hong SB, Oh H, Valera VA, Baba M, Schmidt LS & Linehan WM (2010) Inactivation of the FLCN tumor suppressor gene induces TFE3 transcriptional activity by increasing its nuclear localization. *PLoS ONE* **5:**

Hua X, Miller ZA, Benchabane H, Wrana JL & Lodish HF (2000) Synergism between transcription factors TFE3 and Smad3 in transforming growth factor-beta-induced transcription of the Smad7 gene. *Journal of Biological Chemistry* **275:** 33205–33208

Huan C, Kelly ML, Steele R, Shapira I, Gottesman SRS & Roman CAJ (2006) Transcription factors TFE3 and TFEB are critical for CD40 ligand expression and thymus-dependent humoral immunity. *Nature immunology* **7:** 1082–91

Inamura K, Fujiwara M, Togashi Y, Nomura K, Mukai H, Fujii Y, Yamamoto S, Yonese J, Fukui I & Ishikawa Y (2012) Diverse Fusion Patterns and Heterogeneous Clinicopathologic Features of Renal Cell Carcinoma With t(6;11) Translocation. *The American Journal of Surgical Pathology* **36:** 35–42

Ishiyama N, Lee S-H, Liu S, Li G-Y, Smith MJ, Reichardt LF & Ikura M (2010) Dynamic and static interactions between p120 catenin and E-cadherin regulate the stability of cell-cell adhesion. *Cell* **141:** 117–28

Jaiswal JK, Andrews NW & Simon SM (2002) Membrane proximal lysosomes are the major vesicles responsible for calcium-dependent exocytosis in nonsecretory cells. *The Journal of cell biology* **159:** 625–35

Janda CY, Waghray D, Levin AM, Thomas C & Garcia KC (2012) Structural basis of Wnt recognition by Frizzled. *Science (New York, N.Y.)* **337:** 59–64

de Jong B, Molenaar IM, Leeuw JA, Idenberg VJ & Oosterhuis JW (1986) Cytogenetics of a renal adenocarcinoma in a 2-year-old child. *Cancer genetics and cytogenetics* **21:** 165–9

Kadowaki T, Wilder E, Klingensmith J, Zachary K & Perrimon N (1996) The segment polarity gene porcupine encodes a putative multitransmembrane protein involved in Wingless processing. *Genes & development* **10:** 3116–28

Kaelin WG (2008) The von Hippel-Lindau tumour suppressor protein: O2 sensing and cancer. *Nature reviews. Cancer* **8:** 865–73

Kauffman EC, Ricketts CJ, Rais-Bahrami S, Yang Y, Merino MJ, Bottaro DP, Srinivasan R & Linehan WM (2014) Molecular genetics and cellular features of TFE3 and TFEB fusion kidney cancers. *Nature reviews. Urology***:** 1–11

Kaushik S & Cuervo AM (2012) Chaperone-mediated autophagy: a unique way to enter the lysosome world. *Trends in cell biology* **22:** 407–17

Kim I, Ding T, Fu Y, Li C, Cui L, Li A, Lian P, Liang D, Wang DW, Guo C, Ma J, Zhao P, Coffey RJ, Zhan Q & Wu G (2009) Conditional mutation of Pkd2

causes cystogenesis and upregulates beta-catenin. *Journal of the American Society of Nephrology : JASN* **20:** 2556–69

Kim S, Nie H, Nesin V, Tran U, Outeda P, Bai C-X, Keeling J, Maskey D, Watnick T, Wessely O & Tsiokas L (2016) The polycystin complex mediates Wnt/Ca(2+) signalling. *Nature cell biology* **18:** 752–64

Kim YS, Kang YK, Kim JB, Han SA, Kim KI & Paik SR (2000) beta-catenin expression and mutational analysis in renal cell carcinomas. *Pathology international* **50:** 725–30

Kispert A, Vainio S & McMahon AP (1998) Wnt-4 is a mesenchymal signal for epithelial transformation of metanephric mesenchyme in the developing kidney. *Development (Cambridge, England)* **125:** 4225–34

Klipper-Aurbach Y, Wasserman M, Braunspiegel-Weintrob N, Borstein D, Peleg S, Assa S, Karp M, Benjamini Y, Hochberg Y & Laron Z (1995) Mathematical formulae for the prediction of the residual beta cell function during the first two years of disease in children and adolescents with insulin-dependent diabetes mellitus. *Medical hypotheses* **45:** 486–90

Koesters R, Ridder R, Kopp-Schneider A, Betts D, Adams V, Niggli F, Briner J & von Knebel Doeberitz M (1999) Mutational activation of the beta-catenin proto-oncogene is a common event in the development of Wilms' tumors. *Cancer research* **59:** 3880–2

Komai Y, Fujiwara M, Fujii Y, Mukai H, Yonese J, Kawakami S, Yamamoto S, Migita T, Ishikawa Y, Kurata M, Nakamura T & Fukui I (2009) Adult Xp11 translocation renal cell carcinoma diagnosed by cytogenetics and immunohistochemistry. *Clinical Cancer Research* **15:** 1170–1176

Komatsu M, Waguri S, Ueno T, Iwata J, Murata S, Tanida I, Ezaki J, Mizushima N, Ohsumi Y, Uchiyama Y, Kominami E, Tanaka K & Chiba T (2005) Impairment of starvation-induced and constitutive autophagy in Atg7-deficient mice. *The Journal of cell biology* **169:** 425–34

Korinek V, Barker N, Morin PJ, van Wichen D, de Weger R, Kinzler KW, Vogelstein B & Clevers H (1997) Constitutive transcriptional activation by a beta-catenin-Tcf complex in APC-/- colon carcinoma. *Science (New York, N.Y.)* **275:** 1784–7

Krishnan B & Truong LD (2002) Renal epithelial neoplasms: The diagnostic implications of electron microscopic study in 55 cases. *Human Pathology* **33:**

68–79

Kuiper RP, Schepens M, Thijssen J, van Asseldonk M, van den Berg E, Bridge J, Schuuring E, Shoenmakers EFPM & van Kessel AG (2003) Upregulation of the transcription factor TFEB in t(6;11)(p21;q13)-positive renal cell carcinomas due to promoter substitution. *Human Molecular Genetics* **12:** 1661–1669

Kuiper RP, Schepens M, Thijssen J, Schoenmakers EFPM & van Kessel AG (2004) Regulation of the MiTF/TFE bHLH-LZ transcription factors through restricted spatial expression and alternative splicing of functional domains. *Nucleic Acids Research* **32:** 2315–2322

Kuure S, Popsueva A, Jakobson M, Sainio K & Sariola H (2007) Glycogen synthase kinase-3 inactivation and stabilization of beta-catenin induce nephron differentiation in isolated mouse and rat kidney mesenchymes. *Journal of the American Society of Nephrology : JASN* **18:** 1130–9

Lal M, Song X, Pluznick JL, Di Giovanni V, Merrick DM, Rosenblum ND, Chauvet V, Gottardi CJ, Pei Y & Caplan MJ (2008) Polycystin-1 C-terminal tail associates with beta-catenin and inhibits canonical Wnt signaling. *Human molecular genetics* **17:** 3105–17

Lancaster MA & Gleeson JG (2010) Cystic kidney disease: the role of Wnt signaling. *Trends in molecular medicine* **16:** 349–60

Lantinga-van Leeuwen IS, Leonhard WN, van de Wal A, Breuning MH, Verbeek S, de Heer E & Peters DJM (2006) Transgenic mice expressing tamoxifen-inducible Cre for somatic gene modification in renal epithelial cells. *Genesis (New York, N.Y. : 2000)* **44:** 225–32

Lantinga-van Leeuwen IS, Leonhard WN, van der Wal A, Breuning MH, de Heer E & Peters DJM (2007) Kidney-specific inactivation of the Pkd1 gene induces rapid cyst formation in developing kidneys and a slow onset of disease in adult mice. *Human molecular genetics* **16:** 3188–96

Launonen V, Vierimaa O, Kiuru M, Isola J, Roth S, Pukkala E, Sistonen P, Herva R & Aaltonen LA (2001) Inherited susceptibility to uterine leiomyomas and renal cell cancer. *Proceedings of the National Academy of Sciences of the United States of America* **98:** 3387–92

Leemans JC, Stokman G, Claessen N, Rouschop KM, Teske GJD, Kirschning CJ, Akira S, van der Poll T, Weening JJ & Florquin S (2005) Renal-associated

TLR2 mediates ischemia/reperfusion injury in the kidney. *The Journal of clinical investigation* **115:** 2894–903

Leroy P & Mostov KE (2007) Slug is required for cell survival during partial epithelial-mesenchymal transition of HGF-induced tubulogenesis. *Molecular biology of the cell* **18:** 1943–52

Leroy X, Zini L, Leteurtre E, Zerimech F, Porchet N, Aubert J-P, Gosselin B & Copin M-C (2002) Morphologic subtyping of papillary renal cell carcinoma: correlation with prognosis and differential expression of MUC1 between the two subtypes. *Modern pathology : an official journal of the United States and Canadian Academy of Pathology, Inc* **15:** 1126–30

Levy C, Khaled M & Fisher DE (2006) MITF: master regulator of melanocyte development and melanoma oncogene. *Trends in Molecular Medicine* **12:** 406–414

Li VSW, Ng SS, Boersema PJ, Low TY, Karthaus WR, Gerlach JP, Mohammed S, Heck AJR, Maurice MM, Mahmoudi T & Clevers H (2012) Wnt signaling through inhibition of β-catenin degradation in an intact Axin1 complex. *Cell* **149:** 1245–56 Available at: http://www.ncbi.nlm.nih.gov/pubmed/22682247 [Accessed May 28, 2016]

Lin S-L, Li B, Rao S, Yeo E-J, Hudson TE, Nowlin BT, Pei H, Chen L, Zheng JJ, Carroll TJ, Pollard JW, McMahon AP, Lang RA & Duffield JS (2010) Macrophage Wnt7b is critical for kidney repair and regeneration. *Proceedings of the National Academy of Sciences of the United States of America* **107:** 4194–9

Linehan WM (2012) Genetic basis of kidney cancer: Role of genomics for the development of disease-based therapeutics. *Genome Research* **22:** 2089–2100

Linehan WM & Rathmell WK (2012) Kidney cancer. *Urologic oncology* **30:** 948–51

Linehan WM & Ricketts CJ (2013) The metabolic basis of kidney cancer. *Seminars in Cancer Biology* **23:** 46–55

Linehan WM, Spellman PT, Ricketts CJ, Creighton CJ, Fei SS, Davis C, Wheeler DA, Murray BA, Schmidt L, Vocke CD, Peto M, Al Mamun AAM, Shinbrot E, Sethi A, Brooks S, Rathmell WK, Brooks AN, Hoadley KA, Robertson AG, Brooks D, et al (2015) Comprehensive Molecular Characterization of Papillary Renal-Cell Carcinoma. *The New England journal of medicine*

Linehan WM, Srinivasan R & Schmidt LS (2010) The genetic basis of kidney cancer: a metabolic disease. *Nature reviews. Urology* **7:** 277–85

Linehan WM & Zbar B (1987) Loss of DNA sequences on chromosome 3 in renal cell carcinoma. *Urology* **30:** 404

Luzio JP, Pryor PR & Bright NA (2007) Lysosomes: fusion and function. *Nature reviews. Molecular cell biology* **8:** 622–32

Malouf GG, Camparo P, Oudard S, Schleiermacher G, Theodore C, Rustine A, Dutcher J, Billemont B, Rixe O, Bompas E, Guillot A, Boccon-Gibod L, Couturier J, Molinié V & Escudier B (2010) Targeted agents in metastatic Xp11 translocation/TFE3 gene fusion renal cell carcinoma (RCC): A report from the Juvenile RCC Network. *Annals of Oncology* **21:** 1834–1838

Malouf GG, Su X, Yao H, Gao J, Xiong L, He Q, Compérat E, Couturier J, Molinié V, Escudier B, Camparo P, Doss DJ, Thompson EJ, Khayat D, Wood CG, Yu W, Teh BT, Weinstein J & Tannir NM (2014) Next-generation sequencing of translocation renal cell carcinoma reveals novel RNA splicing partners and frequent mutations of chromatin-remodeling Genes. *Clinical Cancer Research* **20:** 4129–4140

Martina JA, Chen Y, Gucek M & Puertollano R (2012) MTORC1 functions as a transcriptional regulator of autophagy by preventing nuclear transport of TFEB. *Autophagy* **8:** 903–914

Martina JA, Diab HI, Lishu L, Jeong-A L, Patange S, Raben N & Puertollano R (2014) The nutrient-responsive transcription factor TFE3 promotes autophagy, lysosomal biogenesis, and clearance of cellular debris. *Science signaling* **7:** ra9

Martina JA & Puertollano R (2013) Rag GTPases mediate amino acid-dependent recruitment of TFEB and MITF to lysosomes. *The Journal of cell biology* **200:** 475–91

Medina DL, Fraldi A, Bouche V, Annunziata F, Mansueto G, Spampanato C, Puri C, Pignata A, Martina JA, Sardiello M, Palmieri M, Polishchuk R, Puertollano R & Ballabio A (2011) Transcriptional activation of lysosomal exocytosis promotes cellular clearance. *Developmental Cell* **21:** 421–430

Medina DL, Di Paola S, Peluso I, Armani A, De Stefani D, Venditti R, Montefusco S, Scotto-Rosato A, Prezioso C, Forrester A, Settembre C, Wang W, Gao Q, Xu H, Sandri M, Rizzuto R, De Matteis MA & Ballabio A (2015) Lysosomal

calcium signalling regulates autophagy through calcineurin and TFEB. *Nature cell biology* **17:** 288–99

Mindell JA (2012) Lysosomal acidification mechanisms. *Annual review of physiology* **74:** 69–86

Mulligan KA, Fuerer C, Ching W, Fish M, Willert K & Nusse R (2012) Secreted Wingless-interacting molecule (Swim) promotes long-range signaling by maintaining Wingless solubility. *Proceedings of the National Academy of Sciences of the United States of America* **109:** 370–7

Nauli SM, Alenghat FJ, Luo Y, Williams E, Vassilev P, Li X, Elia AEH, Lu W, Brown EM, Quinn SJ, Ingber DE & Zhou J (2003) Polycystins 1 and 2 mediate mechanosensation in the primary cilium of kidney cells. *Nature genetics* **33:** 129–37

Nelson WJ & Nusse R (2004) Convergence of Wnt, beta-catenin, and cadherin pathways. *Science (New York, N.Y.)* **303:** 1483–1487

Network TCGAR, Medicine A working group: BC of, Creighton CJ, Morgan M, Gunaratne PH, Wheeler DA, Gibbs RA, Agency BCC, Robertson GA, Chu A, Institute B, Beroukhim R, Cibulskis K, Hospital B& W, Signoretti S, University B, HsinTa Wu FV, Raphael BJ, Center TU of TC, Verhaak RGW, et al (2013) Comprehensive molecular characterization of clear cell renal cell carcinoma. *Nature* **499:** 43–49

Nickerson ML, Jaeger E, Shi Y, Durocher JA, Mahurkar S, Zaridze D, Matveev V, Janout V, Kollarova H, Bencko V, Navratilova M, Szeszenia-Dabrowska N, Mates D, Mukeria A, Holcatova I, Schmidt LS, Toro JR, Karami S, Hung R, Gerard GF, et al (2008) Improved identification of von Hippel-Lindau gene alterations in clear cell renal tumors. *Clinical cancer research : an official journal of the American Association for Cancer Research* **14:** 4726–34

Nickerson ML, Warren MB, Toro JR, Matrosova V, Glenn G, Turner ML, Duray P, Merino M, Choyke P, Pavlovich CP, Sharma N, Walther M, Munroe D, Hill R, Maher E, Greenberg C, Lerman MI, Linehan WM, Zbar B & Schmidt LS (2002) Mutations in a novel gene lead to kidney tumors, lung wall defects, and benign tumors of the hair follicle in patients with the Birt-Hogg-Dubé syndrome. *Cancer cell* **2:** 157–64

Nusse R & Varmus HE (1982) Many tumors induced by the mouse mammary tumor virus contain a provirus integrated in the same region of the host

genome. *Cell* **31:** 99–109

Palmieri M, Impey S, Kang H, di Ronza A, Pelz C, Sardiello M & Ballabio A (2011) Characterization of the CLEAR network reveals an integrated control of cellular clearance pathways. *Human Molecular Genetics* **20:** 3852–3866

Pan F-Y, Zhang S-Z, Xu N, Meng F-L, Zhang H-X, Xue B, Han X & Li C-J (2010) Beta-catenin signaling involves HGF-enhanced HepG2 scattering through activating MMP-7 transcription. *Histochemistry and cell biology* **134:** 285–95

Panáková D, Sprong H, Marois E, Thiele C & Eaton S (2005) Lipoprotein particles are required for Hedgehog and Wingless signalling. *Nature* **435:** 58–65

Papkoff J, Brown AM & Varmus HE (1987) The int-1 proto-oncogene products are glycoproteins that appear to enter the secretory pathway. *Molecular and cellular biology* **7:** 3978–84

Parikh J, Coleman T, Messias N & Brown J (2009) Temsirolimus in the treatment of renal cell carcinoma associated with Xp11.2 translocation/TFE gene fusion proteins: a case report and review of literature. *Rare tumors* **1:** e53

Park J-S, Valerius MT & McMahon AP (2007) Wnt/beta-catenin signaling regulates nephron induction during mouse kidney development. *Development (Cambridge, England)* **134:** 2533–9

Pavlovich CP, Grubb RL, Hurley K, Glenn GM, Toro J, Schmidt LS, Torres-Cabala C, Merino MJ, Zbar B, Choyke P, Walther MM & Linehan WM (2005) Evaluation and management of renal tumors in the Birt-Hogg-Dubé syndrome. *The Journal of urology* **173:** 1482–6

Perera RM, Stoykova S, Nicolay BN, Ross KN, Fitamant J, Boukhali M, Lengrand J, Deshpande V, Selig MK, Ferrone CR, Settleman J, Stephanopoulos G, Dyson NJ, Zoncu R, Ramaswamy S, Haas W & Bardeesy N (2015) Transcriptional control of autophagy-lysosome function drives pancreatic cancer metabolism. *Nature* **524:** 361–5

Petit CS, Roczniak-Ferguson A & Ferguson SM (2013) Recruitment of folliculin to lysosomes supports the amino acid-dependent activation of Rag GTPases. *The Journal of cell biology* **202:** 1107–22

Pinson KI, Brennan J, Monkley S, Avery BJ & Skarnes WC (2000) An LDL-receptor-related protein mediates Wnt signalling in mice. *Nature* **407:** 535–8

Ploper D, Taelman VF, Robert L, Perez BS, Titz B, Chen H-W, Graeber TG, von Euw E, Ribas A & De Robertis EM (2015) MITF drives endolysosomal

biogenesis and potentiates Wnt signaling in melanoma cells. *Proceedings of the National Academy of Sciences of the United States of America* **112:** E420–9

Pogenberg V, Ogmundsdóttir MH, Bergsteinsdóttir K, Schepsky A, Phung B, Deineko V, Milewski M, Steingrímsson E & Wilmanns M (2012) Restricted leucine zipper dimerization and specificity of DNA recognition of the melanocyte master regulator MITF. *Genes & development* **26:** 2647–58

Qian C-N, Knol J, Igarashi P, Lin F, Zylstra U, Teh BT & Williams BO (2005) Cystic renal neoplasia following conditional inactivation of apc in mouse renal tubular epithelium. *The Journal of biological chemistry* **280:** 3938–45

Ranganathan S, Tan X & Monga SPS beta-Catenin and met deregulation in childhood Hepatoblastomas. *Pediatric and developmental pathology : the official journal of the Society for Pediatric Pathology and the Paediatric Pathology Society* **8:** 435–47

Rao Q, Liu B, Cheng L, Zhu Y & Shi Q (2012) Renal Cell Carcinomas With t(6;11)(p21;q12). **36:** 1327–1338

Rao Q, Zhang XM, Tu P, Xia QY, Shen Q, Zhou XJ & Shi QL (2013) Renal cell carcinomas with t(6;11)(p21;q12) presenting with tubulocystic renal cell carcinoma-like features. *International Journal of Clinical and Experimental Pathology* **6:** 1452–1457

Rehli M, Lichanska A, Cassady AI, Ostrowski MC & Hume DA (1999) TFEC is a macrophage-restricted member of the microphthalmia-TFE subfamily of basic helix-loop-helix leucine zipper transcription factors. *Journal of immunology (Baltimore, Md. : 1950)* **162:** 1559–65

Rijsewijk F, Schuermann M, Wagenaar E, Parren P, Weigel D & Nusse R (1987) The Drosophila homolog of the mouse mammary oncogene int-1 is identical to the segment polarity gene wingless. *Cell* **50:** 649–57

Rivera MN, Kim WJ, Wells J, Driscoll DR, Brannigan BW, Han M, Kim JC, Feinberg AP, Gerald WL, Vargas SO, Chin L, Iafrate AJ, Bell DW & Haber DA (2007) An X chromosome gene, WTX, is commonly inactivated in Wilms tumor. *Science (New York, N.Y.)* **315:** 642–5

Roczniak-Ferguson A, Petit CS, Froehlich F, Qian S, Ky J, Angarola B, Walther TC & Ferguson SM (2012) The transcription factor TFEB links mTORC1 signaling to transcriptional control of lysosome homeostasis. *Science*

signaling **5:** ra42

Rodova M, Islam MR, Maser RL & Calvet JP (2002) The polycystic kidney disease-1 promoter is a target of the beta-catenin/T-cell factor pathway. *The Journal of biological chemistry* **277:** 29577–83

Rodríguez A, Webster P, Ortego J & Andrews NW (1997) Lysosomes behave as Ca2+-regulated exocytic vesicles in fibroblasts and epithelial cells. *The Journal of cell biology* **137:** 93–104]

Saftig P & Klumperman J (2009) Lysosome biogenesis and lysosomal membrane proteins: trafficking meets function. *Nature reviews. Molecular cell biology* **10:** 623–35

Sahu R, Kaushik S, Clement CC, Cannizzo ES, Scharf B, Follenzi A, Potolicchio I, Nieves E, Cuervo AM & Santambrogio L (2011) Microautophagy of cytosolic proteins by late endosomes. *Developmental cell* **20:** 131–9

Sancak Y, Bar-Peled L, Zoncu R, Markhard AL, Nada S & Sabatini DM (2010) Ragulator-rag complex targets mTORC1 to the lysosomal surface and is necessary for its activation by amino acids. *Cell* **141:** 290–303

Sancak Y, Peterson TR, Shaul YD, Lindquist RA, Thoreen CC, Bar-Peled L & Sabatini DM (2008) The Rag GTPases bind raptor and mediate amino acid signaling to mTORC1. *Science (New York, N.Y.)* **320:** 1496–501

Sansom OJ, Griffiths DFR, Reed KR, Winton DJ & Clarke AR (2005) Apc deficiency predisposes to renal carcinoma in the mouse. *Oncogene* **24:** 8205–10

Sardiello M, Palmieri M, di Ronza A, Medina DL, Valenza M, Gennarino VA, Di Malta C, Donaudy F, Embrione V, Polishchuk RS, Banfi S, Parenti G, Cattaneo E & Ballabio A (2009) A gene network regulating lysosomal biogenesis and function. *Science (New York, N.Y.)* **325:** 473–7

Schmidt L, Duh FM, Chen F, Kishida T, Glenn G, Choyke P, Scherer SW, Zhuang Z, Lubensky I, Dean M, Allikmets R, Chidambaram A, Bergerheim UR, Feltis JT, Casadevall C, Zamarron A, Bernues M, Richard S, Lips CJ, Walther MM, et al (1997) Germline and somatic mutations in the tyrosine kinase domain of the MET proto-oncogene in papillary renal carcinomas. *Nature genetics* **16:** 68–73

Schmidt LS & Linehan WM (2015) Molecular genetics and clinical features of Birt-Hogg-Dubé syndrome. *Nature reviews. Urology* **12:** 558–69

Settembre C, De Cegli R, Mansueto G, Saha PK, Vetrini F, Visvikis O, Huynh T, Carissimo A, Palmer D, Klisch TJ, Wollenberg AC, Di Bernardo D, Chan L, Irazoqui JE & Ballabio A (2013a) TFEB controls cellular lipid metabolism through a starvation-induced autoregulatory loop. *Nature cell biology* **15:** 647–58

Settembre C, Fraldi A, Medina DL & Ballabio A (2013b) Signals from the lysosome: a control centre for cellular clearance and energy metabolism. *Nature reviews. Molecular cell biology* **14:** 283–296

Settembre C, Di Malta C, Polito VA, Garcia Arencibia M, Vetrini F, Erdin S, Erdin SU, Huynh T, Medina D, Colella P, Sardiello M, Rubinsztein DC & Ballabio A (2011) TFEB links autophagy to lysosomal biogenesis. *Science (New York, N.Y.)* **332:** 1429–1433

Settembre C, Zoncu R, Medina DL, Vetrini F, Erdin S, Erdin S, Huynh T, Ferron M, Karsenty G, Vellard MC, Facchinetti V, Sabatini DM & Ballabio A (2012) A lysosome-to-nucleus signalling mechanism senses and regulates the lysosome via mTOR and TFEB. *The EMBO journal* **31:** 1095–108

Shao X (2002) A Minimal Ksp-Cadherin Promoter Linked to a Green Fluorescent Protein Reporter Gene Exhibits Tissue-Specific Expression in the Developing Kidney and Genitourinary Tract. *Journal of the American Society of Nephrology* **13:** 1824–1836

Shen C & Kaelin WG (2013) The VHL/HIF axis in clear cell renal carcinoma. *Seminars in cancer biology* **23:** 18–25

Sidhar SK, Clark J, Gill S, Hamoudi R, Crew AJ, Gwilliam R, Ross M, Linehan WM, Birdsall S, Shipley J & Cooper CS (1996) The t(X;1)(p11.2;q21.2) translocation in papillary renal sell carcinoma fuses a novel gene PRCC to the TFE3 transcription factor gene. *Human Molecular Genetics* **5:** 1333–1338

Simons M, Gloy J, Ganner A, Bullerkotte A, Bashkurov M, Krönig C, Schermer B, Benzing T, Cabello OA, Jenny A, Mlodzik M, Polok B, Driever W, Obara T & Walz G (2005) Inversin, the gene product mutated in nephronophthisis type II, functions as a molecular switch between Wnt signaling pathways. *Nature genetics* **37:** 537–43

Stark K, Vainio S, Vassileva G & McMahon AP (1994) Epithelial transformation of metanephric mesenchyme in the developing kidney regulated by Wnt-4. *Nature* **372:** 679–83

Steingrímsson E, Copeland NG & Jenkins N a (2004) Melanocytes and the microphthalmia transcription factor network. *Annual review of genetics* **38:** 365–411

Steingrimsson E, Tessarollo L, Reid SW, Jenkins NA & Copeland NG (1998) The bHLH-Zip transcription factor Tfeb is essential for placental vascularization. *Development (Cambridge, England)* **125:** 4607–4616

Stinchcombe JC & Griffiths GM (1999) Regulated secretion from hemopoietic cells. *The Journal of cell biology* **147:** 1–6

Taelman VF, Dobrowolski R, Plouhinec JL, Fuentealba LC, Vorwald PP, Gumper I, Sabatini DD & De Robertis EM (2010) Wnt signaling requires sequestration of Glycogen Synthase Kinase 3 inside multivesicular endosomes. *Cell* **143:** 1136–1148

Takada R, Satomi Y, Kurata T, Ueno N, Norioka S, Kondoh H, Takao T & Takada S (2006) Monounsaturated fatty acid modification of Wnt protein: its role in Wnt secretion. *Developmental cell* **11:** 791–801

Tanigawa S, Wang H, Yang Y, Sharma N, Tarasova N, Ajima R, Yamaguchi TP, Rodriguez LG & Perantoni AO (2011) Wnt4 induces nephronic tubules in metanephric mesenchyme by a non-canonical mechanism. *Developmental biology* **352:** 58–69

Tassabehji M, Newton VE & Read AP (1994) Waardenburg syndrome type 2 caused by mutations in the human microphthalmia (MITF) gene. *Nature genetics* **8:** 251–5

Thivierge C, Kurbegovic A, Couillard M, Guillaume R, Coté O & Trudel M (2006) Overexpression of PKD1 causes polycystic kidney disease. *Molecular and cellular biology* **26:** 1538–48

Tian G, Erman B, Ishii H, Gangopadhyay SS & Sen R (1999) Transcriptional activation by ETS and leucine zipper-containing basic helix-loop-helix proteins. *Molecular and cellular biology* **19:** 2946–2957

Tolwinski NS, Wehrli M, Rives A, Erdeniz N, DiNardo S & Wieschaus E (2003) Wg/Wnt signal can be transmitted through arrow/LRP5,6 and Axin independently of Zw3/Gsk3beta activity. *Developmental cell* **4:** 407–18

Tonk V, Wilson KS, Timmons CF, Schneider NR & Tomlinson GE (1995) Renal cell carcinoma with translocation (X;1). Further evidence for a cytogenetically defined subtype. *Cancer genetics and cytogenetics* **81:** 72–5

Tsuda M, Davis IJ, Argani P, Shukla N, McGill GG, Nagai M, Saito T, Laé M, Fisher DE & Ladanyi M (2007) TFE3 fusions activate MET signaling by transcriptional up-regulation, defining another class of tumors as candidates for therapeutic MET inhibition. *Cancer Research* **67:** 919–929

Ugurel S, Houben R, Schrama D, Voigt H, Zapatka M, Schadendorf D, Bröcker EB & Becker JC (2007) Microphthalmia-associated transcription factor gene amplification in metastatic melanoma is a prognostic marker for patient survival, but not a predictive marker for chemosensitivity and chemotherapy response. *Clinical cancer research : an official journal of the American Association for Cancer Research* **13:** 6344–50

Vainio SJ & Uusitalo MS (2000) A road to kidney tubules via the Wnt pathway. *Pediatric nephrology (Berlin, Germany)* **15:** 151–6

Del Valle-Pérez B, Arqués O, Vinyoles M, de Herreros AG & Duñach M (2011) Coordinated action of CK1 isoforms in canonical Wnt signaling. *Molecular and cellular biology* **31:** 2877–88

Vanharanta S, Buchta M, McWhinney SR, Virta SK, Peçzkowska M, Morrison CD, Lehtonen R, Januszewicz A, Järvinen H, Juhola M, Mecklin J-P, Pukkala E, Herva R, Kiuru M, Nupponen NN, Aaltonen LA, Neumann HPH & Eng C (2004) Early-onset renal cell carcinoma as a novel extraparaganglial component of SDHB-associated heritable paraganglioma. *American journal of human genetics* **74:** 153–9

Varela I, Tarpey P, Raine K, Huang D, Ong CK, Stephens P, Davies H, Jones D, Lin M-L, Teague J, Bignell G, Butler A, Cho J, Dalgliesh GL, Galappaththige D, Greenman C, Hardy C, Jia M, Latimer C, Lau KW, et al (2011) Exome sequencing identifies frequent mutation of the SWI/SNF complex gene PBRM1 in renal carcinoma. *Nature* **469:** 539–42

Verhage M & Toonen RF (2007) Regulated exocytosis: merging ideas on fusing membranes. *Current opinion in cell biology* **19:** 402–8

Verheyen EM & Gottardi CJ (2010) Regulation of Wnt/beta-catenin signaling by protein kinases. *Developmental dynamics : an official publication of the American Association of Anatomists* **239:** 34–44

Voronkov A & Krauss S (2013) Wnt/beta-catenin signaling and small molecule inhibitors. *Current pharmaceutical design* **19:** 634–64

Wagner AJ, Goldberg JM, Dubois SG, Choy E, Rosen L, Pappo A, Geller J,

Judson I, Hogg D, Senzer N, Davis IJ, Chai F, Waghorne C, Schwartz B & Demetri GD (2012) Tivantinib (ARQ 197), a selective inhibitor of MET, in patients with microphthalmia transcription factor-associated tumors: results of a multicenter phase 2 trial. *Cancer* **118:** 5894–902

Wakita K, Tetsu O & McCormick F (2001) A mammalian two-hybrid system for adenomatous polyposis coli-mutated colon cancer therapeutics. *Cancer research* **61:** 854–8

Wei W, Chua M-S, Grepper S & So S (2010) Small molecule antagonists of Tcf4/beta-catenin complex inhibit the growth of HCC cells in vitro and in vivo. *International journal of cancer. Journal international du cancer* **126:** 2426–36

van de Wetering M, Cavallo R, Dooijes D, van Beest M, van Es J, Loureiro J, Ypma A, Hursh D, Jones T, Bejsovec A, Peifer M, Mortin M & Clevers H (1997) Armadillo coactivates transcription driven by the product of the Drosophila segment polarity gene dTCF. *Cell* **88:** 789–99

Weterman MJ, van Groningen JJ, Jansen A & van Kessel AG (2000) Nuclear localization and transactivating capacities of the papillary renal cell carcinoma-associated TFE3 and PRCC (fusion) proteins. *Oncogene* **19:** 69–74

Willert K, Brown JD, Danenberg E, Duncan AW, Weissman IL, Reya T, Yates JR & Nusse R (2003) Wnt proteins are lipid-modified and can act as stem cell growth factors. *Nature* **423:** 448–52

Willert K & Nusse R (2012) Wnt proteins. *Cold Spring Harbor perspectives in biology* **4:** a007864

Wu A, Kunju LP, Cheng L & Shah RB (2008) Renal cell carcinoma in children and young adults: analysis of clinicopathological, immunohistochemical and molecular characteristics with an emphasis on the spectrum of Xp11.2 translocation-associated and unusual clear cell subtypes. *Histopathology* **53:** 533–44

Xu H & Ren D (2015) Lysosomal physiology. *Annual review of physiology* **77:** 57–80

Yang Y, Valera V, Sourbier C, Vocke CD, Wei M, Pike L, Huang Y, Merino MA, Bratslavsky G, Wu M, Ricketts CJ & Linehan WM A novel fumarate hydratase-deficient HLRCC kidney cancer cell line, UOK268: a model of the Warburg effect in cancer. *Cancer genetics* **205:** 377–90

Zbar B, Alvord WG, Glenn G, Turner M, Pavlovich CP, Schmidt L, Walther M, Choyke P, Weirich G, Hewitt SM, Duray P, Gabril F, Greenberg C, Merino MJ, Toro J & Linehan WM (2002) Risk of renal and colonic neoplasms and spontaneous pneumothorax in the Birt-Hogg-Dubé syndrome. *Cancer epidemiology, biomarkers & prevention : a publication of the American Association for Cancer Research, cosponsored by the American Society of Preventive Oncology* **11:** 393–400

Zhang F, White RL & Neufeld KL (2000) Phosphorylation near nuclear localization signal regulates nuclear import of adenomatous polyposis coli protein. *Proceedings of the National Academy of Sciences of the United States of America* **97:** 12577–82

Zhao GQ, Zhao Q, Zhou X, Mattei MG & de Crombrugghe B (1993) TFEC, a basic helix-loop-helix protein, forms heterodimers with TFE3 and inhibits TFE3-dependent transcription activation. *Molecular and cellular biology* **13:** 4505–4512

Zhou LT, Liu FY, Li Y, Peng YM, Liu YH & Li J (2012) Gpnmb/osteoactivin, an attractive target in cancer immunotherapy. *Neoplasma* **59:** 1–5

Zhu X, Kanai Y, Saito A, Kondo Y & Hirohashi S (2000) Aberrant expression of beta-catenin and mutation of exon 3 of the beta-catenin gene in renal and urothelial carcinomas. *Pathology international* **50:** 945–52